NUREG/CR-5875
BNL-NUREG-52325

Experimental Modeling of Heat and Mass Transfer in a Two-Fluid Bubbling Pool With Application to Molten Core-Concrete Interactions

Prepared by
G. A. Greene

Brookhaven National Laboratory

Prepared for
U.S. Nuclear Regulatory Commission

AVAILABILITY NOTICE

Availability of Reference Materials Cited in NRC Publications

Most documents cited in NRC publications will be available from one of the following sources:

1. The NRC Public Document Room, 2120 L Street, NW., Lower Level, Washington, DC 20555

2. The Superintendent of Documents, U.S. Government Printing Office, P.O. Box 37082, Washington, DC 20013-7082

3. The National Technical Information Service, Springfield, VA 22161

Although the listing that follows represents the majority of documents cited in NRC publications, it is not intended to be exhaustive.

Referenced documents available for inspection and copying for a fee from the NRC Public Document Room include NRC correspondence and internal NRC memoranda; NRC bulletins, circulars, information notices, inspection and investigation notices; licensee event reports; vendor reports and correspondence; Commission papers; and applicant and licensee documents and correspondence.

The following documents in the NUREG series are available for purchase from the GPO Sales Program: formal NRC staff and contractor reports, NRC-sponsored conference proceedings, international agreement reports, grant publications, and NRC booklets and brochures. Also available are regulatory guides, NRC regulations in the *Code of Federal Regulations*, and *Nuclear Regulatory Commission Issuances*.

Documents available from the National Technical Information Service include NUREG-series reports and technical reports prepared by other Federal agencies and reports prepared by the Atomic Energy Commission, forerunner agency to the Nuclear Regulatory Commission.

Documents available from public and special technical libraries include all open literature items, such as books, journal articles, and transactions. *Federal Register* notices, Federal and State legislation, and congressional reports can usually be obtained from these libraries.

Documents such as theses, dissertations, foreign reports and translations, and non-NRC conference proceedings are available for purchase from the organization sponsoring the publication cited.

Single copies of NRC draft reports are available free, to the extent of supply, upon written request to the Office of Administration, Distribution and Mail Services Section, U.S. Nuclear Regulatory Commission, Washington, DC 20555.

Copies of industry codes and standards used in a substantive manner in the NRC regulatory process are maintained at the NRC Library, 7920 Norfolk Avenue, Bethesda, Maryland, for use by the public. Codes and standards are usually copyrighted and may be purchased from the originating organization or, if they are American National Standards, from the American National Standards Institute, 1430 Broadway, New York, NY 10018.

NUREG/CR-5875
BNL-NUREG-52325

Experimental Modeling of Heat and Mass Transfer in a Two-Fluid Bubbling Pool With Application to Molten Core-Concrete Interactions

Prepared by
G. A. Greene

Brookhaven National Laboratory

Prepared for
U.S. Nuclear Regulatory Commission

AVAILABILITY NOTICE

Availability of Reference Materials Cited in NRC Publications

Most documents cited in NRC publications will be available from one of the following sources:

1. The NRC Public Document Room, 2120 L Street, NW., Lower Level, Washington, DC 20555

2. The Superintendent of Documents, U.S. Government Printing Office, P.O. Box 37082, Washington, DC 20013-7082

3. The National Technical Information Service, Springfield, VA 22161

Although the listing that follows represents the majority of documents cited in NRC publications, it is not intended to be exhaustive.

Referenced documents available for inspection and copying for a fee from the NRC Public Document Room include NRC correspondence and internal NRC memoranda; NRC bulletins, circulars, information notices, inspection and investigation notices; licensee event reports; vendor reports and correspondence; Commission papers; and applicant and licensee documents and correspondence.

The following documents in the NUREG series are available for purchase from the GPO Sales Program: formal NRC staff and contractor reports, NRC-sponsored conference proceedings, international agreement reports, grant publications, and NRC booklets and brochures. Also available are regulatory guides, NRC regulations in the *Code of Federal Regulations*, and *Nuclear Regulatory Commission Issuances*.

Documents available from the National Technical Information Service include NUREG-series reports and technical reports prepared by other Federal agencies and reports prepared by the Atomic Energy Commission, forerunner agency to the Nuclear Regulatory Commission.

Documents available from public and special technical libraries include all open literature items, such as books, journal articles, and transactions. *Federal Register* notices, Federal and State legislation, and congressional reports can usually be obtained from these libraries.

Documents such as theses, dissertations, foreign reports and translations, and non-NRC conference proceedings are available for purchase from the organization sponsoring the publication cited.

Single copies of NRC draft reports are available free, to the extent of supply, upon written request to the Office of Administration, Distribution and Mail Services Section, U.S. Nuclear Regulatory Commission, Washington, DC 20555.

Copies of industry codes and standards used in a substantive manner in the NRC regulatory process are maintained at the NRC Library, 7920 Norfolk Avenue, Bethesda, Maryland, for use by the public. Codes and standards are usually copyrighted and may be purchased from the originating organization or, if they are American National Standards, from the American National Standards Institute, 1430 Broadway, New York, NY 10018.

DISCLAIMER NOTICE

NUREG/CR-5875
BNL-NUREG-52325

Experimental Modeling of Heat and Mass Transfer in a Two-Fluid Bubbling Pool With Application to Molten Core-Concrete Interactions

Manuscript Completed: April 1992
Date Published: June 1992

Prepared by
G. A. Greene

Brookhaven National Laboratory
Upton, NY 11973

Prepared for
Division of Systems Research
Office of Nuclear Regulatory Research
U.S. Nuclear Regulatory Commission
Washington, DC 20555
NRC FIN L1259

ABSTRACT

This report describes the results of seven series of experiments conducted to investigate heat and mass transfer phenomena in multicomponent bubbling pools with application to the modeling of interlayer heat and mass transfer between immiscible liquid layers and interfacial heat transfer to vertical and horizontal boundaries for the CORCON computer code. Criteria for the onset of entrainment between immiscible liquids, as well as the rate of entrainment and the rate of settling are developed, which are applicable for modeling of mass transport during core-concrete interactions. Heat transfer models are developed for the case of stratified layers as well as the case with mass entrainment between the layers. Finally, models for heat transfer with bubbling to horizontal, drilled surfaces as well as bubbling along vertical surfaces are presented which are appropriate for boundary heat transfer analyses during molten core-concrete interactions.

TABLE OF CONTENTS

LIST OF FIGURES

LIST OF FIGURES (continued)

LIST OF TABLES

EXECUTIVE SUMMARY

The purpose of this report is to provide the experimental basis for modeling of multiphase heat and mass transfer processes that may occur in hypothetical core-concrete interactions. The models so developed are to form the basis for the analyses of hydrodynamic mixing and interlayer heat transfer in a multicomponent, bubbling pool of molten core debris for the CORCON computer code. The inclusion of these hydrodynamics and heat transfer models in CORCON will represent a significant advancement in the code's capability to analyze the effects of molten core-concrete interactions. By allowing the present constraint of segregated immiscible layering of oxide and metal layers to be relaxed and, in its place, the capability to mechanistically calculate the morphology of each layer (mixed or segregated) and the subsequent interlayer and boundary heat transfer rates to be activated, the distribution of heat sources and fission products and the melt temperatures will be more reliably calculated and, as a result, the analyses of containment loads, performance, and fission product release will be greatly improved.

A series of seven experimental investigations were performed during this study which form the basis for the modeling of interlayer and interfacial heat and mass transfer for the CORCON code. In all cases, the gas bubbling is to simulate the effect of rising concrete decomposition gases in the pool. The first series of experiments investigated the enhancement to heat transfer between stratified immiscible liquids by gas bubbling across the interface. The objective of these tests was to evaluate and/or improve the existing modeling in CORCON for stratified fluid layer heat transfer. Three series of tests were performed; the heavy fluid was mercury and the three light fluids tested were 10 cs. and 100 cs. silicone oils and water. The mercury was chosen to suppress mixing while the water and oils were chosen to cover the widest possible range of fluid Prandtl number. An improved interlayer heat transfer model was developed and implemented in CORCON to replace the original interlayer heat transfer model.

The second series of experiments that was performed investigated the onset of entrainment between immiscible liquid layers due to rising gas bubbles across the interface. The objective of these tests was to develop a mechanistic and reliable physical model to predict the conditions necessary to support mass entrainment from the lower fluid layer into the upper fluid layer, i.e., the onset of mixing. Experiments were performed with eight different fluid pairs to cover the widest possible range of the governing scaling parameters for entrainment onset. A first-principle analysis led to the theoretical criterion for the threshold volume of gas bubble necessary to cause entrainment. Application of this entrainment onset criterion to the modeling in the CORCON code will insure that the code calculations will reliably discriminate between conditions which support mixing between core oxide and metal layers during core-concrete interactions, and those conditions that will remain stratified.

The third series of experiments that was performed investigated the amount or rate of mass entrainment between initially stratified immiscible liquid layers due to gas bubbles rising across the liquid-liquid interface. The objective of these tests was to develop a physically-based correlation model to predict the amount of mass transferred by a single gas bubble rising across the liquid-liquid interface under conditions that have been shown to exceed the onset of

entrainment criterion. Experiments were performed with the same eight fluid pairs used in the entrainment onset study. The most significant variables which affect entrainment rate are liquid densities, liquid viscosities, and liquid-liquid interfacial tension. The fluid pairs studied covered ranges of these properties that were wide enough to support reliable correlation of the experimental data. The correlation can be used to calculate the mass transferred or entrained by a single gas bubble. By knowing the size and rate of all core-concrete gas bubbles, simple multiplication will result in the rate of entrainment. Application of this entrainment rate model to the modeling in the CORCON code will insure that hydrodynamic mixing and layer mixture properties are reliably calculated. This will ensure that the morphology of the core debris layers are accurately predicted, and that the distribution of heat sources and fission products that are calculated by CORCON will be accurate and reliable.

The fourth series of experiments that was performed investigated the phenomenon of heat transfer between partially stratified liquid layers with mass transport across the interface. This is the configuration most expected under molten core-concrete interaction conditions. The objective of these tests was to develop a generalized heat transfer model which incorporates the stratified heat transfer, entrainment onset, and entrainment rate models previously developed. Two series of experiments were performed with immiscible liquid layers that are known to support entrainment under conditions of gas bubbling. Silicone oil (10 cs.) and water were chosen as the fluid pair for these tests since their entrainment volume characteristics were optimum for quantification of heat transfer. The entrainment heat transfer model that was synthesized exhibited excellent agreement with the entrainment heat transfer data over two orders of magnitude in the heat transfer coefficient without adjustment. In the absence of entrainment, this heat transfer model reduces to the stratified layer model. Inclusion of this generalized entrainment heat transfer model in CORCON will greatly improve the accuracy and reliability of interlayer heat transfer analyses and insure consistency with hydrodynamic conditions of stratification or entrainment.

A fifth series of experiments that was performed investigated the phenomenon of drag and instability of entrained liquid droplets settling in another immiscible liquid. The objective of these tests was to develop a model for the settling velocity of liquid droplets that have been created by the entrainment process over a wide range of Reynolds and Weber numbers. This model, along with the entrainment rate model, will determine the mixture composition of the liquid layer into which the entrainment is occurring. Eight series of experiments were conducted with eight different pairs of fluids to examine the droplet drag characteristics over the entire length of the drag curve. Both stable and unstable drag regimes were modeled, as well as the locus of conditions which represent the transition from stable to unstable droplet drag. Inclusion of these drag models into the mixing model of the CORCON code will complete the formulation needed to reliably and accurately calculate heat and mass transfer between immiscible liquid layers under conditions characteristic of molten core-concrete interactions.

In addition to the five series of experiments for the modeling of interlayer heat and mass transfer between immiscible liquid layers, two other series of experiments are reported which investigated boundary heat transfer with gas bubbling. One of these experiments investigated heat transfer from a liquid pool in bubbly flow to a vertical wall; the second experiment investigated heat

transfer from a horizontal bubbling surface to an overlying liquid pool. Both experiments covered a range of gas flow rates appropriate to the modeling of the quasi-steady state period of molten core-concrete interactions. The experiments on bubbling heat transfer to a vertical boundary resulted in a detailed correlation that is appropriate for comparison to CORCON's lateral heat transfer model for non-metallic layers.

NOMENCLATURE

A	Test plate surface area
c_p	Specific heat
C_d	Drag coefficient
d	Equivalent spherical diameter
d_b	Spherical equivalent bubble diameter
Fr	Froude number
g	Gravitational acceleration
G	Coolant mass flux
Gr_1	Grashof number ($= g\beta\Delta T r_b^3/\nu^2$)
Gr_2	Grashof number ($= g\alpha^2 r_b^3/\nu^2$)
Gr_3	Grashof number ($= g\alpha r_b^3/\nu^2$)
h	Heat transfer coefficient
j_e	Superficial entrainment flux
j_g	Superficial gas velocity
k	Thermal conductivity
K	Droplet heat transfer efficiency
Nu	Nusselt number ($=hr_b/k$)
Pr	Prandtl number
q	Heat flux
r_b	Spherical equivalent bubble radius
R	Radius
Re	Reynolds number ($= ud/\nu$)
Re	Superficial Reynolds number ($=j_g r_b/\nu$)
Re_e	Entrainment Reynolds number ($=j_e d_b/\nu_2$)

NOMENCLATURE (continued)

$Re_{1,2}$	Bubble Reynolds number in layer 1 or 2 ($=u_b d_b/\nu$)
St	Stanton number
S	Shape factor for gas bubble
T	Temperature
u	Velocity
u_b	Bubble rise velocity
u_∞	Bubble terminal rise velocity
V	Volume
V_{go}	Entrainment onset bubble volume
V_g^*	Minimum bubble penetration volume
$V_{m,e}$	Maximum theoretical entrainment volume
We	Weber number ($= \rho u^2 d/\sigma$)

Greek Symbols

α	Void fraction, thermal diffusivity
β	Coefficient of thermal expansion
β	Column contact angle
ϵ	Entrainment efficiency
ρ	Density
ρ^*	Density ratio
μ	Dynamic viscosity
σ	Surface tension
σ_{12}	Interfacial tension
ν	Kinematic viscosity
ω	Dimensionless bubble volume
ϕ	Dimensionless excess bubble volume

NOMENCLATURE (continued)

ϕ	Dimensionless superficial gas velocity (= j_g/u_∞)

Subscripts

b	Bubble
crit	Critical value
d	Droplet
e	Entrainment
g	Gas
i	Side of interface (i = 1 or 2)
in	Coolant inlet
ℓ	Liquid
m	Maximum
out	Coolant outlet
plate	Test plate average
pool	Liquid pool average
SR	Surface removal
SURF	Surface
T	Total
w	Wall
1	Upper light liquid
2	Lower heavy liquid

1. INTRODUCTION

Reassessments of the public risk due to unterminated severe accidents in nuclear power reactors have pointed to the need for a better understanding of the heat and mass transfer processes in gas-sparged multi-fluid bubbling pools. In the case of severe core meltdown accidents in nuclear power reactors, the public risk is a direct function of the physical threat to the reactor containment and the release of radionuclides from the molten core to the environment during the stage of the accident termed the molten core-concrete interaction (MCCI) stage. The MCCI presupposes that the core meltdown has proceeded uninterrupted, that the high temperature core-melt has penetrated the reactor pressure vessel, and that the core has been deposited on the concrete floor below. Heat transfer from the molten core debris is sufficient to melt the concrete, which will then release H_2O and CO_2 gases due to the decomposition of hydroxides and carbonates in the concrete as well as the vaporization of water. As these gases rise through the molten pool of core debris, they can react exothermically with molten metals in the pool, releasing more energy into the core debris, converting H_2O and CO_2 into H_2 and CO, and chemically transforming some condensed phase radionuclides into intermediate volatile species by reactive vaporization. Since the core debris consists of molten oxides (UO_2, ZrO_2, FeO, etc.) and molten metals (Zr, Fe, Ni, Cr, etc.) which are immiscible, the molten pool would be vertically stratified in the absence of the gas bubbling action of the concrete decomposition gases. It is the action of the rising gas bubbles that enhances the boundary surface (bottom and side) and interfacial heat transfer rates and that drives the entrainment mass transport across the interface between the stratified layers of oxides and metals.

If the rising gas bubbles are not able to entrain the lower liquid into the upper layer, the pool will remain stratified and heat transfer between the liquids will be across a well-defined interface. Heat transfer across this interface will be enhanced by surface renewal processes, as would be heat transfer at the lower bubbling surface and along the vertical walls of the cavity or container. Under some circumstances, the rising bubbles may drive mass transport across the interface. If the rate of mass entrainment can be balanced by the rate of settling of the entrained droplets, the upper layer will become a heterogenous mixture layer; if the rate of entrainment exceeds the rate of settling of the droplets, the pool will eventually become completely mixed and the liquid-liquid interface will disappear. In either case, heat transfer from one layer to the other would be augmented even more than for the stratified case.

In the last decade, there has been a significant increase in research activity in the area of heat, mass, and momentum transfer in gas-sparged multi-fluid bubbling pools. Some have looked at the heat transfer processes across a liquid-liquid interface due to the bubble action across the interface. Other studies have examined the bubbling enhanced heat transfer at solid boundaries. Attention has been focused on both horizontal and vertical surfaces; in addition, some investigations have considered surfaces with bubbling along the boundary layer while others have considered surfaces with gas injected through the surface itself. There has been little activity in the study of the criterion for onset of entrainment between liquid layers due to gas bubbles rising across their interface, and similarly little activity in the investigation of the rate of mass entrainment by the rising bubbles and the subsequent rate of settling of the

entrained droplets.

The objectives of this report are to present the results of a series of seven separate experimental investigations which the author has conducted in order to develop a comprehensive set of models for incorporation in the CORCON computer code which models molten core-concrete interactions. The results of these seven separate investigations will be discussed and the mathematical models for each of the processes that are described will be presented. Finally, the remaining uncertainties and areas which could benefit from further investigation and model development will be presented.

2. ENHANCEMENT TO HEAT TRANSFER BETWEEN STRATIFIED IMMISCIBLE LIQUIDS BY GAS BUBBLING ACROSS THE INTERFACE

In early nuclear safety analyses, the core debris was assumed segregated into overlying immiscible layers of core oxides, core metals, and melted concrete slag in a vertical, cylindrical geometry. When the core oxide layer became diluted by concrete decomposition products to the extent that it became less dense than the metallic layer, these two layers would physically invert. The core oxide layer and the overlying slag layer would then combine into one layer. These layers would be continuously sparged by concrete decomposition gases from below, keeping the individual layers well mixed and isothermal. It is this gas flux which would drive the heat and mass transfer processes between the overlying layers. Separate analyses and experimental evidence have revealed that under a wide range of conditions, bubble-induced entrainment may dominate the interlayer transport processes (Greene et al., 1982, 1988a). However, under conditions in which the rising bubbles are unable to support entrainment, transport processes between liquid layers would be controlled by bubble agitation and turbulence at the liquid-liquid interface. In the stratified state, fission products and their decay heat would be concentrated in the oxide layer while chemically reactive metals, principally zirconium, and their heats of reaction would be concentrated in the metallic layer. Interfacial heat transfer between layers would determine not only the temperature of each layer but also the upward-to-downward heat transfer split. This in turn would control the downward concrete erosion vs. upward radiative or boiling heat flux.

In the absence of models for mixing and entrainment, early assessments of the consequences of molten core-concrete interactions were based solely upon analyses which assumed this stratified configuration. Modeling of this stratified heat transfer mode between immiscible liquid layers with gas-sparging, intended to represent molten core metals and oxides, will be discussed in this section.

2.1 Background

The earliest stratified interlayer heat transfer model that was developed was a version of the Konsetov model (1966) for heat transfer to a surface with bubble agitation, modified by Blottner (1979) to include two effects: (1) a lower asymptotic limit for natural convection in the absence of bubbling and, (2) an arbitrary increase in the coefficient of the void fraction term from 0.4 to 50.0 to shift the model into better agreement with some limited experimental data. Blottner's interfacial relationship, applicable for each fluid, is as follows,

$$h_i = k(Pr\ g/\nu^2)^{1/3}\ (0.00274\beta\Delta T + 50\alpha^2)^{1/3}. \qquad (1)$$

This relationship can be non-dimensionalized as follows,

$$Nu = (0.00274\ Gr_1 + 50\ Gr_2)^{1/3}\ Pr^{1/3} \qquad (2)$$

where Gr_1 is the Grashof number based upon the thermal buoyancy and Gr_2 is the Grashof number based upon void fraction-induced buoyancy. Gr_2 is not unlike that derived by Greene et al. (1989) except that the void fraction dependance is arbitrarily quadratic instead of linear. In nearly all cases, the term involving Gr_1 is much less than the term involving Gr_2 and can be neglected.

Another model for heat transfer across liquid-liquid interfaces agitated by bubbles was developed by Szekely (1963) using surface renewal principles which assume periodic destruction of temperature gradients at the liquid-liquid interfaces by the arrival of bubbles. His result was further modified by Blottner (1979), resulting in the following interfacial heat transfer coefficient for either fluid,

$$h_i = 1.69\left[\frac{\rho c k J_g}{r_b}\right]^{1/2} . \qquad (3)$$

This relationship can be non-dimensionalized as follows,

$$Nu = 1.69\ Re^{1/2}\ Pr^{1/2} \qquad (4)$$

where Re is the Reynolds number based on the superficial gas velocity and the volume equivalent bubble radius.

A third model for heat transfer across stratified liquid-liquid interfaces agitated by bubbles was developed by Lee et al. (1984). Using Szekely's original result, as modified by Blottner, further adjustments in the modeling assumptions were made to cause the bubble arrival period to be inversely proportional to the bubble frequency. This was done to force the heat transfer coefficient to be proportional to the superficial gas velocity, a behavior apparently supported by some available experimental data. Introducing the bubble rise velocity as a parameter, Lee arrived at the following relationship for the overall heat transfer coefficient across the two layers,

$$h_{1\text{-}2} = 12.5\left[\frac{k_1\alpha_1^{-1/2} + k_2\alpha_2^{-1/2}}{k_1\alpha_1^{-1/2} + k_2\alpha_2^{-1/2}}\right] \times \left[\frac{g\sigma(\rho_1-\rho_g)}{\rho_1^2}\right]^{-1/8} \left[\frac{J_g}{d_b^{1/2}}\right] \qquad (5)$$

where subscripts 1 and 2 in this equation refer to the lower and upper fluids, respectively.

If the heat transfer resistance for one layer is neglected, several terms may be omitted, resulting in an interfacial heat transfer relationship similar to Equation (3). The resulting relationship may then be made dimensionless as follows,

$$Nu = 8.8\left[Re\ Pr\ J_g^*\right]^{1/2} \qquad (6)$$

where $J_g^+ = J_g/[g\sigma(\rho_l-\rho_g)/\rho_l^2]^{1/4}$. In this form, it becomes apparent that the only change from Equation (4) is the inclusion of an additional term involving J_g^+ in an effort to force Nu to be a linear function of J_g.

These three models were subsequently compared to some early experimental data of Werle (1982) and Greene (1982) with surprisingly mixed results. Equations (1), (3) and (5) all were found to compare favorably with the data of Werle for the 10 cs. oil/Wood's metal system. None were able to predict the water/mercury data of Greene with any success with the exception of Equation (5), which was essentially forced to do so. An attempt was made to reproduce the data of Werle to try to resolve this apparent discrepancy. It was found that Werle's data could not be reproduced and, in fact, were lower than Greene's data for water/mercury by almost an order of magnitude. On this basis, any appearance of favorable comparison between the three models just discussed and the data base for interlayer heat transfer between overlying, stratified liquid layers was dispelled. As a result of this comparison, the experimental investigation to be described was initiated.

2.2 Experimental Apparatus and Procedure

An experimental apparatus with which to investigate heat transfer between immiscible liquid layers with gas agitation was constructed. The apparatus (see Figure 1) was a Pyrex glass cylinder, 10 cm in diameter and 1 meter deep. The apparatus was insulated to minimize radial heat losses by a two-inch thick cylindrical blanket of Fibrefrax insulation. A porous stainless steel frit was mounted in the base to provide a spatially uniform gas flux from below. Internal heating of the lower fluid layer (mercury) was accomplished by a cartridge heating assembly which penetrated the side of the cylindrical test vessel into the fluid chamber. Power was measured by a precision watt meter. The flow through the porous frit was measured by a bank of air rotameters. Bubble size was characterized photographically as a function of the pressure and flow rate. Over the range of pressure and flow rate covered by these experiments, the volume equivalent bubble radius was correlated to the superficial gas velocity as,

$$r_b\ (\text{cm}) = 0.233 + 0.109\ J_g\ (\text{cm/s}). \qquad (7)$$

This relationship was developed only to determine the bubble size in this study and not as a general formula. A vertical traversable thermocouple assembly was installed along the centerline axis of the pool for determination of the temperature distribution in each layer and the temperature difference across layers. Ten thermocouples were aligned at a nominal separation of one inch. Fluid pairs chosen for these non-entrainment interlayer heat transfer tests were mercury-water and mercury-silicone oil. The fluid pairs utilized in this study were chosen in an attempt to maintain a stratified configuration in the presence of gas bubbling, as well as to encompass the widest range possible for the appropriate dimensionless scaling parameters. In the experiments, the superficial gas velocity was varied over the range 0.33-7.75 cm/s; this spans the characteristic range expected during the stage of an MCCI in which the pool could remain stratified as shown in Table 1. By chosing simulant fluids with the appropriate physical and transport properties, the ranges of Reynolds, Prandtl, and Nusselt numbers of the data were able to span the ranges expected during MCCI conditions as shown in Table 1. Mercury was chosen as the lower fluid to

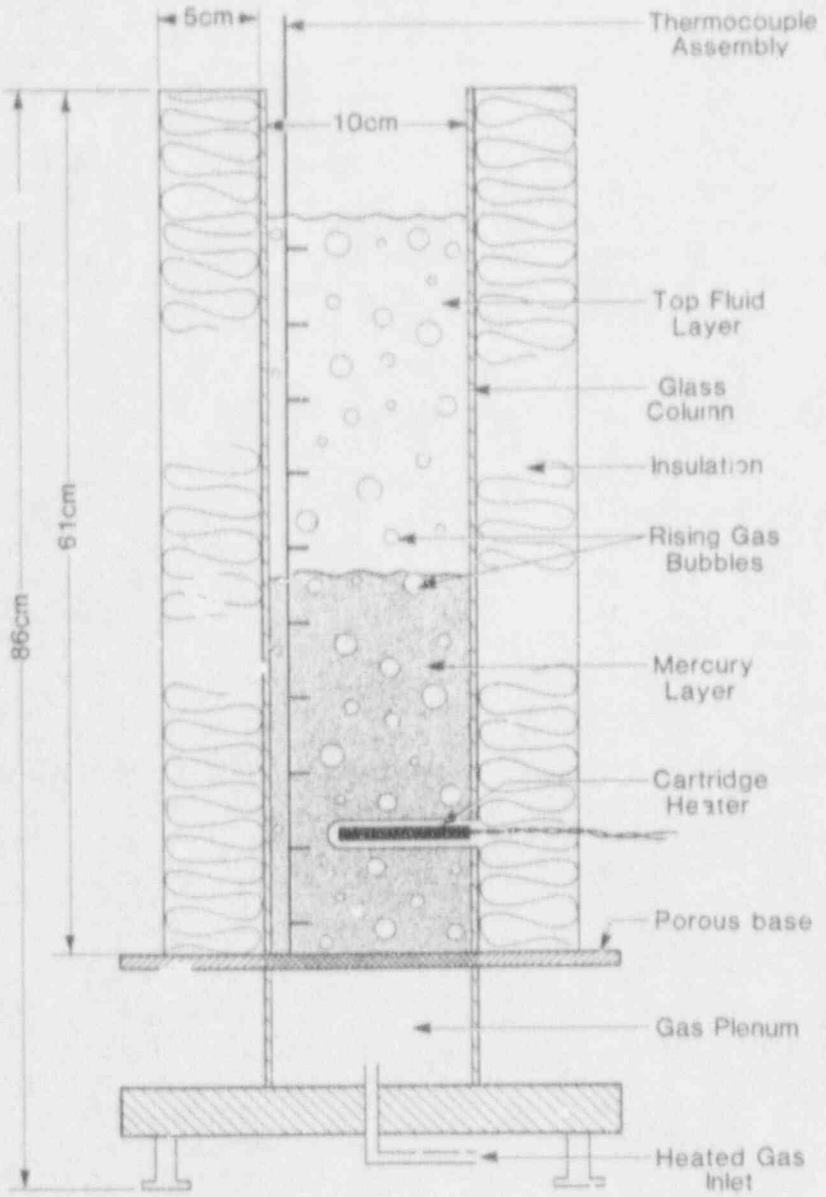

Figure 1. Schematic of experimental apparatus.

Table 1

Ranges of Scaling Parameters
for Interfacial Heat Transfer

Scaling Parameter	Experimental Range	Characteristic NPP Range*
Jg (cm/s)	0.33 - 7.75	3.3 - 5.5
Re	0.19 - 1099.	87. - 220.
Pr	4.0 - 540.	6.0 - 9.0
Nu	37. - 2500.	176. - 461. (calculated by Eqn. 8)

*Calculated from CORCON-MOD 2.04 Standard Problem.

suppress entrainment and to have a minimal resistance to heat transfer. With respect to stratification vs entrainment, a necessary condition for entrainment by bubbles rising across a liquid-liquid interface was derived by Greene (1988a). Application of that criterion to the water (or oil)/mercury system indicates that rising gas bubbles are unable to support liquid entrainment for the fluid pairs used in the present study. This behavior has been verified experimentally. With respect to resistance to heat transfer, one can assume for the time being that the interfacial heat transfer process is a transient surface renewal process on both sides of the interface. Examination of the physical properties, in particular the thermal diffusivities of each liquid layer, suggests that the resistance to heat transfer on the mercury side of the interface would be, for the worst case, at least a factor of ten less than on the water side. Neglecting this resistance would result in an uncertainty in the heat transfer coefficient of, at most, 10% for the water/mercury tests and negligible uncertainty for the two oils over mercury. In this fashion, the measured overall heat transfer coefficient would be approximately equal to the heat transfer coefficient on the oil or water side of the liquid-liquid interface. Fluid density and viscosity were measured in the laboratory. Specific heat and thermal conductivity values were taken from the literature or from vendor-supplied data. The apparatus was charged with the test fluids and power supplied by the immersed cartridge heating assembly. The temperature distribution in the liquids was monitored until steady-state conditions were achieved at a prescribed heat flux. The overall heat transfer coefficient was calculated as the net power input divided by the interfacial temperature difference and the cross-sectional area. The superficial gas velocity was calculated as the volumetric gas flux divided by the cross-sectional area. Each data point to be presented represents an average value of from five to as many as thirteen tests, with the individual data variations being in most cases less than 6%.

2.3 EXPERIMENTAL RESULTS

The experiments were performed in three series as listed in Table 1. The number in parentheses next to each heat transfer coefficient listed is the standard deviation of the value presented. The superficial gas velocity covered the range 0.30 - 8.35 cm/s and the measured heat transfer coefficient varied from 2986 to 50216 W/m^2K. The dimensional experimental data for the three fluid pairs are shown in Figure 2. The experimental data greatly exceed the data from Werle (1982) for the same fluids by as much as a factor of ten. With one exception, the data exceed the model predictions of Equations (1) and (3) by as much as a factor of 7-14 at the highest superficial gas velocities investigated. The only exception is the comparison of the water/mercury heat transfer data to Equation (1), which lies a factor of two below the data.

It was found that Equation (5) deviates from the oil/mercury data as badly as Equations (1) and (3). It agrees with the water/mercury data only in the lower range of j_g = 1 cm/s; the comparison rapidly deteriorates at higher gas velocity. Since the lower range of gas velocity is not the range of most interest, it was concluded that the overall comparison of Equation (5) to the present experimental data is at least as poor as Equations (1) and (3). The heat transfer coefficient was cast as a Nusselt number and the superficial gas velocity as a Reynolds number based upon the volume equivalent bubble radius and the properties of the water or oil layer. The Prandtl number was similarly chosen as that of the water or oil layer. The correlation that was developed to

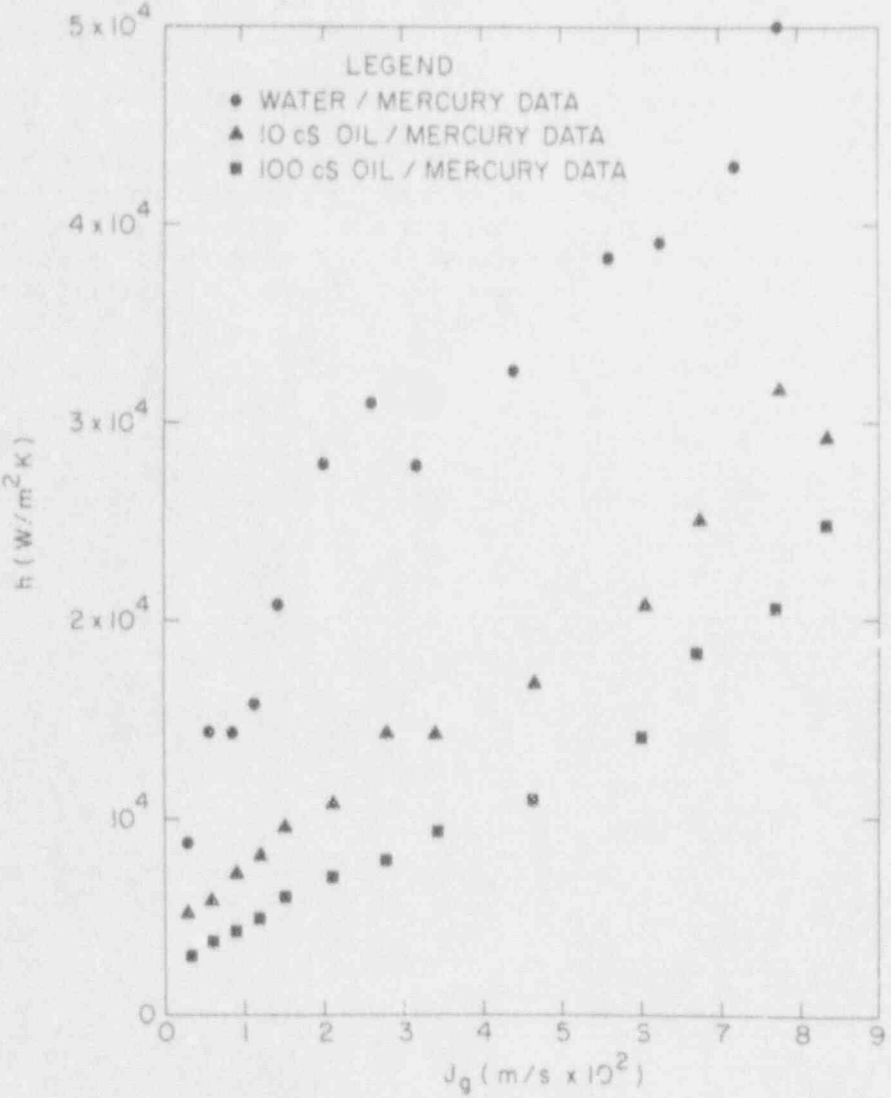

Figure 2. Interfacial heat transfer coefficients vs. superficial gas velocity.

predict interlayer heat transfer between overlying immiscible liquid layers agitated by rising bubbles is shown in Figure 3. The form of the correlation is,

$$Nu = 1.95\ Re^{0.72}\ Pr^{0.72} \tag{8}$$

and is the relationship recommended for interlayer heat transfer.

2.4. Summary

The data cover a range of Prandtl numbers from 4.0 to 540, as listed in Table 2. Therefore, the correlation given by Equation (8) would be expected to be reasonably accurate for situations in which one fluid layer has a Prandtl number greater than unity (core oxides), and the other fluid layer has a negligible resistance to heat transfer (core metals). This is precisely the situation in the case of a molten core-concrete interaction. In practice it is recommended that Equation (8) be applied to the fluids on each side of the interface and then calculate the overall heat transfer resistance across the interface from the bulk temperature of one fluid layer to the bulk temperature of the second fluid layer. Application of this equation to the modeling of stratified layer heat transfer in the CORCON code will insure reliable calculations of the energy balance between molten core metals and oxides during core-concrete interactions, thus insuring accurate analyses of melt temperature and concrete erosion rate. As will be discussed in Section 5, this model will be necessary for the analysis of interlayer heat transfer with entrainment as well.

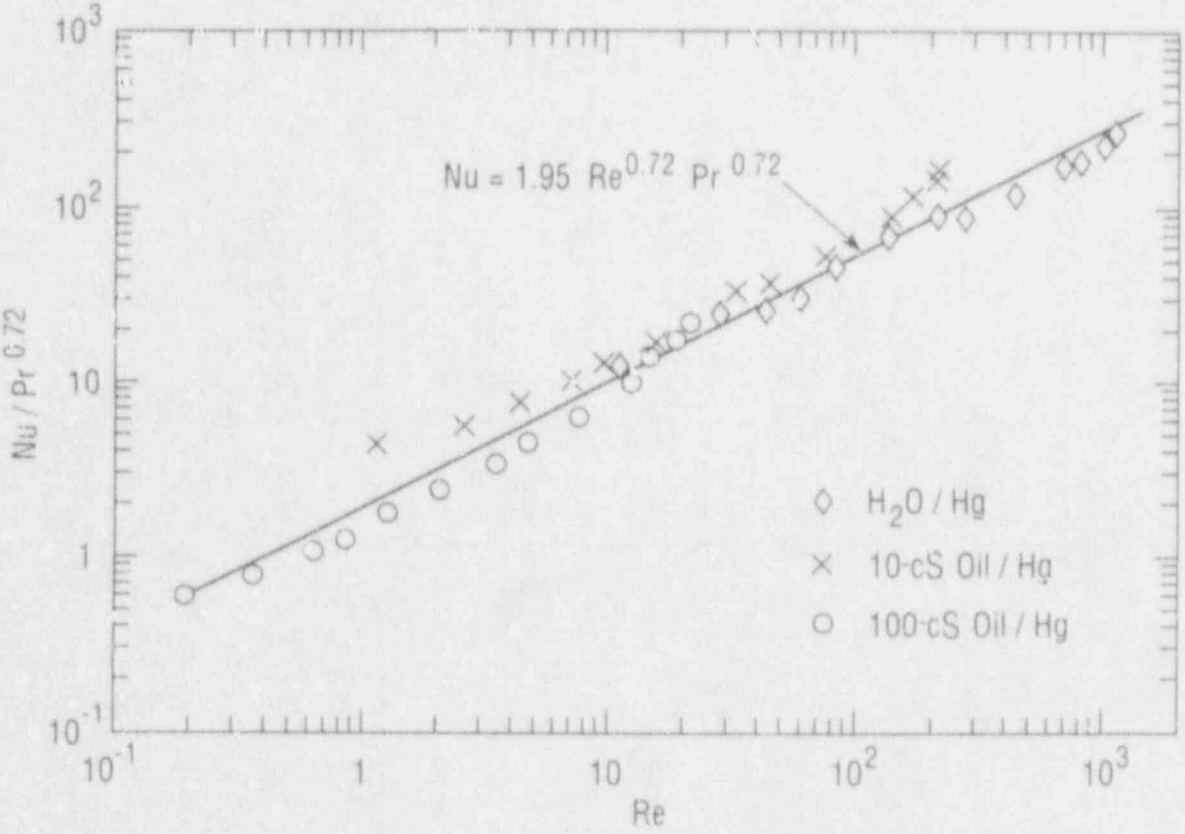

Figure 3. Dimensionless correlation of interfacial heat transfer data.

Table 2
Listing of Experimental Data
for Stratified Heat Transfer

Run (-)	h (W/m^2K)	J_g (cm/s)	T (°C)	Nu (-)	Re (-)	Pr (-)
			Water/Mercury			
1	8823 (1023)	0.30	37	37.9	11.4	4.60
2	14424(4317)	0.59	45	67.6	28.5	4.00
3	14309(1687)	0.88	40	74.6	43.2	4.32
4	15842(1837)	1.17	37	90.8	59.5	4.60
5	20831(2174)	1.47	39	128.7	83.6	4.41
6	27907(4222)	2.05	38	203.8	134.7	4.51
7	31039(8117)	2.65	41	254.6	208.8	4.23
8	27766(1767)	3.23	39	259.6	277.8	4.41
9	32458(3079)	4.38	38	367.5	434.9	4.71
10	38158(5766)	5.63	37	516.5	675.9	4.60
11	38946(4910)	6.28	36	571.5	808.1	4.71
12	42805(1364)	7.21	35	698.6	993.8	4.81
13	50216(4800)	7.75	33	873.3	1101.3	5.07
			10 cs Oil/Mercury			
14	5177 (118)	0.30	56	104.3	1.18	79.4
15	5796 (68)	0.60	56	129.8	2.63	79.4
16	7196 (128)	0.90	56	177.2	4.34	79.4
17	8146 (164)	1.22	63	224.9	7.17	72.6
18	9609 (127)	1.52	63	296.8	9.65	72.6
19	10784 (40)	2.13	63	376.2	15.9	72.6
20	14395 (250)	2.81	77	580.1	32.8	52.8
21	14347 (415)	3.41	77	642.4	44.2	52.8
22	16870 (290)	4.64	77	931.6	74.2	52.8
23	20674 (416)	6.06	82	1373.0	136.2	44.9
24	24980 (631)	6.74	82	1808.0	165.1	44.9
25	31604(1239)	7.74	82	2547.0	211.1	44.9
26	29105 (842)	8.35	77	2476.0	205.6	52.8
			100 cs Oil/Mercury			
27	2986 (32)	0.33	61	52.4	0.19	501.0
28	3750 (42)	0.61	56	73.1	0.35	540.0
29	4338 (47)	0.91	61	93.0	0.63	501.0
30	4924 (66)	1.21	56	115.1	0.85	540.0
31	6052 (25)	1.52	61	157.2	1.27	501.0
32	7073 (54)	2.13	61	215.9	2.09	501.0
33	7885 (133)	2.80	78	276.5	3.51	445.0
34	9382 (169)	3.43	72	371.6	4.76	457.0
35	10930 (193)	4.63	72	525.2	7.79	457.0
36	14082 (175)	6.03	78	813.8	12.5	445.0
37	18328 (845)	6.70	78	1142.0	14.9	445.0
38	20566 (577)	7.71	78	1429.0	19.1	445.0
39	24737 (480)	8.34	72	1831.0	21.6	457.0

*Number in parentheses indicates the standard deviation of the measured heat transfer coefficient.

3. ONSET OF ENTRAINMENT BETWEEN IMMISCIBLE LIQUID LAYERS DUE TO RISING GAS BUBBLES

In the previous section, the enhancement to heat transfer across a stratified liquid-liquid interface due to rising gas bubbles was treated. It was explained that this situation is found in such diverse applications as metallurgical processing and nuclear reactor safety. In all these occurrences, one is concerned with the possibility of entraining the denser liquid from the bottom layer into the top layer of lighter liquid by the rising gas bubbles. Such entrainment can significantly increase both heat and mass transfer between the two immiscible liquid layers, a phenomenon which could be either detrimental or desirable depending upon the specific application. In the absence of such a criterion for the onset of entrainment, the molten layers are required to remain stratified in spite of the action of the rising gas bubbles. In this section we describe the investigations of entrainment onset and the criteria developed which allow relaxation of the stratification constraint.

3.1. Background

Previous investigations reported in the literature indicate that entrainment between the liquid layers is clearly observed in some cases while apparently not present in other cases. Szekely (1963) deals with the case of a bubble-stirred interface between the two immiscible liquids without entrainment. Porter, Richardson, and Subramanian (1966) report observations of aqueous solutions overlying liquid mercury with no apparent entrainment of the mercury into the aqueous phase. Poggi, Minto, and Davenport (1969) report experimental indications of entrainment occurring between pools of glycerin-water over mercury, fused salt over lead, and slag over molten copper. More recently, Werle (1982) and Greene (1982) investigated the fluid mechanics and heat transfer behavior of silicone oil and water over liquid metal pools of Wood's metal and mercury, and silicone oil over water pools, both cases with gas bubbling from below. It was found in both investigations that the rates of heat transfer between the two overlying immiscible liquid layers driven by gas bubbles rising through the interface were strongly dependent upon whether the system exhibited entrainment or stratification. The gas bubbling was able to support entrainment for the oil over water system, however the water/oil over Wood's metal/mercury systems remained stratified with no mass transfer between phases. As reported by the authors, the fluid systems which underwent entrainment exhibited rates of interlayer heat transfer that greatly exceeded those measured for the fluid systems that remained stratified. Epstein et al. (1981) tested stratified pools of organic liquid and water with nitrogen as the bubbling gas. These authors reported that a well-mixed emulsion of the two liquid phases was formed upon exceeding some critical value of gas flux. Gonzalez and Corradini (1987) and Suter and Yadigaroglu (1988) also reported clear indications of mixing between stratified layers of liquids under certain operating conditions.

The accumulated evidence indicates that entrainment between the immiscible liquid layers could occur or not occur depending on the specific liquid system and operating conditions. The objective of this section is to develop a criterion for predicting the onset of interfacial entrainment between the liquid layers. A conceptual limiting criterion is developed and then compared with experimental observations.

3.2 Physical Phenomena

Consider a pool consisting of stratified layers of two immiscible liquids. If gas is injected at the bottom of the pool and flows upward through the liquid layers, entrainment and mixing of the heavier liquid (density ρ_2) into the lighter liquid (density ρ_1) can occur, as reported above. Our objective is to develop a criterion that can predict the minimum gas flow needed to cause such entrainment. Clearly, the phenomenon is affected by the two-phase flow regime of gas in the lower liquid pool. As gas flux increases, the two-phase flow regime changes from bubbly flow, to churn-turbulent flow, annular flow, and eventually to dispersed flow. Since our concern is with the minimum gas flow that would induce entrainment, attention is centered on the regime of discrete bubbly flow.

In the first part of this study, a series of photographic records were obtained to aid in qualitative understanding of the physical phenomenon. Stratified layers of silicone oil over colored aqueous solutions of copper sulfate in a transparent 10 cm diameter column were used for these experiments. Single bubbles of air were injected at the bottom of the column and photographed as they penetrated the interface between the two liquids. Examples of the photographic records of the phenomenon are shown in Figure 4. It is seen in Figures 4a-b that as the gas bubble penetrates the liquid interface, it begins to drag a column of the denser fluid in its wake into the lighter fluid. As the bubble continues to rise [Figures 4c-d], this "wake" column elongates and then necks down and finally snaps to free a glob of the denser fluid which is then successfully entrained into the upper fluid by the rising gas bubble. In these experiments, depending on the size of the gas bubble, globules of the lower liquid would be so entrained or not entrained into the upper pool. In the latter case, a raised column (such as in Figure 4a) could still occur but then the column would be pulled back into the lower pool by surface tension without necking down and breaking off as an entrained globule. It was also observed that small gas bubbles would sometimes be trapped at the two-fluid interface and be prevented from penetrating into the upper layer of lighter liquid.

The question to be addressed is, "Under what conditions does a rising bubble penetrate the interface between the two liquid pools and entrain some volume of the denser liquid into the lighter liquid." Our interpretation of the photographic records indicated that the entrainment process was caused by the rising gas bubble having sufficient buoyancy to penetrate the liquid-liquid interface and to drag in its wake a globule of the denser fluid into the upper pool, with sufficient force to overcome interfacial tension between the two liquids as well as the negative buoyancy of the denser fluid. In the following discussion, a criterion is developed based on this hypothesized mechanism to estimate the minimum size gas bubble able to cause entrainment for a given pair of immiscible liquids.

3.3 Formulation of Criterion

Consider a gas bubble of volume V_g as it rises through the lower liquid layer and approaches the interface. To successfully entrain fluid of density ρ_2 into the fluid of density ρ_1, the gas bubble must necessarily meet both of the following requirements:

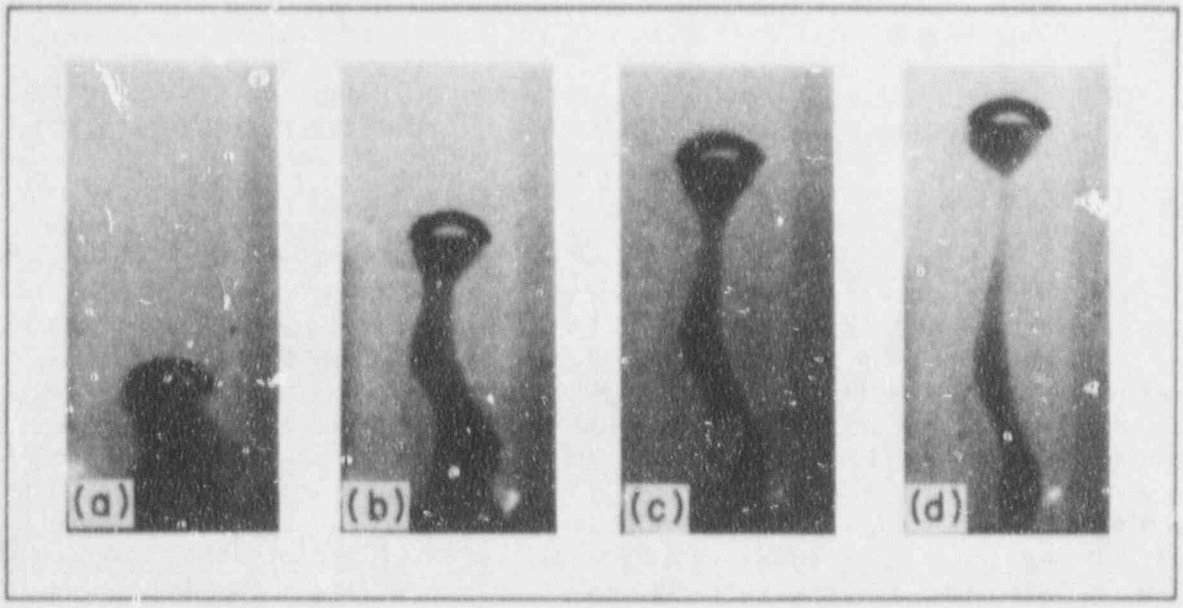

Figure 4. Photograph of entrainment phenomenon.

(a) Successfully penetrate the liquid-liquid interface and rise into the upper liquid layer,

(b) Successfully drag a globule of the ρ_2 fluid in its wake, into the upper liquid layer, a sufficient distance so as to detach the globule from the liquid-liquid interface.

We will formulate the necessary criterion for each of these two requirements.

The following simplifying assumptions are taken as reasonable hypotheses:

(a) Consider only individual bubbles, i.e., no interaction between successive or neighboring bubbles.

(b) Cylindrical symmetry about the vertical axis of the rising bubble.

(c) One-dimensional motion in the vertical direction only.

(d) Limit to low velocities so that inertial and viscous shear forces are negligible compared to buoyancy and surface tension forces.

3.3.1 Penetration

First consider a bubble of volume V_g as it passes the liquid-liquid interface. Visual observations in this investigation and elsewhere [Suter, 1988] indicate the tendency for a small "film" of the ρ_2 liquid to surround the bubble as it attempts to penetrate the interface. Neglecting dynamic effects, the forces acting on the bubble-film assembly are upward buoyancy and downward surface tension. The effective buoyancy force decreases as the bubble passes from the heavier ρ_2 fluid into the lighter ρ_1 fluid. At the same time, the downward component of the surface tension force increases as the angle changes from 0 to $\pi/2$. Therefore, the critical moment is when all of V_g is in the upper layer and the angle θ is equal to $\pi/2$. For successful penetration by the gas bubble, this minimum net upward force must be greater than zero. Neglecting the mass of the thin film around the bubble, and for the limiting case of a spherical bubble, the penetration criterion can be written as,

$$V_g\,(\rho_1-\rho_g)g - 3.90\,\sigma_{12}\,(V_g)^{1/3} > 0 \qquad (9)$$

That is, for the gas bubble to penetrate the interface, its volume V_g must exceed a critical volume V_g^* given by,

$$V_g^* = \left[\frac{3.9\,\sigma_{12}}{g\,(\rho_1-\rho_g)}\right]^{3/2} \qquad (10)$$

where σ_{12} is the interfacial tension between the two liquids.

3.3.2 Entrainment

Next consider a gas bubble of volume V_g after it penetrates the liquid interface, as shown in Figure 5. Under buoyancy driven motion, the gas volume rises through the upper lighter liquid and attempts to pull in its wake a column of the heavier lower liquid. Let V_2 indicate the volume of the denser fluid pulled above the liquid interface and R_2 denote the column radius, with interfacial contact angle β as indicated in Figure 5a. A vertical force balance on the combined $V_g + V_2$ configuration indicates an upward buoyancy force of,

$$\text{Buoyancy (up)} = [V_g (\rho_1 - \rho_g) - V_2 (\rho_2 - \rho_1)] \cdot g$$

and a downward force due to surface tension of,

$$\text{Surface tension (down)} = 2\pi R_2 \cdot \sigma_{12} \cdot \sin \beta$$

For the entrainment process to continue successfully, the upward force must exceed the downward force, hence,

$$V_g (\rho_1 - \rho_g) - V_2 (\rho_2 - \rho_1) > \frac{2\pi R_2 \sigma_{12}}{g} \cdot \sin \beta \qquad (11)$$

The surface tension force is maximum when $(\sin \beta)$ approaches unity, corresponding to the situation shown in Figure 5b. In this state, assuming a hemispherical volume, the wake volume V_2 corresponds to,

$$V_2 \geq \frac{2}{3} \pi R_2^3 \qquad \text{at } \beta = \pi/2 \qquad (12)$$

The photographic records indicate that radius of the wake column (R_2) is approximately equal to the projection radius of the leading gas bubble. Hence one can write the approximate relationship between R_2 and V_g as follows,

$$R_2 = \left(\frac{3}{4\pi} V_g\right)^{1/3} \cdot S \qquad (13)$$

where S is a shape function for the gas bubble, measuring its projection radius versus the radius of a sphere,

S = 1 for spherical bubble

S > 1 for spherical-cap bubble.

For the minimum condition, take S = 1, resulting in the following necessary criterion for entrainment of ρ_2 fluid into the ρ_1 layer:

$$V_g > \left[\frac{7.8 \sigma_{12}}{g(3\rho_1 - \rho_2 - 2\rho_g)}\right]^{3/2} \qquad (14)$$

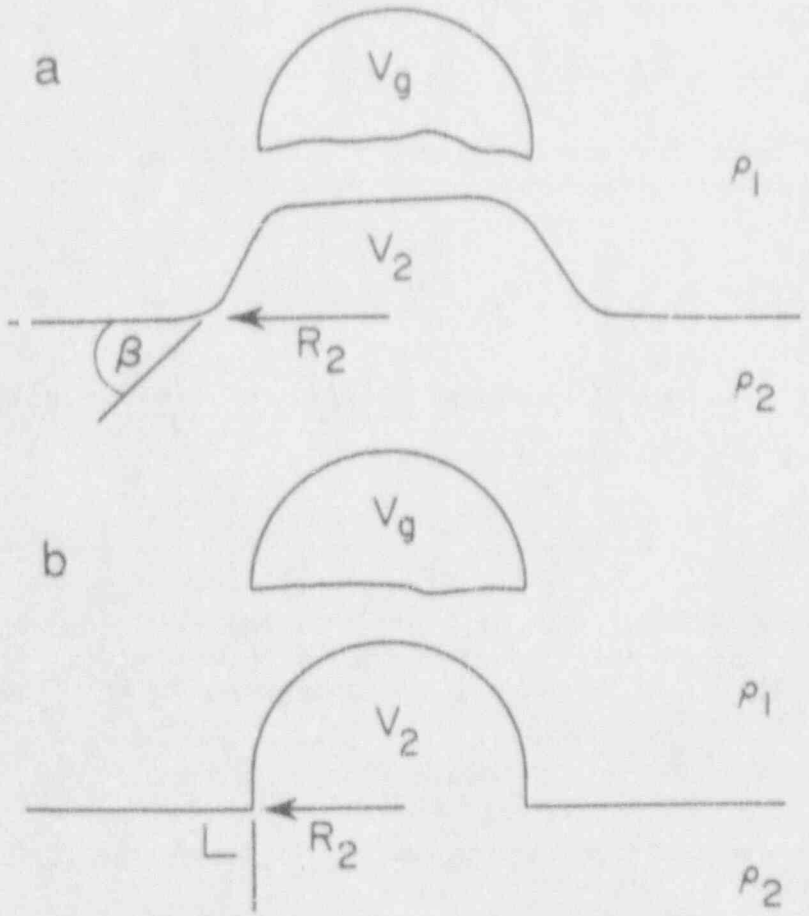

Figure 5. Geometrical system for analysis.

We can define a dimensionless bubble volume by normalizing with respect to the minimum penetration gas volume (V_g^*), as given by Equation (10),

$$w \equiv \frac{V_g}{V_g^*} = V_g \cdot \left[\frac{g(\rho_1 - \rho_g)}{3.9\,\sigma_{12}}\right]^{3/2} \tag{15}$$

The criterion for interface penetration by the rising gas bubble becomes,

$$w > 1 \tag{16}$$

and the criterion for possible entrainment of heavier liquid into the lighter liquid is,

$$w > \left[\frac{2(\rho_1 - \rho_g)}{3\rho_1 - \rho_2 - 2\rho_g}\right]^{3/2} \tag{17}$$

For most cases, the gas density is negligible compared to the liquid densities, and Equation (17) simplifies to,

$$w > \left[\frac{2}{3 - \rho^*}\right]^{3/2} \tag{18}$$

where $\rho^* = \rho_2/\rho_1$.

The results are plotted in Figure 6, showing the regimes where,

(a) Gas bubbles do not penetrate the liquid-liquid interface,

(b) Bubbles penetrate the interface, but cannot entrain the heavier liquid into the upper layer of lighter liquid,

(c) Entrainment is possible,

(d) Entrainment is not possible by single bubbles by this mechanism.

Equation (18) indicates that entrainment by this single bubble process is not possible when the ratio of liquid densities exceeds the limit,

$$\rho^* > 3 \tag{19}$$

This is consistent with the observations of Porter et al. (1966), Werle (1982), and Greene et al. (1982) that no entrainment occurred for water over mercury ($\rho^* \simeq 13$) or for water over Wood's metal ($\rho^* \simeq 9.5$). It should be emphasized that this formulation treats only entrainment by single bubbles, giving a necessary criterion for entrainment. Thus, this deals primarily with

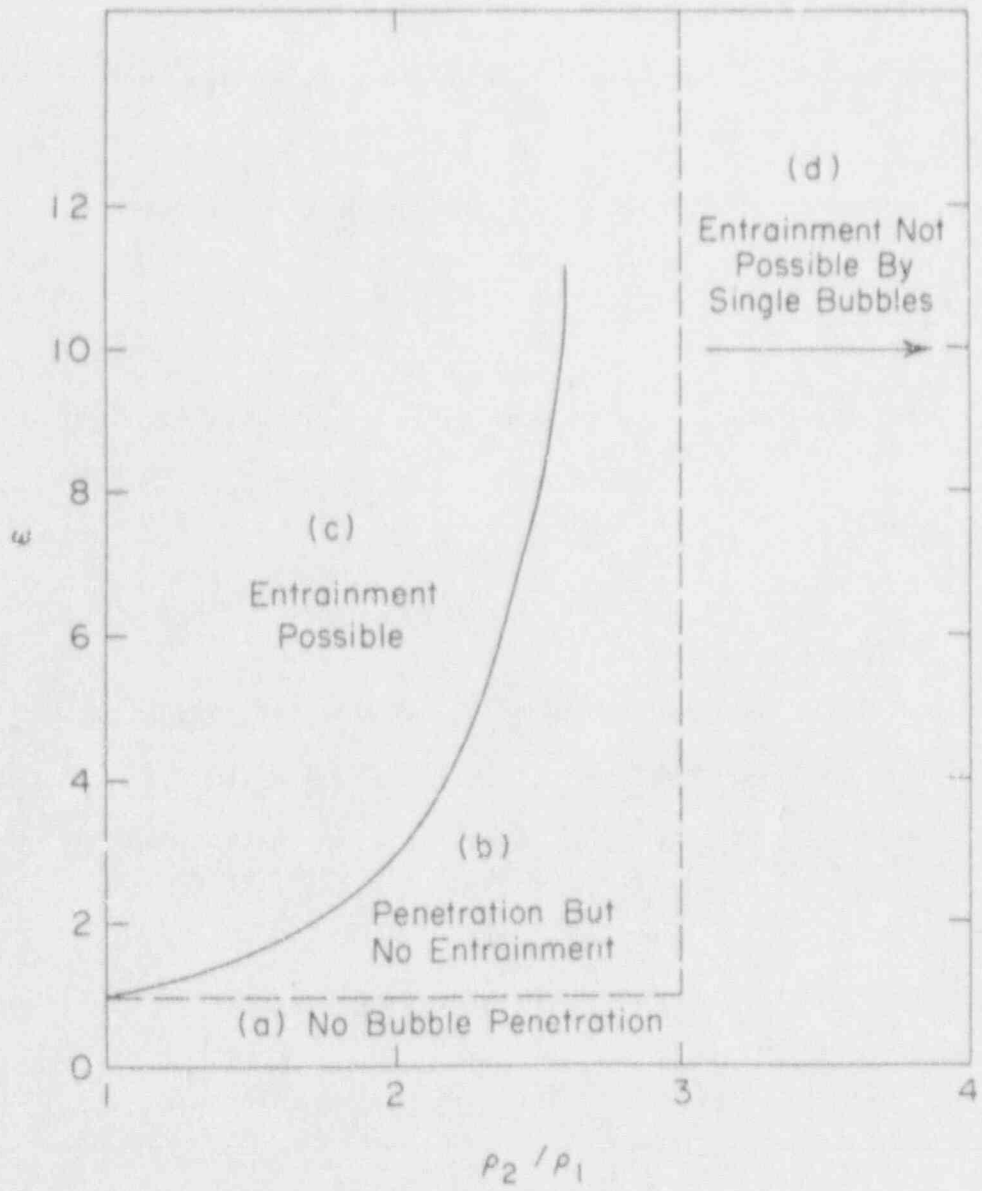

Figure 6. Map of possible penetration and entrainment regimes.

applications at the lower range of gas flow rates, where bubbly flow exists.

3.4 Experiment

In order to test the criterion for bubble penetration and entrainment derived above, experiments were carried out with eight different pairs of immiscible liquids. For each pair of fluids, gas bubbles of varying sizes were injected to determine the regimes of entrainment and non-entrainment. The fluid pairs and range of bubble volumes were chosen to encompass the widest range possible for the appropriate scaling parameters for entrainment onset. The parameters that were found to be most important are V_g^*, ρ^*, σ_{12}/ρ_1, and ω. The ranges encompassed by these parameters in the experiments are listed in Table 3, along with characteristic values expected during MCCI conditions. The resulting ranges of the scaiing parameters was as wide as practically possible, and the results may be applied to MCCI conditions reliably.

As illustrated in Figure 7, the experimental apparatus consisted of a vertical glass column having two sections and provided with devices for injecting and measuring gas bubble volumes and for collection of entrained liquid globules. The denser and lighter liquids were contained in the lower (6.0 cm i.d. X 23.5 cm length) and upper (16 cm i.d. X 14.5 cm length) sections of the glass column, respectively. In operation, the liquid-liquid interface would be adjusted to lie just below the junction plane of the two sections. A mechanical shutter was mounted just above the junction plane to collect any volume of the denser liquid that is entrained into the lighter liquid.

Air bubbles of varying sizes could be injected at the bottom of the glass column by means of a micrometer syringe and holding-cup mechanism. After initial purging, a metered volume of gas would be injected by the syringe into the inverted holding cup. When ready, the cup would be quickly turned upward, allowing the injected gas to rise through the liquid layers as a single bubble. An inverted funnel, with attached burette mounted at the top of the test section, permitted trapping of the rising gas bubble and measuring its volume with a precision of 0.002 cm^3.

The liquid properties were measured as a part of the test program. Densities were obtained by gravimetric measurements to a precision of 0.01 gm/cm^3 and surface tensions were measured with a Fisher Surface Tensiomat (Model 21) to a precision of 0.05 dyne/cm. The tabulated values are averages obtained from 10 measurements for each fluid. It should be noted that surface tension is sensitive to small amounts of impurities or additives (e.g., copper sulfate used to color the water) and direct measurements had to be obtained with the actual test fluids.

In the experiments, a pair of liquids would be charged into the apparatus and adjusted to set the liquid-liquid interface at the desired height. A specified volume of air would be injected into the holding cup, then permitted to rise as a single bubble through the two liquid layers. Visual observation and video recordings would be made during the time of bubble transit. The morphology observed was as qualitatively described above and illustrated in Figure 4. Entrainment of the denser fluid into the upper liquid pool was discernible by eye and from the video films whenever it occurred. All experiments, with the exception of those using R11 refrigerant, were performed at room temperature.

Table 3

Ranges of Scaling Parameters
for Entrainment Onset

Scaling Parameter	Experimental Range	Characteristic NPP Value**
Vg^* (cm^3)	0.002 - 0.90	0.50
ρ^*	1.0 - 3.0	1.21
σ_{12}/ρ_1	3.0 - 80.0	83.
w	0.7 - 60.0	~4.*
w_{onset}	variable	1.2

*Assumes V_{bbl} = 2 cm^3

**Calculated from CORCON-MOD 2.04 Standard Problem.

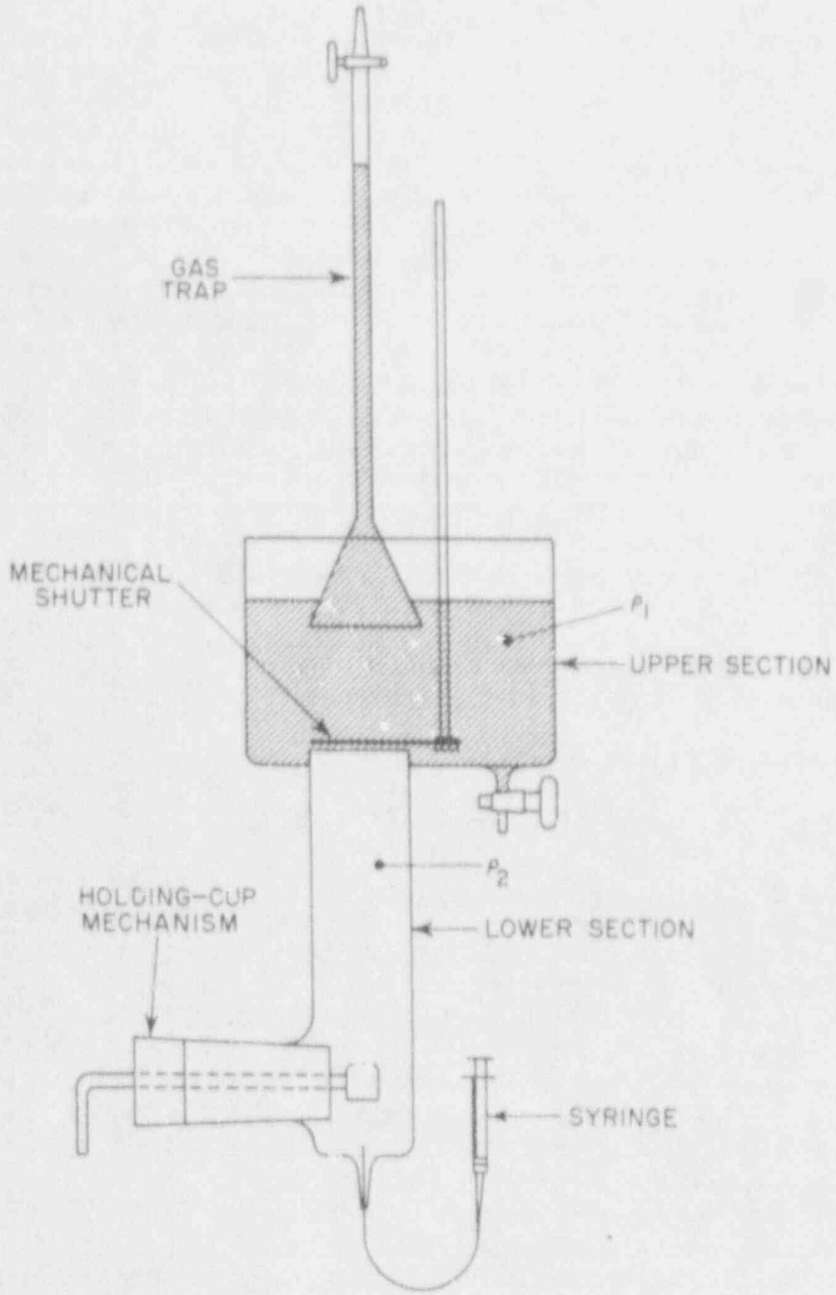

Figure 7. Schematic diagram of experimental entrainment apparatus.

Due to the low boiling point, the R11 fluid had to be slightly refrigerated to prevent its vaporization during the tests.

3.5 Results

Sample results are shown in Figures 8a-b for the eight pairs of test fluids. The numerical results are listed in Table 4. Each point represents a test condition where multiple observations were made. Due to second-order perturbations, there was some stochastic variation in whether or not a specific bubble of a given size would induce entrainment. If bubbles of a given size were observed to cause entrainment in 75% (or more) of the repetitions, that condition was considered to be an "entrairment" point. Usually, the bubble volume that satisfied this 75% threshold was also close to the minimum bubble size with observable entrainment. In Figures 8a-b, the cases with and without entrainment are indicated by dark and open symbols, respectively. The threshold criterion for entrainment, given by Equation (14), is indicated by the horizontal line for each pair of test fluids. There is a 500-fold range in the predicted bubble volume for onset of entrainment for these widely different fluids. The results of Figures 8a-b show generally good agreement between experiment and theory, with the onset of significant entrainment occurring close to the proposed thresholds. The acetone/glycerine fluid pair exhibited an interesting but unexplained quirk, that is an onset-of-entrainment transition followed by a subsequent return to conditions not supporting entrainment. This anomalous behavior has not been investigated further at present, and for the purposes of this paper, the first onset-of-entrainment volume was chosen for analysis.

According to the theory proposed above, the onset criterion for entrainment is affected primarily by just two physical property groups:

ratio of liquid densities, ρ^*

ratio of interfacial tension/liquid density, σ_{12}/ρ_1

The eight pairs of liquids used in these experiments covered a 20-fold range in σ_{12}/ρ_1 and almost a 3-fold range in ρ^*. These data were examined to test the effects of physical properties on the entrainment onset criterion. Figure 9a plots the conditions corresponding to onset of entrainment determined experimentally for the eight pairs of test fluids as a function of the density ratio, ρ^*. The gas volume for onset, V_g, is normalized with respect to the penetration volume, V_g^*, to give the dimensionless onset volume, ω, as defined by Equation (15). The points in Figure 9a represent the smallest ω that caused significant entrainment for each pair of fluids. It is seen that the 3-fold range in ρ^* caused two orders-of-magnitude change in the onset ω. The curve in the figure represents the theoretical criterion for onset of entrainment, as given by Equation (18). Good agreement between experiment and theory was obtained; the theory not only predicted the parametric effect of ρ^* but also gave good estimates of the magnitude of ω.

Figure 9b examines the parametric effect of the property group, σ_{12}/ρ_1. According to the proposed theory, the group

$$V_g * [g(3-\rho^*)/7.8]^{3/2}$$

Table 4

Comparison of Measured and Calculated
Minimum Bubble Volume for Entrainment Onset

d Pair	Minimum Bubble Volume for Entrainment Onset*		
	Measured**	Measured Range	Calculated
licone oil/ olored with $CuSO_4$	0.015	0.010 - 0.020	0.011
silicone oil/ (colored with $CuSO_4$)	0.030	0.020 - 0.035	0.048
11 (refrigerant)	0.050	0.030 - 0.050	0.046
Water/Bromoform	0.90	0.55 - 1.40	1.20
Hexane/Water	0.17	0.15 - 0.21	0.22
Glycerine/Bromoform	0.04	0.03 - 0.09	0.043
Acetone/Glycerine	0.002	0.001 - 0.003	0.002
100 cs silicone oil/ Glycerine	0.07	0.05 - 0.09	0.058

* Bubble volume in cm^3.

**Entrainment occurred in 75% of the cases at this volume.

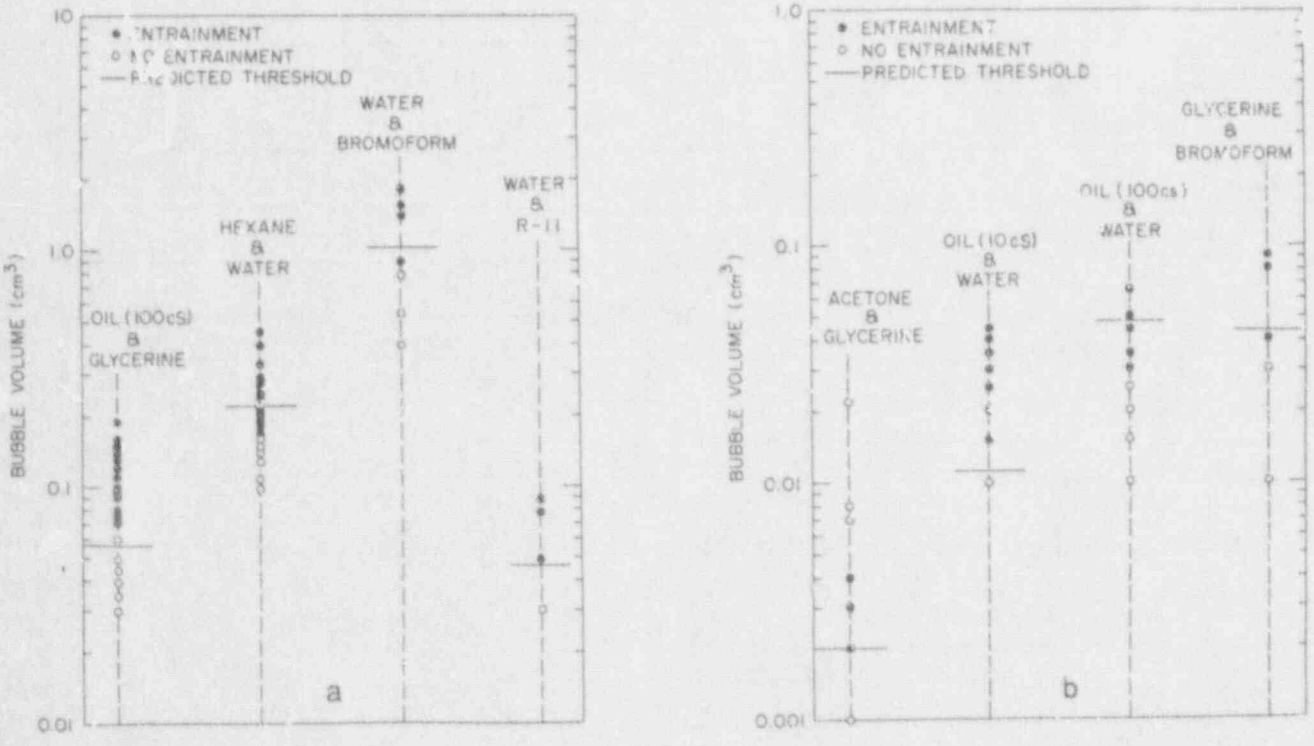

Figure 8. Sample entrainment onset results.

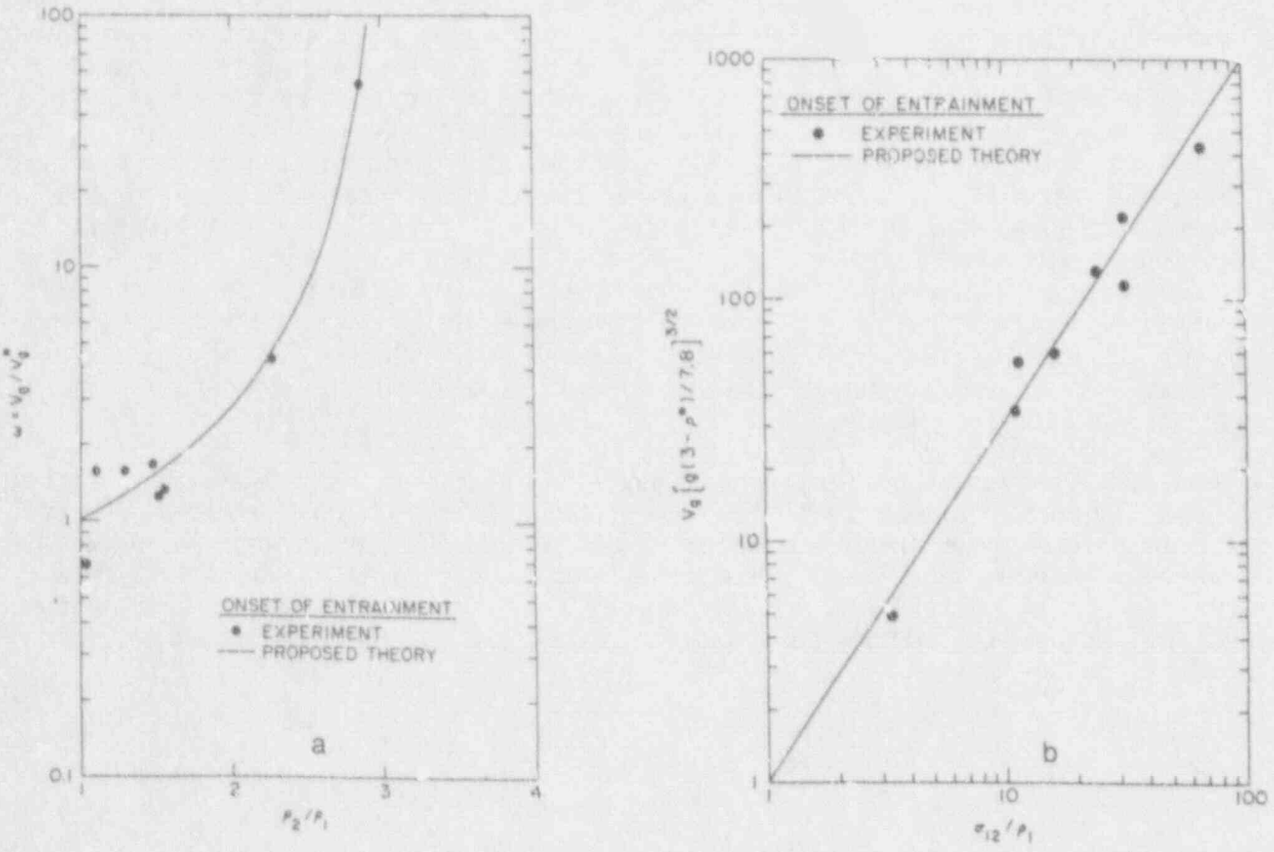

Figure 9. Effect of a) liquid densities, and b) interfacial tension-liquid density ratio on entrainment onset.

should be equal to $(\sigma_{12}/\rho_1)^{3/2}$, where V_g is the threshold volume of the gas bubble to cause entrainment. The experimental measurements for the test fluids are plotted in Figure 9b and confirm this prediction over a 20-fold range of σ_{12}/ρ_1. The theoretical prediction, Equation (14), is also plotted and shows very good agreement with the experimental results over the 100-fold range of the threshold volume. The axes in this figure are in CGS units. The proposed theory, based on first-principles, obtained this good agreement with measurements without the use of any empirical parameters.

3.6 Summary

The problem of entrainment between stratified layers of immiscible liquids caused by rising gas bubbles was examined to develop a criterion for onset of entrainment. Visualization experiments led to a hypothesis that entrainment by single bubbles is caused by the levitation of a small column of the denser fluid in the wake of the bubble as the bubble passes across the liquid-liquid interface. A first-principle analysis led to a theoretical criterion for the threshold volume of gas bubble necessary to cause entrainment, indicating a strong dependence on the liquid-liquid density ratio (ρ^*) and the interfacial tension-liquid density ratio (σ_{12}/ρ_1). Experiments were conducted to measure actual onset of entrainment for eight different pairs of fluids. The experiments covered a 3-fold range in ρ^*, a 20-fold range in σ_{12}/ρ_1, and a 2000-fold range in the gas bubble volume. The proposed theoretical criterion, with no empirical parameters, was able to predict the experimental measurements with good agreement over the entire test range.

Application of the entrainment onset criterion to the modeling in the CORCON code will insure that the code calculations will reliably be able to discriminate between conditions which support mixing between core oxide and metal layers during core-concrete interactions, and those conditions which will remain stratified. This will be important in so far as entrainment will determine the heat balance in the molten core debris as well as the distribution of fission products in the melt.

4. BUBBLE INDUCED ENTRAINMENT BETWEEN INITIALLY STRATIFIED LIQUID LAYERS

As illustrated in Figure 4, it is known that gas bubbles of sufficient size rising through stratified layers can entrain some volume of the denser liquid from the lower layer into the upper layer of lighter liquid. This entrainment pheromenon has significant effects on both heat and mass transfer between the two liquid layers (Szekeley, 1963; Greene, et al., 1988b). This situation is encountered and is of concern in a number of applications. Some examples are chemical processing, assessments of severe nuclear reactor accidents, and in metallurgical processing. In the previous section, an entrainment onset criterion was developed which enabled relaxation of the limiting constraint requiring the two liquid layers to be stratified under the action of gas bubbles rising across their interface. In this section, a model is developed and presented which will enable the amount of the lower liquid which is entrained by the rising gas bubbles to be calculated. A model for entrainment between immiscible layers of molten core debris is needed for CORCON in order to be able to calculate the mixture properties of the layers, the rate of heat transfer between the layers, and the distribution of fission products in the core debris.

4.1 Background

Greene et al. (1988a) showed that discrete gas bubbles must exceed a certain minimum volume to cause entrainment of the denser liquid into the upper pool; a theoretical criterion was developed to predict this onset condition. The objective of the present section is to determine the volume of the denser fluid that will be entrained by a discrete bubble, once this onset criterion is exceeded. The study is limited to that regime of gas flux which results in bubbly flow. Higher gas fluxes would lead to alternate flow regimes (e.g., churn turbulent flow) which may have very different mechanisms for fluid mixing between the two immiscible liquids.

Previous investigations reported in the literature indicate that entrainment between overlying immiscible liquid layers by bubbling gas is clearly observed for some fluid systems while apparently not observed for other fluids. Szekely (1963) and Greene et al. (1988a) report on studies of liquid systems which did not support entrainment, but rather remained stratified. Szekely presents a theoretical analysis of transient heat transfer at the interface by surface renewal principles, while Greene et al. present experimental results for interfacial heat transfer and a dimensionless correlation of their data.

Mercier et al. (1974) report on visual observations in which a minimum bubble volume threshold was observed (0.020 cm^3) for onset of entrainment between water and a variety of mineral oils. A similar observation is reported by Mori et al. (1977) who observed a minimum bubble volume for penetration of an aqueous glycerol-R113 interface; for bubbles larger than this penetration threshold value (0.020-0.045 cm^3), entrainment of the lower fluid always occurred and increased with increasing bubble volume. Epstein et al. (1981) report on the onset of mixing and stratification in bubbling systems; they suggest that it is only necessary to know the mixture density to predict the pool configuration. In a similar study, however, Suter and Yadigaroglu (1988) develop an entrainment criterion on the basis of stability considerations which include density and interfacial and surface tensions. Greene et al. (1988a) present a theoretical

and experimental study of entrainment in which they report both a bubble penetration threshold and an entrainment onset threshold. The model is a function of the densities of the gas and two liquids, the interfacial tension between the liquids and the bubble volume; entrainment onset data for eight separate fluid pairs were found to be in good agreement with the entrainment onset criterion. The bubble penetration criterion was in agreement with the experimental observations of Mori et al. (1977).

That the rate of entrainment between immiscible liquid layers increased with increasing bubble volume for a particular pair of fluids is reported by Poggi et al. (1969), Cheung et al. (1986), Veeraburus and Philbrook (1959), and Mori et al. (1977). Mori et al. present data for glycerol-R113 which demonstrate an increase in entrained volume with an increase in bubble volume and a decrease in the viscosity of the light liquid. Entrainment mechanisms of film and bubble transport were observed by Poggi (1969), Veeraburus (1959), and Mori et al. (1977). Cheung et al. (1986) observed that entrainment could be affected by non-uniform gas bubbling. Although no model for the rate of entrainment is presented, Gonzalez and Corradini (1987) report experimental results for entrainment onset and emulsification for several fluid pairs as a function of the superficial gas velocity.

Heat transfer between overlying liquids both with and without entrainment is reported by Greene et al. (1982, 1988b) and Werle (1982). Both authors observed that pools could be stratified, mixed, or homogenized depending upon the fluid properties and volumetric gas flux. The component of heat flux due to entrainment was observed to substantially increase the interlayer heat transfer over the stratified situation. Greene and Schwarz (1982) present a model for calculating the entrainment heat transfer as a combination of the stratified component and that due to direct mass transfer. The analysis requires a model for the rate of mass entrainment which, until now, was not available. It should be noted that Suo-Anttila (1988) recently proposed a framework for calculating entrainment and entrainment heat transfer between overlying liquid with gas bubbling. However, models for the various processes involved are not offered.

4.2 Experiment

In order to investigate the phenomenon of bubble-induced entrainment between stratified liquids, the experimental investigation to be described was initiated. In this section we will discuss in detail the experimental apparatus and the experimental procedure. It became necessary during this investigation to measure the physical and transport properties of the fluids that were used, as well as the bubble rise velocities for each of the fluids. These measurements will be discussed as well.

As was the case for the entrainment onset studies, the fluid pairs that were utilized in the entrainment rate studies were chosen in an attempt to encompass the widest possible range for the appropriate scaling parameters. For the most part, the fluid pairs chosen were the identical ones as utilized in the entrainment onset experiments. The significant scaling parameters, both dimensional and dimensionless, are listed in Table 5, along with the ranges of these parameters that were covered by the experiments. Note that in all cases, the characteristic values for these parameters that could be expected under MCCI conditions are spanned by the ranges covered in the experiments. Therefore, the results may be applied to MCCI conditions reliably.

Table 5

Ranges of Scaling Parameters
for Volumetric Entrainment Between
Overlying Immiscible Liquids
by Rising Bubbles

Scaling Parameter	Experimental Range	Characteristic NPP Value*
$V_{g,o}$ (cm^3)	0.0025 - 1.02	0.62
ϕ	0.28 - 1396.0	2.0-5.0
$V_{m,e}$ (cm^3)	0.27 - 54.9	~13.
ϵ	0.006 - 0.366	~0.2
Re_1	0.87 - 8752.	~1200.
Re_2	0.48 - 12815.	~8800.

*Calculated from CORCON-MOD 2.04 Standard Problem.

The experimental apparatus was previously illustrated in Figure 7. It consisted of a vertical glass column having two cylindrical sections, and installed with devices for injecting and measuring gas bubbles of precise volumes and for collection of the entrained liquid volume. The denser and lighter fluids were contained in the lower and upper sections of the glass column, respectively. A mechanical shutter was mounted just above the junction plane to collect the volume of the denser, lower liquid that would be entrained into the lighter, upper liquid by a rising bubble.

In the experiments, a pair of immiscible liquids would be charged into the apparatus and adjusted to set the liquid-liquid interface at the junction of the two cylindrical sections. A specified volume of air would be injected into the holding cup, then allowed to rise as a single bubble through the two layers. Visual observations and video recordings would be made during the time of bubble transit and entrainment. The volume of the lower, heavy fluid that was entrained in the wake of the rising bubble would be intercepted by the mechanical shutter device. The shutter would be simply rotated in a horizontal, sweeping motion to cover the junction at the interface of the two liquids, capturing the entrained liquid volume as it once again settled. The bubble would continue to rise until trapped in the burette, at which point an accurate determination of the actual bubble volume could be made. The entrained droplets were recovered from the shutter plate, separated from the lighter liquid, and measured. All experiments, with the exception of those using R11 refrigerant, were performed at room temperature. Due to its low boiling point, the R11 fluid had to be refrigerated to 40-50 F to prevent vaporization during the tests. However, the properties of the R11 that were used in the data analysis were measured at this refrigerated temperature.

4.3 Bubble Rise Velocity

It was necessary to know the bubble rise velocities for these tests in order to calculate the bubble Reynolds number. No theory was found which would accurately and reliably predict the bubble rise velocity in any fluid other than water. Therefore, the bubble terminal rise velocities were measured for air bubbles in each of the test fluids as art of the experimental program. A separate cylindrical test column was constructed into which the bubble holding-cup mechanism could be installed. Bubbles, which covered the size range used in the entrainment experiments, were released and their time-of-flight was timed over two separate courses in their ascent. It was required that the velocities over both courses be identical in order for it to be considered at terminal velocity. The terminal velocities indicated in Figure 10 represent the average of twenty runs for each bubble size tested.

4.4 Results

This section presents sample experimental results and discusses their implications.

4.4.1 Observations of Phenomenon

Figure 4 shows a series of frames from a high-speed photographic record of a single discrete bubble rising through the stratified liquid layers. During this series of frames, the gas bubble has passed into the upper pool and a volume of the denser liquid is clearly seen to be entrained in its wake, having

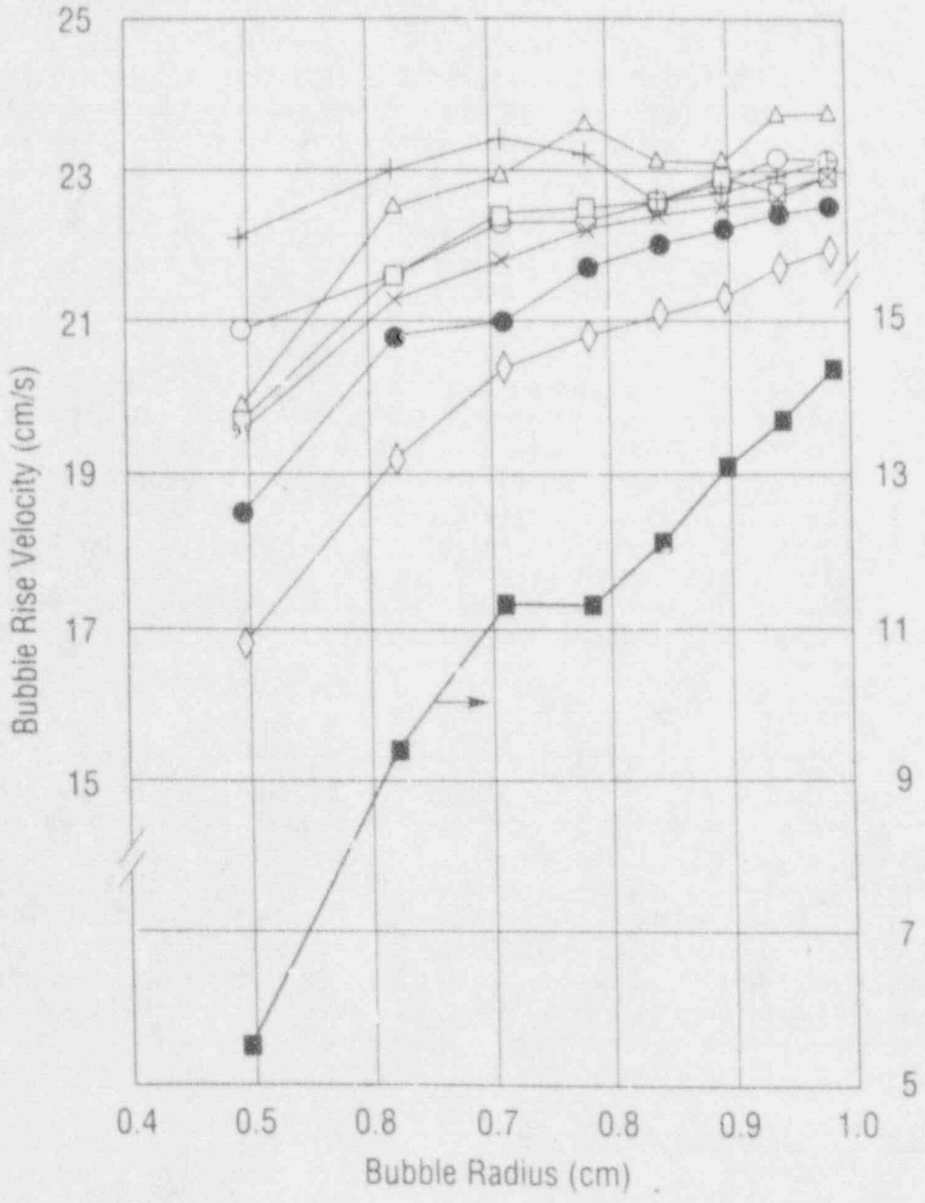

Figure 10. Measured bubble rise velocities: +-Water, O-Acetone, △-R11, □-Hexane, X-10 cs. Silicone Oil, ●-Bromoform, ◊-100 cs. Silicone Oil, ■-Glycerine.

been pulled through the interface between the two liquid layers. Studies of the high-speed movies showed that entrainment starts when a gas bubble of sufficient volume penetrates the surface and pulls a column of the lower liquid in its wake into the upper pool. If the bubble volume is of insufficient size, the levitated column falls back to the lower pool and the gas bubble continues to rise through the upper pool without having caused any entrainment. For sufficiently large gas bubbles, the levitated column rises to a sufficient height that it becomes hydrodynamically unstable; as it elongates, it necks down to snap free a glob of the denser fluid which is then considered to be successfully entrained into the upper fluid layer. Our experiment permitted the capture and measurement of the volume of such entrained globules. Observations of the phenomena from the visual recordings indicated that the volume of entrainment would be affected not only by the size of the gas bubble but also by the densities of the two liquid fluids, their viscosities, and the interfacial tension between the two liquids. Experimental indications of these parametric effects are described below.

4.4.2 Effect of Heavy-Liquid Density

Figure 11a shows the experimental data indicating volumes of entrained liquid for individual bubbles of various sizes (volumes). Results are plotted for two pairs of fluids, water overlying Refrigerant-11 and water overlying bromoform. The major parametric difference between these two pairs is the density of the heavier liquid, bromoform being 2.9 times more dense than water. It is seen that the entrainment volume for a given bubble volume decreased very significantly with increasing density of the heavy liquid, the water/bromoform entrainment volumes being almost an order-of-magnitude lower than the corresponding entrainment volumes for water/R11.

4.4.3 Effect of Light-Liquid Density

The effect of the light-liquid density is just the opposite. Figure 11b shows data for two pairs of fluids, silicone oil over water and hexane over water. The major parametric difference between these two pairs is the density of the upper layer light fluid, hexane, with a specific density of 0.7 as compared to silicone oil with a specific density of 0.9. These results clearly show that entrainment volumes increased with increasing density of the light liquid. For the fluids indicated, a density ratio of 1.5 in the upper layer fluid resulted in a factor of approximately four in the entrainment volumes, for the same bubble volume. Combined with the observation of Figure 11a, the experimental results demonstrate the importance of buoyancy difference between the two liquids.

4.4.4 Effect of Interfacial Tension

Measurements obtained with the two pairs of fluids, water over Refrigerant-11 and hexane over water, can be compared to evaluate the effect of interfacial tension on entrainment. Both of these pairs have a relative density difference of approximately 0.4 g/cm^3 between the heavier and lighter liquids so that relative buoyancy should not be a factor. The major parametric difference between these two pairs is the interfacial tension (σ_{12}) which differed by almost a factor of ten. The results showed that there is little discernible difference in the entrainment volumes between these two pairs of fluids. However, the minimum gas bubble volumes for which measurable entrainment

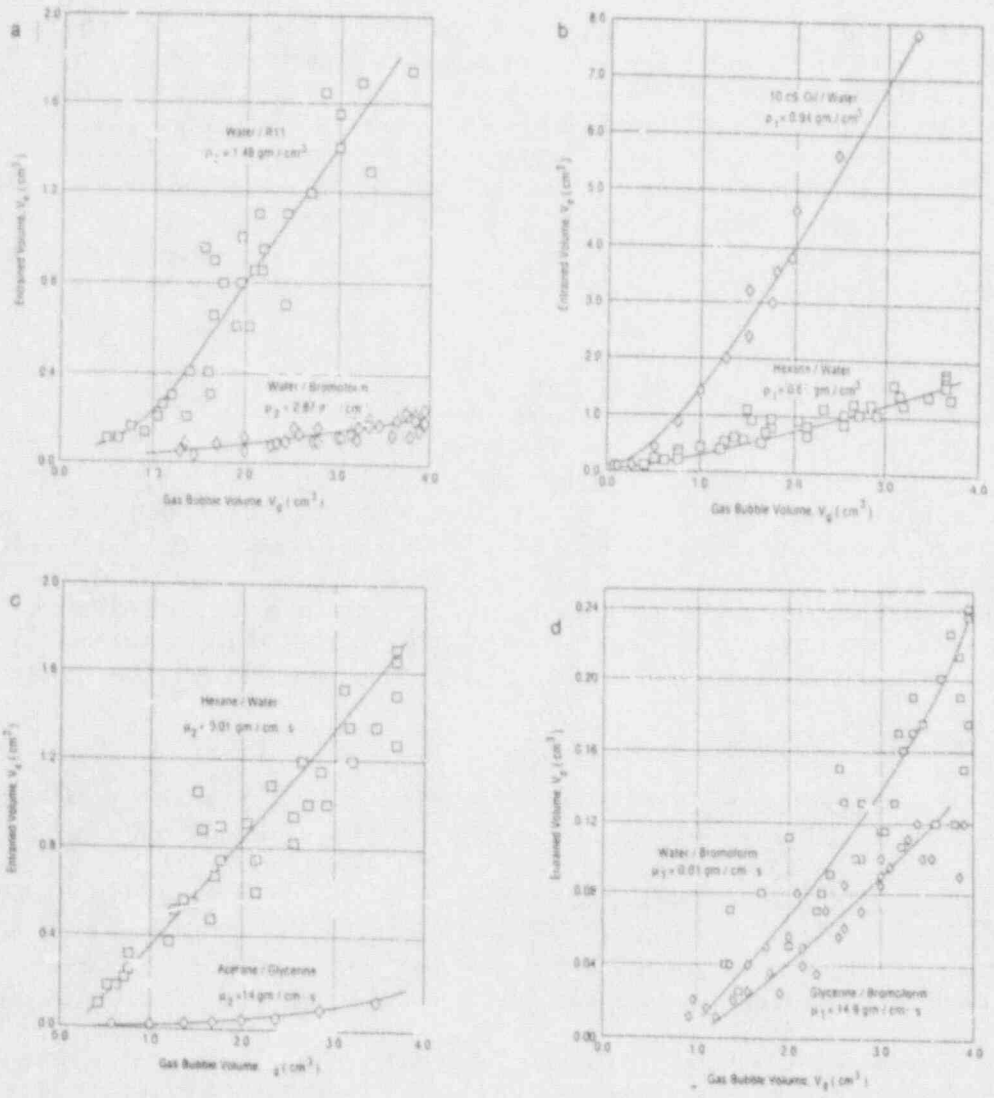

Figure 11. Parametric effects of a) heavy-liquid density, b) light-liquid density, c) heavy-liquid viscosity, and d) light-liquid viscosity upon entrainment.

could be obtained was found to be 0.03 cm^3 for water over R11 and 0.002 cm^3 for hexane over water. The conclusions from this observation is that the interfacial tension affected the onset of entrainment but had relatively small effect on the volume of entrainment. The first effect is consistent with the results reported in Greene et al. (1988a).

4.4.5 Effect of Heavy-Liquid Viscosity

While the liquid viscosities do not affect static force balances, they would be expected to affect bubble rise velocities which in turn influence the characteristics of the bubble wake. Figure 11c examines the potential effect of the liquid viscosity of the heavier liquid in the lower pool. The two pairs of fluids illustrated in this figure have essentially identical viscosities in the lighter fluid and also similar density differences; the major parametric dependence is in the viscosity of the heavy liquids which differ by a factor of over 1000 for water and glycerin. The experimental results show a strong influence on the entrainment volumes. The low viscosity case (hexane/water) had entrainment volumes greater than 10 times that of the high viscosity case (acetone/glycerin).

4.4.6 Effect of Light-Liquid Viscosity

Figure 11d illustrates the effect of different viscosities for the light liquids in the upper pool. Data are plotted for water over bromoform and glycerin over bromoform. These two pairs of test fluids had the same heavier liquid (bromoform) and similar buoyancy density differences. Thus this figure illustrates the parametric effect of the upper fluid (light liquid) viscosity. It is seen that while there is a discernible increase in entrainment volume for the less viscous case, the magnitude of the effect for changing light-liquid viscosity is much less than that for changing viscosity of the heavy-liquid.

4.5 Correlation of Data

The experimental results clearly indicate that the volume of entrainment from the lower pool into the upper pool by a discrete gas bubble is a function of the gas bubble volume, the densities of the two liquids, the viscosity of the two liquids, and the interfacial tension between the two liquids. Over the range of experimental tests for eight different fluid pairs, the resultant entrainment volume per bubble varied over two orders-of-magnitude. The development of a correlation to represent this experimental data base is presented here.

It was first noted that, for a given pair of liquids, entrainment would be possible by discrete gas bubbles only if the bubble volume exceeded the criterion for onset presented by Greene et al. (1988a),

$$V_g \geq V_{go} \quad . \tag{20}$$

V_{go} was theoretically derived by Greene et al. (1988a), and is given by

$$V_{go} = \left[\frac{7.8\,\sigma_{12}}{g(3\rho_1 - \rho_2 - 2\rho_g)} \right]^{3/2} \tag{14}$$

A static force balance was performed (assuming negligible inertial forces) to determine the maximum theoretical liquid volume that could be entrained across the liquid-liquid interface by a rising gas bubble which exceeds this entrainment onset volume. As the bubble (in this analysis the bubble is assumed to be a spherical cap) rises across the liquid-liquid interface, it is observed that a column of the lower, heavy fluid rises with it due to buoyancy and wake effects associated with the bubble. We will consider a control volume consisting of the rising gas bubble and the levitated column of the lower, heavy liquid. By considering the upward lifting force due to the buoyancy of the bubble on the column of entraining fluid, the restoring force on the fluid column due to interfacial tension with the upper fluid, and negative buoyancy of the entrained column in the upper layer, the following force balance was derived.

$$(\rho_1 - \rho_g)\, gV_g = 2\pi\left[\frac{3V_g}{2\pi}\right]^{1/3} \sigma_{12} + V_{m,e}\,(\rho_2 - \rho_1)g \qquad (21)$$

The first term is due to ... ble buoyancy, the second term represents the effect of interfacial tension as the levitated column attempts to tear free from the lower layer, and the third term is the restoring buoyancy of the entraining column. This can be rearranged to solve for the maximum volume of lower liquid ($V_{m,e}$) that can be levitated into the lighter upper liquid as follows:

$$V_{m,e} = \frac{V_g(\rho_1 - \rho_g) - (\sigma_{12}/g)(12\,\pi^2\,V_g)^{1/3}}{(\rho_2 - \rho_1)} \qquad (22)$$

One can consider an "efficiency" of entrainment (ϵ) by taking the ratio of actual entrainment volume (V_e) to the maximum entrainable volume ($V_{m,e}$).

$$\epsilon = \frac{V_e}{V_{m,e}} \qquad (23)$$

Figure 12 shows plots of the experimentally obtained entrainment efficiencies versus the gas bubble volume for two sample liquid pairs. It is seen that for a given pair of fluids, ϵ initially increases rapidly when V_g exceeds V_{go}, but then seems to approach asymptotic limits at higher V_g values. For the cases tested, the entrainment efficiency varied over two orders-of-magnitude but did not exceed 0.3. Other pairs of test fluids presented parametric curves similar to those plotted in Figure 12.

A normalized driving force for entrainment can be defined, based on the excess bubble volume beyond that required to cause onset of entrainment, as

$$\phi = \frac{V_g - V_{go}}{V_{go}} \qquad (24)$$

When the entrainment efficiencies are plotted versus ϕ, approximately linear line segments are obtained on log-log coordinates. Parametric variations in the magnitude of ϵ are obviously related to the fluid properties of the stratified

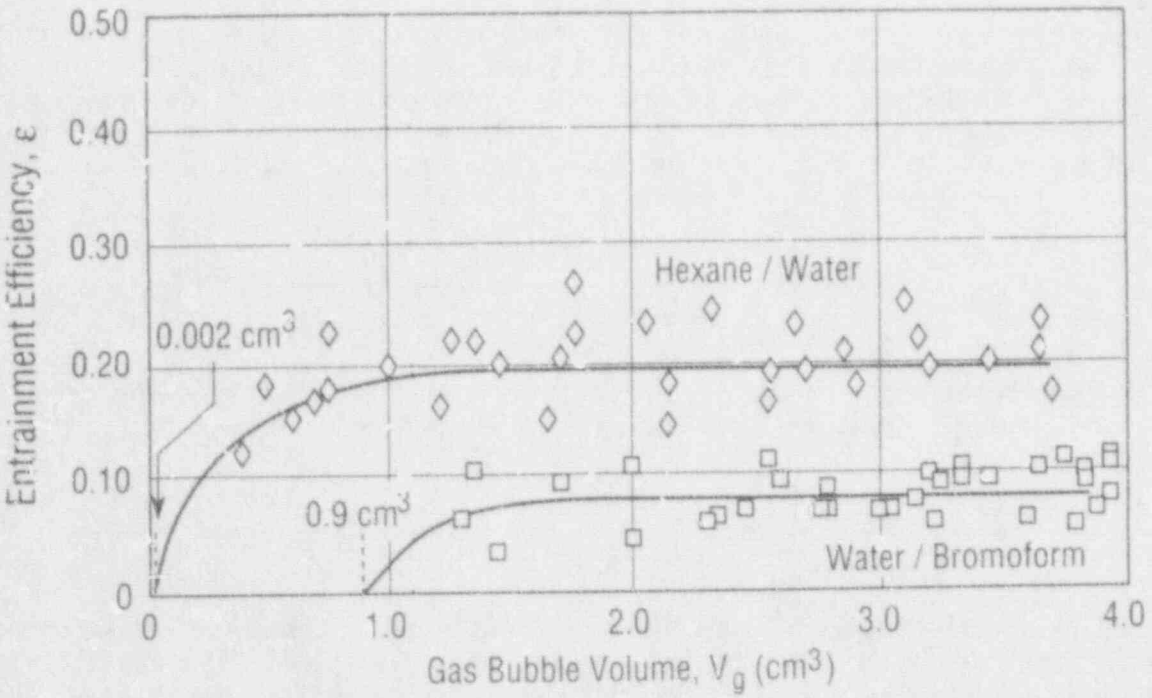

Figure 12. Examples of entrainment efficiencies.

liquid layers.

As indicated above, photographic observations had indicated that entrainment occurs by capturing a volume of the dense liquid in the wake, as the gas bubble passes through the liquid-liquid interface. It seems reasonable to expect that any inefficiency in the entrainment process would be associated with the size and character of the bubble wakes. The bubble wakes are in turn affected by bubble diameter and velocity, the fluid viscosity, and density. These parameters are conveniently grouped in the bubble Reynolds number,

$$Re_1 = \frac{\rho_1 u_{b1} d_b}{\mu_1} \qquad \text{for lighter liquid}$$

$$Re_2 = \frac{\rho_2 u_{b2} d_b}{\mu_2} \qquad \text{for denser liquid} \tag{25}$$

where d_b is taken to be the bubble diameter for an equivalent spherical volume of gas. In this investigation, the terminal rise velocities (u_{b1}, u_{b2}) were experimentally determined as a function of the gas volume (V_g) for each fluid. In situations when experimental determination is not possible, published correlations can be used (Wallis, 1969).

Following this reasoning, a functional relationship of form,

$$\epsilon = f(\phi, Re_1, Re_2)$$

was sought. The final correlation was represented as,

$$\frac{\phi}{\epsilon} (Re_1)^a (Re_2)^b = K\phi^c \tag{26}$$

where the constants were empirically determined to be,

$$a = .119$$

$$b = .380$$

$$c = .84C$$

$$K = 806$$

Figure 13 shows a graphical comparison of this correlation with all the experimental data obtained in this investigation. The statistical fit corresponds to a mean deviation of 0.35 in the ratio of measured to calculated entrainment efficiency.

4.6 Summary

The process of liquid entrainment between stratified liquid layers by rising gas bubbles was experimentally investigated for eight different pairs of

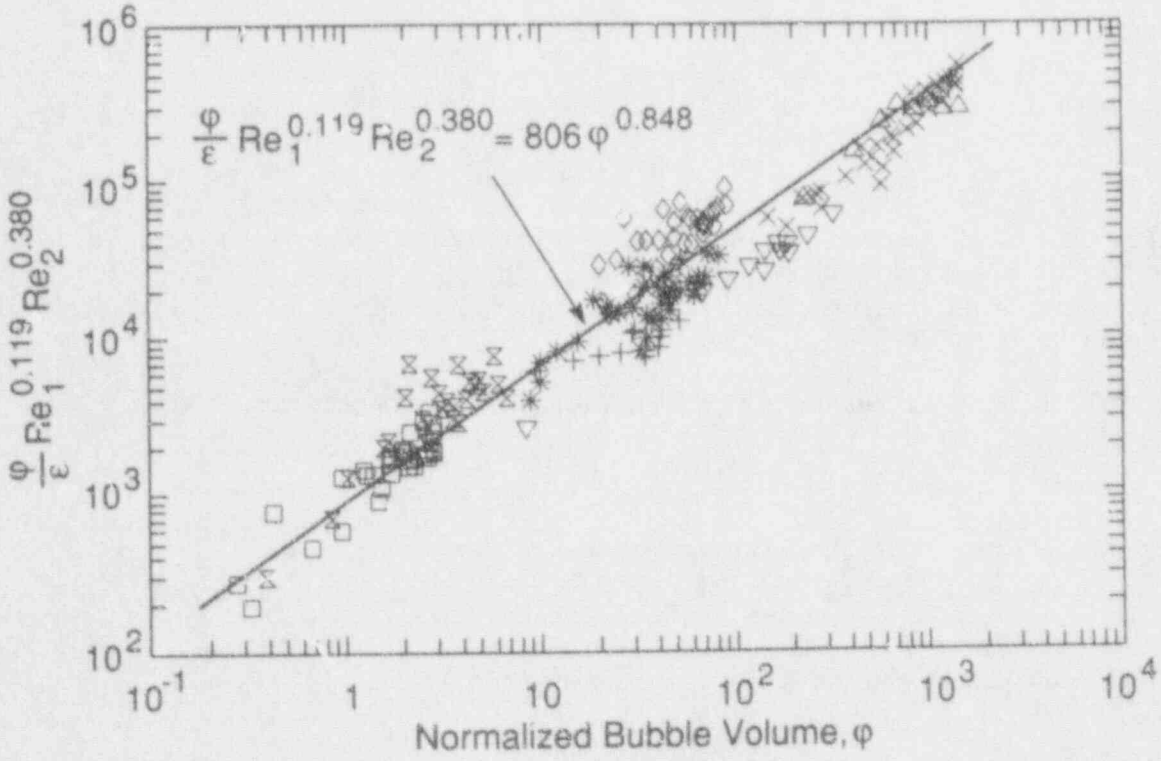

Figure 13. Correlation of data: □-Water/Bromoform, ◊-100 cs. Silicone Oil/Bromoform, ▽-10 cs. Silicone Oil/Water, *-Water/R11, +-100 cs. Silicone Oil/Water, ⊠-Glycerine/Bromoform, △-Acetone/Glycerine, X-Hexane/Water.

liquids, covering a wide range of physical properties. In addition to photographic observations, quantitative measurements of the entrained liquid volumes were obtained for a range of gas bubble size. The results indicated that once the gas bubble exceeded the necessary minimum size to cause onset of entrainment, measurable entrainment occurred which increased with excess gas volume (above the required onset volume). The efficiency of entrainment, defined as the ratio of entrained volume to maximum entrainable volume as derived from a limiting static force balance, was found to range over two orders-of-magnitude but did not exceed 0.3 for any of the test cases. A dimensionless correlation was obtained to represent the entrainment efficiency as a function of the excess gas volume (ϕ), and the gas bubble Reynolds numbers in each liquid (Re_1,Re_2). Agreement between the proposed correlation and the 189 experimental data points indicated a mean deviation of 0.35.

Application of the entrainment rate model in the CORCON code will insure that hydrodynamic mixing and layer mixture properties are reliably calculated. This will insure that the morphology of the core debris layers is accurately predicted, and that the heat transfer between the layers and the distribution of fission products that are calculated by CORCON are reliable.

5. HEAT TRANSFER BETWEEN STRATIFIED LIQUIDS WITH ENTRAINMENT ACROSS THE INTERFACE

Consider the case of two immiscible liquids in initially stratified layers and agitated by rising gas bubbles as illustrated in Figures 14a-c. As gas bubbles rise upwards through the liquid-liquid interface, they not only disturb the temperature gradients on both sides of the interface, but may entrain the lower, heavy liquid into the upper, lighter layer, further increasing the heat transfer from liquid to liquid. If the rising bubbles are not able to support entrainment, the stratified state will prevail, and heat transfer will be across a well-defined interface between two well-mixed pools at different temperatures. This is the configuration presented in Figure 14a and discussed in Section II. Under some circumstances, the rising gas bubbles not only agitate the liquid-liquid interface but also drive a mass transfer process by entraining the lower heavy liquid upwards in the wakes of the rising gas bubbles. If the rate of entrainment of the lower phase can be balanced by the rate of droplet settling (or de-entrainment) a partially mixed configuration will result in which the liquid-liquid interface will be preserved between a homogenous lower layer and a heterogenous upper mixture layer. This is the pool configuration presented in Figure 14b. Criteria for onset of entrainment and rate of entrainment were discussed in Sections III and IV, respectively. De-entrainment will be discussed in Section VIII. If the rate of entrainment is greater than the rate of settling of the entrained droplets, the two liquids will form a pool that is fully mixed, or fully entrained; there will only be one heterogeneous liquid layer and the concept of interlayer heat transfer will not be applicable. This is the configuration that is presented in Figure 14c. This configuration will not be addressed in this discussion.

5.1 Heat Transfer in Stratified Configuration

If conditions are such that entrainment of the lower fluid into the upper fluid cannot be supported by the rising gas bubbles, the liquid layers will remain stratified as illustrated in Figure 14a. In this stratified configuration, the rate of heat transfer between the two layers is controlled by the rate of bubble agitation at the liquid-liquid interface. Szekely developed an analytical solution for the surface renewal heat transfer coefficient for each side of the interface (representing the heat flux divided by the average bulk layer-to-interface temperature difference) by integrating the time-dependent heat flux on each side of the interface over the period of arrival of successive bubbles. He arrived at the following result for the heat transfer coefficient on each side of the interface,

$$h_i = 1.69\left[\frac{\rho c_p k j_g}{r_b}\right]^{1/2} \tag{3}$$

which was cast in dimensionless form as,

$$Nu_i = 1.69\ Re_i^{1/2}\ Pr_i^{1/2} \tag{4}$$

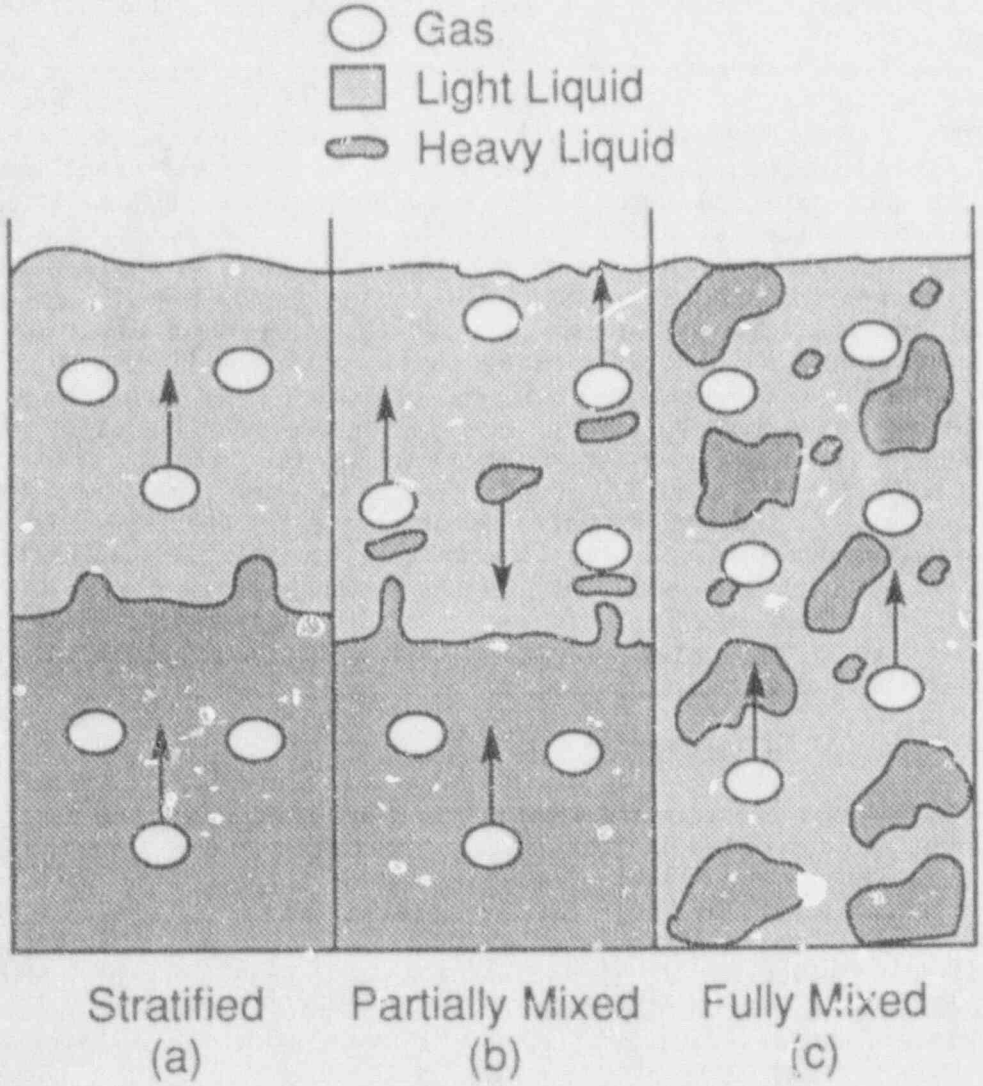

Figure 14. Configurations of multifluid bubbling pools.

where $Re_i = j_g r_b/\nu$ and i = 1 or 2, representing the upper or lower liquid layer, respectively. The overall heat transfer would be evaluated by summing the two series resistances on both sides of the interface. Due to the absence of data with which to evaluate this model, Greene and Irvine (1988b) performed an experimental investigation into heat transfer between overlying, stratified immiscible liquids with bubble agitation. The fluids that were tested were water, and 10 cs. and 100 cs. silicone oils over a layer of mercury. Three sets of experiments were performed. The experimental data were non-dimensionalized as in Equation (4) and an empirical correlation was developed. The resulting correlation is given by,

$$Nu_i = 1.95\ Re_i^{0.72}\ Pr_i^{0.72} \tag{8}$$

This is the model that is recommended for surface renewal heat transfer driven by gas bubbling at a liquid-liquid interface in the absence of mass entrainment.

5.2 Onset of Bubble-Induced Entrainment

Experiments with liquids such as water or light oils over a pool of mercury (and other heavy metals as well) have shown that the stratified configuration is possible, even under the influence of gas bubbling across the interface. However, there is evidence from other studies that indicate that with some fluid pairs, the gas bubbling can drive mass transfer across the interface if some threshold entrainment condition is satisfied.

Greene et al. (1988a) performed a systematic experimental and analytical investigation of the conditions for the onset of mass entrainment across a stratified liquid-liquid interface due to single rising gas bubbles. Experiments were performed for eight fluid pairs with single air bubbles. The bubble volumes in the entrainment onset experiments covered over three orders of magnitude. For each of the fluid pairs, a distinct bubble volume at which entrainment onset occurred was observed. The onset volume was observed, however, to be strongly dependent upon the fluid pair, ranging from 0.002 cm^3 for acetone/glycerine to 1.0 cm^3 for water/bromoform.

An analytical criterion for the prediction of entrainment onset was developed, based upon a static force balance on the bubble/liquid system as it attempts to levitate a column of the lower, heavy liquid, and interfacial tension which acts to restrain the entrainment. The mathematical criterion for onset of entrainment that was developed is given by the dimensionless inequality,

$$\omega > \frac{V_{go}}{V_g^*} \equiv \left[\frac{2(\rho_1 - \rho_g)}{(3\rho_1 - \rho_2 - 2\rho_g)}\right]^{3/2} \tag{17}$$

where ω is the dimensionless bubble volume equal to V_g/V_g^*, V_g is the bubble volume, V_g^* is the necessary bubble volume to penetrate the interface, and V_{go} is the entrainment onset bubble volume. These are defined as

$$V_{go} = \left[\frac{7.8\ \sigma_{12}}{(3\rho_1 - \rho_2 - 2\rho_g)g}\right]^{3/2} \tag{14}$$

and

$$V_g^* = \left[\frac{3.9\,\sigma_{12}}{(\rho_1-\rho_g)g}\right]^{3/2} \tag{10}$$

The proposed theoretical criterion (Eqns. 10, 14, 17), with no empirical parameters, was found to predict the experimental measurements with good agreement over the entire test range.

5.3 Rate of Bubble-Induced Entrainment

There is clear evidence in the literature that entrainment between overlying immiscible liquid layers by gas bubbling from below occurs for some fluid pairs, and is a function of the bubble volume as well as the physical and transport properties of the liquids and the gas. This is the configuration shown schematically in Figure 14b. Greene et al. (1990) performed a systematic experimental investigation of the parameters that contribute to the volume of heavy liquid that can be entrained by a gas bubble rising across a liquid-liquid interface to develop a general entrainment rate model. Experiments were performed with eight separate fluid pairs and single air bubbles as previously described for the entrainment onset studies (Greene et al. 1988a). The experimental results clearly indicate that the volume of entrainment from the lower pool into the upper pool by a discreet gas bubble is a complicated function of the gas bubble volume, densities and viscosities of both liquids, and the interfacial tension between the two liquids. An analysis based upon a static force balance was developed to predict the maximum volume that can be entrained, neglecting inertial forces as,

$$V_{m,e} = \frac{V_g(\rho_1-\rho_g)-(\sigma_{12}/g)(12\pi^2 V_g)^{1/3}}{(\rho_2-\rho_1)} \tag{22}$$

One can consider an entrainment efficiency, ϵ, by taking the ratio of the actual measured entrained volume, V_e, to the maximum entrainable volume, $V_{m,e}$,

$$\epsilon = V_e/V_{m,e} \tag{23}$$

It is reasonable to expect that any inefficiencies in the entrainment process would be associated with the size and character of the bubble wakes. The bubble wakes are affected by Re_1 and Re_2, the bubble Reynolds numbers in the upper (1) and lower (2) liquids, respectively. A functional relationship for the entrainment efficiency was sought of the form, $\epsilon=f(\phi, Re_1, Re_2)$, where ϕ is the dimensionless excess bubble volume beyond that required for onset of entrainment,

$$\phi = \frac{V_g-V_{go}}{V_{go}} \tag{24}$$

The final relationship was found to be,

$$\frac{\phi}{\epsilon} \; Re_1^{0.119} \; Re_2^{0.380} = 806 \; \phi^{0.848} \tag{26}$$

This correlation and the experimental data were found to be in good agreement.

5.4 Overall Interlayer Heat Transfer with Entrainment

In order to evaluate the magnitude of the heat transfer between overlying immiscible liquid layers with bubbling induced entrainment across the interface, the configuration shown in Figure 14b, it is necessary to calculate the component due to surface renewal as well as that due to the entrained mass. The total heat transferred between the two liquid layers is assumed to be the sum of the heat transfer across the interface and the heat transfer from the entrained drops of the lower, heavy fluid while suspended in the upper layer. The overall surface renewal heat transfer coefficient, h_{SR}, is constructed by summing the series resistances to heat transfer on both sides of the interface, h_1 and h_2, as follows:

$$h_{SR}^{-1} = \left[\frac{1}{h_1} + \frac{1}{h_2}\right] \tag{27}$$

Both h_1 and h_2 can be computed from the surface renewal heat transfer correlation, Equation (8), by simply substituting the fluid properties appropriate to the continuous fluid on each side of the interface, i = 1 and 2.

The heat transferred by the entrained droplets while suspended in the upper, light liquid layer is modeled as a fraction of total excess (or deficit) enthalpy transferred from the drops to the continuous liquid. This can be represented in terms of an entrainment heat transfer coefficient, h_e, as follows:

$$h_e = K\rho_2 c_{p2} j_e \tag{28}$$

where j_e is the superficial (volumetric) entrainment flux, analogous to the superficial gas velocity, j_g (≡volumetric gas flux/interfacial cross-sectional area). The superficial entrainment flux, j_e, is defined as the product of the superficial gas velocity and the ratio of entrained volume per bubble to the bubble volume:

$$j_e = j_g \left(\frac{V_e}{V_g}\right) \tag{29}$$

Both Equations (27) and (29) illustrate the importance of not only the physical and transport properties of both liquids, but the size of the rising bubbles as well, in evaluating the heat transfer under entraining conditions. The size of the bubbles was directly measured in the course of these tests. The parameter K in Equation (28) is an efficiency factor for the droplet-liquid heat transfer which represents the actual fraction of excess enthalpy transferred from the drop to the surrounding liquid. For the experimental data to be presented, K was found to be almost always nearly equal to one, and will be assumed equal to one for this model. The total interlayer heat transfer coefficient can now be represented by summing Equations (27) and (28) as follows,

$$h_T = h_{SR} + \rho_2 c_{p2} j_e \tag{30}$$

where the first term on the right hand side is the contribution due to surface renewal effects and the second term is due to mass transport effects. This heat transfer coefficient is multiplied by the overall temperature difference from bulk layer to bulk layer to calculate the overall heat flux. It is possible to non-dimensionalize Equation (30) by multiplying both sides by the quantity (d_b/k_2), resulting in the following dimensionless form of the total interlayer heat transfer model,

$$Nu_T = Nu_{SR} + Re_e Pr_2 \tag{31}$$

where $Nu_T = h_T d_b/k_2$, $Nu_{SR} = h_{SR} d_b/k_2$, $Re_e = j_e d_b/\nu_2$, and Pr_2 is the Prandtl number of the lower, heavy liquid layer. This form of the model may be useful for evaluating data for additional fluid pairs as they become available.

In order to evaluate the model for total interlayer heat transfer with entrainment (Figure 14b, Equation 30), a series of two heat transfer experiments were performed (Greene et al., 1982). These entrainment heat transfer experiments differed from the stratified heat transfer experiments which were discussed in Section II only in the choice of the immiscible fluid pairs tested. For the stratified heat transfer studies, one of the fluids chosen was mercury; this ensured that the liquids would remain stratified since the fluid pairs did not satisfy the entrainment onset criterion. In addition, the resistance to heat transfer on the mercury side of the interface was negligible, allowing direct comparison of the data to models that were applicable for only one side of the interface. In this manner, the uncertainty in the data and models would not be compounded by having two comparable heat transfer resistances in series. In the heat transfer experiments with entrainment across the interface, the fluid pair was chosen to admit entrainment across the interface by the rising gas bubbles. Therefore, the overall heat transfer measured would be the sum of the contribution due to surface renewal processes in series on both sides of the interface (stratified contribution) and the contribution due mass transport of the lower, heavy liquid into the upper, light layer by the rising gas bubbles (entrainment contribution). The experiments utilized 10 cs. silicone oil over water with gas bubbling from a porous frit installed in the test section base. The test apparatus was previously discussed in Section II. The heat transfer coefficient that was measured in these tests was the net overall heat transfer coefficient, including both the surface renewal and entrainment components. The resulting experimental heat transfer data for the two series of tests are listed in Table 6. The heat transfer coefficient was then calculated by Equation (30) and compared to the measured heat transfer coefficient, as shown in Figure 15. The measured overall heat transfer coefficient is defined as the overall heat flux divided by the difference in bulk temperature between the two fluid layers. Equation (30) was found to be in good agreement with the experimental data over two orders of magnitude in measured heat transfer coefficient.

5.5 Summary

A framework for evaluating the total rate of heat transfer between overlying immiscible liquid layers with bubble induced entrainment was presented. It was found to be a synthesis of surface renewal heat transfer and that due to direct

Table 6
Entrainment Heat Transfer Data
10 cs. Silicone Oil/Water

RUN	J_g(cm/s)	$h_{measured}$ (W/m^{2}K)
101	0.17	2578
102	0.17	2490
103	0.25	3819
104	0.25	3953
105	0.38	7115
106	0.38	7490
107	0.63	27344
108	0.63	28646
110	1.25	75300
200	0.12	2136
210	0.19	4143
220	0.25	7382
230	0.38	12058
240	0.63	23670
250	1.00	52513

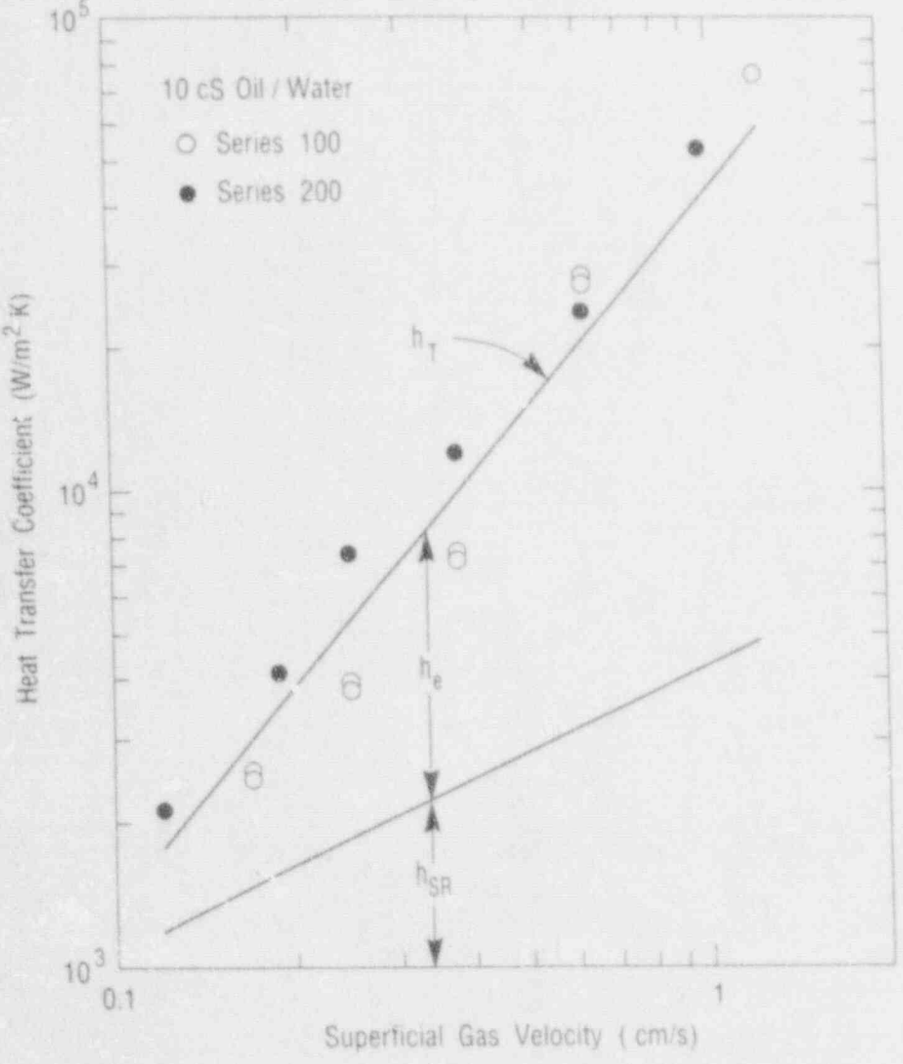

Figure 15. Measured overall heat transfer vs. gas velocity.

heat transfer from the entrained drops. Models for surface renewal heat transfer, entrainment onset, and entrainment rate were presented and compared to available experimental data. The models and data were found to be in very good agreement. These models were then combined to construct the overall heat transfer model, Equation (30). When the total interlayer heat transfer model was compared to available heat transfer data for bubbling pools of 10 cs. silicone oil over water, the model and data which both included the effects of entrainment, were found to be in very good agreement over two orders of magnitude in the measured total heat transfer coefficient.

Application of the entrainment heat transfer model to the CORCON code will extend the ability of the code to calculate interlayer heat transfer from the stratified layer configuration to conditions in which mass transfer across the layer interface is occurring. This model relies on accurate modeling of stratified heat transfer, entrainment onset, and entrainment rate in the gas-sparged core debris. This will insure reliable and accurate analysis of melt temperature and concrete erosion rate with interlayer mixing.

6. HEAT TRANSFER FROM A LIQUID POOL IN BUBBLY FLOW TO A VERTICAL WALL

In a number of cases of bubbling of a non-condensable gas through an overlying liquid pool, it is desirable to know, not only the rate of heat transfer between overlying immiscible liquid layers, but heat transfer rates to the boundaries of the vessel as well. These structural boundaries include the base as well as the vertical sidewalls of the vessel. In this section, we shall consider the bubbling enhancement to the heat transfer from the bubbling liquid pool to the vertical sidewalls of the vessel. This modeling is needed for the CORCON code to be able to accurately and reliably predict lateral heat loads on the vertical walls of confining structures such as concrete pedestals and Mark I steel shells. In the subsequent section, we shall consider bubbling ennanced heat transfer to the bottom surface.

6.1 Physical Phenomena

Consider a liquid pool with an internal heat source which is held in a container. In the absence of gas bubbling, the heat transfer from the heated pool to its surroundings would be controlled by free convective processes driven by the temperature differences between the pool and its walls. In the free convection configuration, the magnitude of the boundary heat transfer coefficient is typically on the order of 100-500 W/m^2K. Boundary layers are stable under these conditions and may, in fact, be laminar over a considerable portion of the boundary surface.

If a non-condensable gas is injected into the pool from below, a two-phase flow environment would be created. The rising gas bubbles would create severe circulation patterns and turbulence. Depending upon the rate of gas injection, the flow regime may be bubbly or churn-turbulent. The length and velocity scales of the turbulence in the pool would be functions of the characteristic bubble size and gas injection velocity, respectively, particularly in the bubbly flow regime which is characterized by distinct rising bubbles. As the bubbles rose in the pool, they would interact with the wall boundary layer. The kinetic energy of the turbulent eddies would be orders-of-magnitude greater than that of the boundary layer flow per unit volume, resulting in destruction of the boundary layer processes. This could occur by two mechanisms: direct interaction of the bubbles with the wall boundary layer, and convection of turbulence from the bubbling core of the pool to the boundaries.

It is expected that the heat flux from the bubbling pool to the boundaries would be considerably enhanced over the free convection case. The heat flux along the wall may be spatially uniform and cannot be predicted by free convection or single-phase flow considerations. This situation just described is what would be encountered in gas-sparged contactors, metallurgical furnaces, and molten core-concrete interactions.

6.2 Previous Studies

There have been several previous studies concerning bubbling heat transfer to vertical surfaces. The first was an experimental study by Kolbel et al. (1958). They investigated bubbling heat transfer in a vertical cylinder to a cylindrical heat transfer element. They investigated eight fluids ranging in

viscosity from 0.85 to 946.5 cs. They observed that if the viscosity was increased, the heat transfer coefficient was decreased. For water, in particular, they observed that for superficial gas velocities in the range 3-10 cm/s, the heat transfer coefficient was in the range 4000-5000 W/m^2K. They accounted for the viscosity effect in a Reynolds number but neglected modeling the heat transfer as a function of Prandtl number. They offered the following relations for heat transfer in terms of a Nusselt number:

$$Nu = 43.7\ Re^{0.22}, \quad Re > 150$$

$$\text{for } j_g \leq 10 \text{ cm/s} \qquad (32)$$

$$Nu = 22.4\ Re^{0.355}, \quad Re < 150$$

The Reynolds and Nusselt numbers in Equation (32) employ the diameter of the heating surface and the superficial gas velocity. Note, however, the absence of any Prandtl number dependance.

Subsequently, Fair et al., (1962) reported on their study of heat transfer and gas holdup in a gas sparger. The technique they used was somewhat different than Kolbel. Air and water were injected into a cylindrical test section simultaneously. A heater was submerged in the flowing air-water pool and the enthalpy rise of the overflowing water was used to calibrate the electrical power input. Using the temperature difference between the electrical heating surface and the water, and the area of the heating element, they calculated a heat transfer coefficient. They found their data best correlated, in dimensional terms, as:

$$h\ (W/m^2K) = 3300\ J_g^{0.22}\ (cm/s) \qquad (33)$$

This dimensional relationship was found to be in good agreement with Kolbel's water data, for superficial gas velocities in the range 0.3 to 15 cm/s.

Hart (1976) reported that the available literature on heat transfer from bubble-agitated systems was inadequate either due to the dimensional nature of the correlations developed or because the dimensionless representation neglected important parameters and variables. Hart used dimensional arguments to identify the dominant variables (superficial gas velocity, gravity, density, viscosity, specific heat, and thermal conductivity) which determine the heat transfer coefficient, and to reject the container dimensions as the significant length scale. He then proceeded by dimensional analysis to develop a general dimensionless structure for the heat transfer coefficient as shown below,

$$St\ Pr^{\beta} = \alpha\ (Re\ Fr)^{\gamma} \qquad (34)$$

where $St = h/\rho C_p j_g$ and $Re \cdot Fr = \rho j_g^3/\mu g$. Experiments similar to those of Fair were performed with water and ethylene glycol. The temperature difference between the heater and the flowing water, along with the power and heater area, were used to calculate the heat transfer coefficient. Once again, dimensional trends in the data were used to determine the coefficients and exponents in Equation (34). It was found that $\alpha = 0.125$, $\beta = 0.6$, and $\gamma = -0.25$. This formulation predicts $h \sim j_g^{.25}$, which is in reasonable agreement with the trends reported by Kolbel

(1958) and Fair (1962), previously.

Konsetov (1966) developed an analytical solution to the problem of heat transfer to a boundary during bubbling of gas through the pool. In his approach, Konsetov assumed that the pool was turbulent and that heat transfer was determined by the size and velocity of these turbulent eddies. He estimated the size of the turbulent eddies to be one-sixth the apparatus diameter, in accordance with some existing theories. Using the data of Kolbel, he arrived at the following dimensional relationship for the bubbling heat transfer coefficient to an apparatus wall,

$$h = 0.25\ k\ (Pr\ \alpha\ g/\nu^2)^{1/3}\ (\mu/\mu_w)^{.14} \tag{35}$$

where the term $(\mu/\mu_w)^{.14}$ can be neglected for most practical applications. This relationship was later modified by Blottner (1979) to tailor it in a more general form for inclusion in CORCON. Blottner included a free convective term which would extend the applicability of Equation (35) to the case of the free convective asymptote when the superficial gas velocity, and therefore the void fraction, was equal to zero. After changing the coefficient to improve comparison to the data of Hart (1976), Blottner arrived at the following dimensional relationship.

$$h = k\ (Pr\ g/\nu^2)^{1/3}\ (0.00274\ \beta\Delta T + 0.05\ \alpha)^{1/3} \tag{36}$$

However, it can be easily shown that for almost all cases with bubbling, the free convective term is negligible and Equation (36) can be simplified to:

$$h = 0.37\ k\ (Pr\ \alpha\ g/\nu^2)^{1/3} \tag{37}$$

It is clear that the only difference between Equations (35) and (37) is in the magnitude of the coefficient, which reflects the data base preference of the authors. Neither Equation (35) or (37) has an explicit length scale in the formulation. However, the development of Konsetov did involve consideration of turbulent eddy size, so a length scale is implicitly considered. In the Konsetov and Blottner formulations the heat transfer coefficient is proportional to $\alpha^{1/3}$. Since, in bubbly flow, the void fraction is approximately linearly dependant upon j_g, this is equivalent to $j_g^{1/3}$. This compares relatively well with the observations of Kolbel (1958), Fair (1962), and Hart (1976).

Significant questions remained unanswered concerning bubbling heat transfer from a liquid pool to a vertical boundary. Dependance upon bubble size has not been established. The dependance of the heat transfer coefficient upon the gas superficial velocity has been reported to vary from $j_g^{.22}$ to $j_g^{.33}$. Some studies suggest a forced convective behavior (Reynolds number) while others suggest a buoyancy-type (Grashof number) or a mixed convection dependance. Finally, the dependance upon the Prandtl number has yet to be established on a firm technical basis. In order to address these concerns and to develop a reliable model of bubbling heat transfer to a vertical boundary, the following experiment was performed.

6.3 Experiment

A rectangular test vessel was fabricated out of one-inch plexiglass stock and had the following inside dimensions: length = 16.9 cm, width = 15.3 cm, depth = 41 cm, resulting in a horizontal platform cross-sectional area = 258 cm^2. In the base was installed a porous plenum assembly through which the gas was injected into the pool. Submerged in the test pool was a horizontal, coiled calrod heater capable of dissipating nominally 2.5 kW into the pool fluid. It was installed in such a manner as to reside directly over the gas injection plenum. The gas was metered through a bank of rotameters and preheated to the pool temperature prior to injection. The calrod heater power was measured by a precision Wattmeter as well as by RMS voltage and amperage. Discrepancies in calculated power were always negligible.

A vertically-oriented instrumented test wall was submerged in the pool. It was constructed out of micarta in a window-frame design. A one-fourth inch thick copper plate was installed in such a manner that one surface was exposed to the bubbling pool, flush with the micarta frame, and the back-side was exposed to a serpentine coolant passage through which water was circulated to cool the test plate. Two thermocouples were installed in the coolant inlet and outlet ports to measure the coolant enthalpy rise. A vertical rake of ten thermocouples was installed along the pool centerline to measure the average pool temperature. Five microthermocouples were installed in the copper plate to perform precise local surface temperature measurements along the vertical axis of the test wall.

The water pool depth would be set to cover the test wall (approximately 30 cm). The gas flux, pool heater, and test plate coolant would be set to specifications. The gas heater was energized and monitored in order to keep the pool temperature and gas temperature as equal as practical. The pool temperature was targeted to 41°C in order to keep the coolant temperature rise around 5°C. The gas flux was varied to cover a range of superficial gas velocities from 2 to 25 mm/s. The size of the bubbles generated by the gas plenum was approximately 3 mm in equivalent spherical radius and essentially constant over the range of the experiments. The test fluid was water and the water properties were evaluated at 41°C for all test runs. All tests were executed under steady-state conditions and each data point to be presented represents the average of five separate tests under nominally identical conditions.

6.4 Results

The modeling approach adopted by Konsetov (1966) and Blottner (1979) requires knowledge of the void fraction in order to correlate the heat transfer data, and a model to predict the void fraction in order to apply the heat transfer model. As a result, the void fraction was measured in the course of these tests.

6.4.1 Void Fraction Measurements

The pool-average void fraction was evaluated as a function of the superficial gas velocity as part of this investigation. The data were visually observed to all reside in the bubbly flow regime, an observation that is in accord with observations of transition to churn-turbulent flow in a pool with bottom gas injection at a superficial gas velocities of approximately 10 cm/s.

A variety of models have been developed to predict this pool-average void fraction. The one which will be compared to the data was reported by Blottner (1979). The form of the void model developed by Blottner, assuming that the two-phase distribution parameter is equal to unity, is shown below,

$$\alpha = \frac{\phi}{1 + \phi} \tag{38}$$

where ϕ is the dimensionless superficial gas velocity. The void data were compared to Equation (38). The results of the comparison, shown in Figure 16, were quite favorable.

6.4.2 Heat Transfer Measurements

The measured temperature throughout the bubbling liquid pool was found to be spatially uniform. The variations in surface temperature along the plate were found to be small compared to the temperature difference from the pool to the plate, generally less than 0.1 K, within the range of the calibration uncertainty of the measurement system. The pool-to-plate temperature difference was generally on the order of 5 K. The wall heat transfer coefficient was calculated according to the following formula,

$$h = \frac{G\, c_p\, (T_{out} - T_{in})}{A\, (T_{pool} - T_{plate})} \tag{39}$$

where the numerator represents the enthalpy rise of the test wall coolant and the temperature difference in the denominator represents the average temperature difference across the wall boundary layer.

The measured heat transfer coefficients from two series of tests are shown in Figure 17 as a function of the superficial gas velocity. It was found that the heat transfer coefficient is a monotonically increasing function of the superficial gas velocity in the bubbly flow regime. The lowest superficial gas velocity at which data were taken was approximately 2 mm/s. The wall heat transfer coefficient at this lowest superficial gas velocity was measured to be nearly 2000 W/m^2K, a factor of five or more greater than calculated for free convection on a vertical plate. This suggests that the bubbles very readily caused the pool to become turbulent, essentially at the onset of any bubbling, causing a discontinuous large increase in the heat transfer coefficient, quite similar to the approach assumed by Konsetov (1966). The heat transfer coefficient was found to increase with increasing superficial gas velocity, and was measured to be approximately 5000 W/m^2K at a superficial gas velocity of only 2.36 cm/s.

The trend of the heat transfer coefficient data was observed to be similar to that reported by Kolbel (1958), Fair (1962), and Hart (1976). Whereas Kolbel and Fair found the heat transfer coefficient proportional to $j_g^{.22}$, and Hart found proportionality to $j_g^{.25}$, the present data on the average were found best approximated as proportional to $j_g^{.33}$ in agreement with the results of Konsetov (1966) and Blottner (1979).

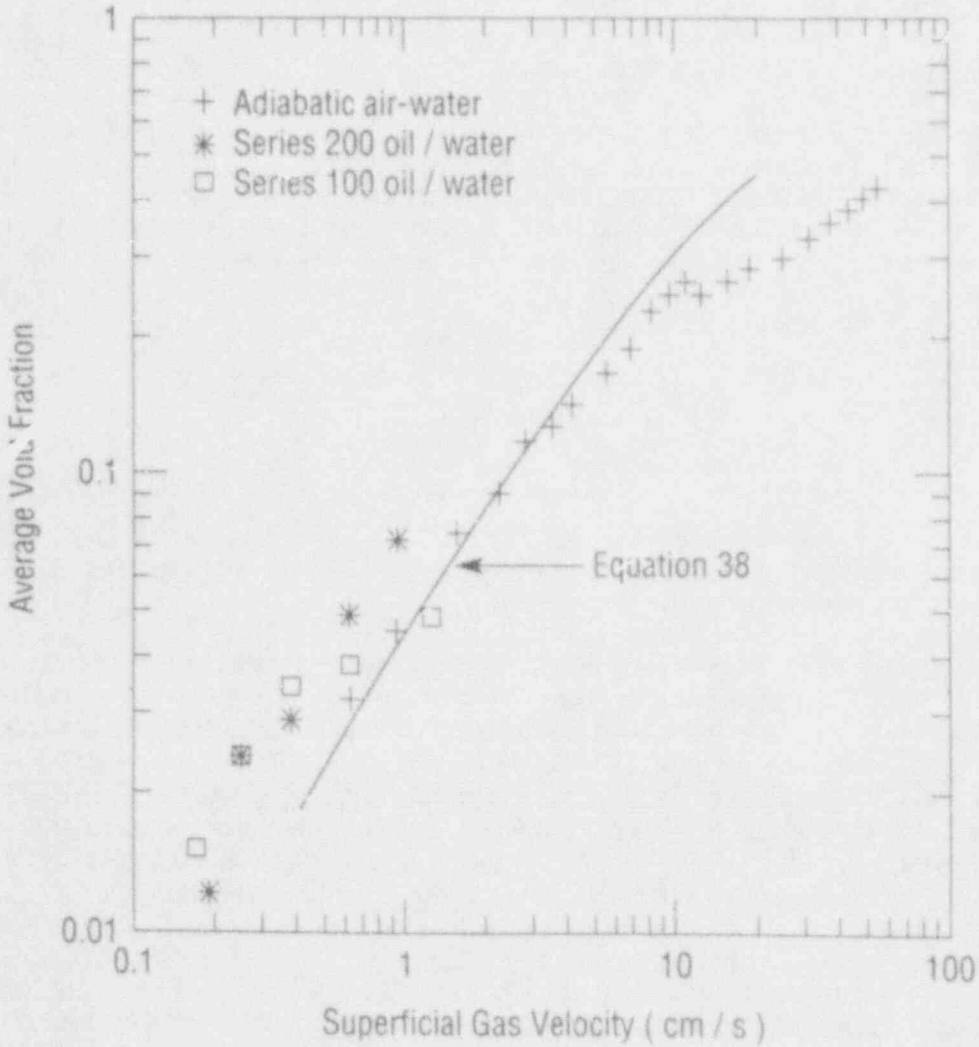

Figure 16. Average void fraction in bubbling pools with bottom gas injection.

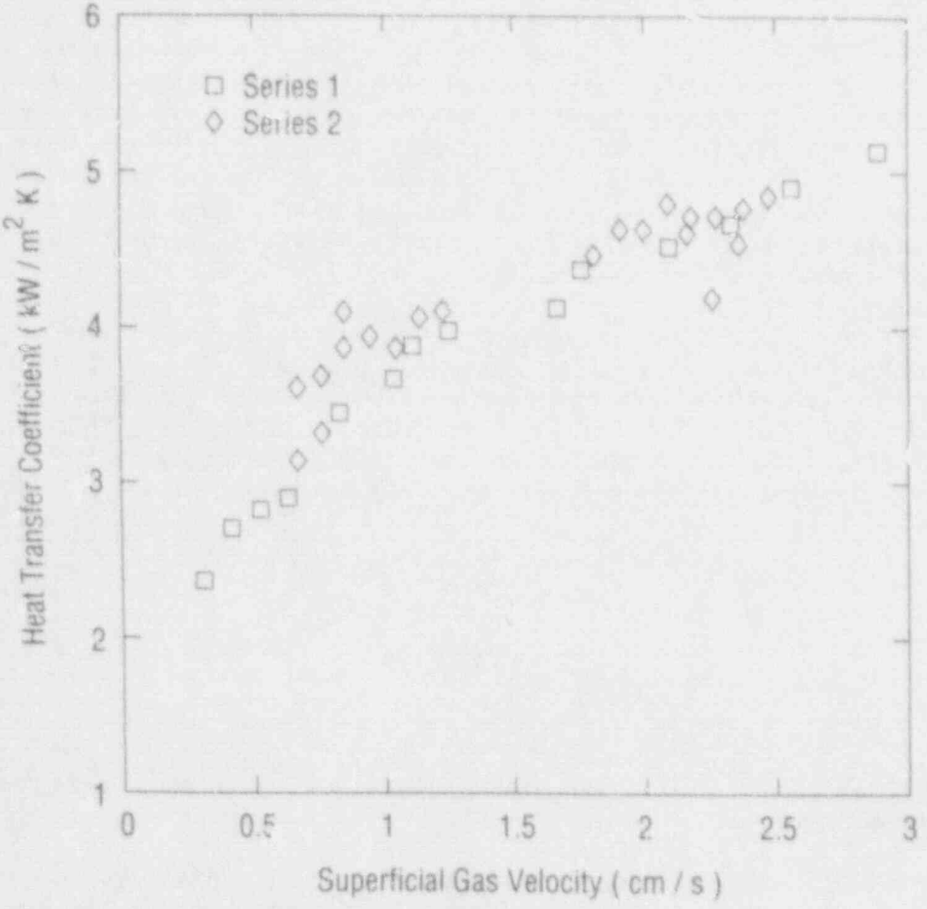

Figure 17. Bubbling heat transfer coefficients vs. superficial gas velocity for a water pool to a vertical wall.

6.5 Model Development

A composite of all the heat transfer data from a bubbling pool to a vertical instrument is displayed in Figure 18. Included in the figure are the data of Greene (1989), Kolbel (1958), Hart (1976), and Fair (1962). These data all demonstrate the trend of increasing heat transfer coefficient with increasing superficial gas velocity as previously observed. The large spread in the data for the heat transfer coefficient (200 - 5400 W/m^2K) is due to the large range of Prandtl number reflected by this data base, from 2.5 to 7500. It is desirable to develop a model that would be applicable over this range of Prandtl number.

The experimental data that were used to construct the correlation model were chosen, both from the present experiments and from the literature, to encompass the widest possible range for the appropriate dimensionless scaling parameters. The dimensionless parameters are listed in Table 7, along with the ranges of these parameters covered by the experimental data and a range considered characteristic of MCCI conditions. Note that, for the most part, the characteristic MCCI ranges fall within the ranges of these parameters covered by the experimental data; as a result of this comparison, the resulting correlation model is expected to be reliable for application to MCCI conditions for pools with Prandtl number greater than unity.

The present data will be compared to the analytical model of Konsetov (1966), since it is the only model which was presented that has a theoretical basis, and the modified version reported by Blottner (1979). Neither the Konsetov nor the Blottner model are in dimensionless form. Introducing the Nusselt number and Grashof number as defined in the Nomenclature, it is straight forward to transform Equations (35) and (37) to dimensionless form as shown below,

$$Nu = 0.25\ Gr_3^{1/3}\ Pr^{1/3} \tag{35a}$$

and

$$Nu = 0.37\ Gr_3^{1/3}\ Pr^{1/3} \tag{37a}$$

In the application of either of these equations, the void fraction may be estimated from Equation (38).

All the heat transfer data displayed in Figure 18 were non-dimensionalized and correlated according to the same format just described for the Konsetov and Blottner models. The dimensionless model that was developed covers a range of Grashof number (Gr_3) of seven orders of magnitude and is shown in Figure 19. The dimensionless correlation that was developed is shown below;

$$Nu = 0.37\ Gr_3^{1/3}\ Pr^{1/3} \tag{37a}$$

This equation is identical to the dimensionless form of Blottner's (modified Konsetov) equation, and is applicable for fluids with Prandtl number greater than unity.

Table 7

Ranges of Dimensionless Scaling Parameters
for Bubbling Heat Transfer to a Vertical Wall

Dimensionless Group	Experimental Range	Characteristic NPP Range*
Gr	10^2 - 1.3×10^5	5×10^3 - 10^5
Pr	2.5 - 7400.	6.0 - 9.0
Nu	1.6 - 26.6	6.3 - 35.7

*Calculated from CORCON-MOD 2.04 Standard Problem.

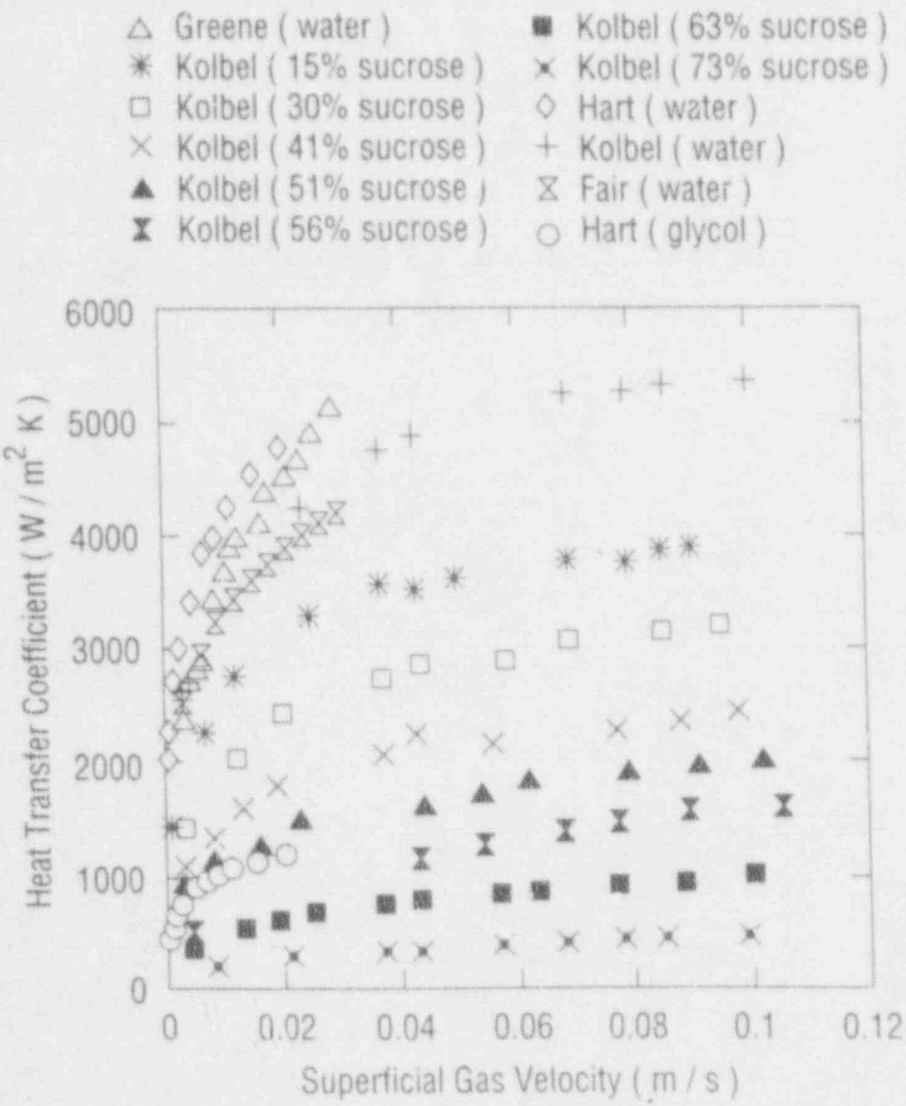

Figure 18. Composite data for bubbling heat transfer coefficients vs. superficial gas velocity: Prandtl number range 2.5-7500.

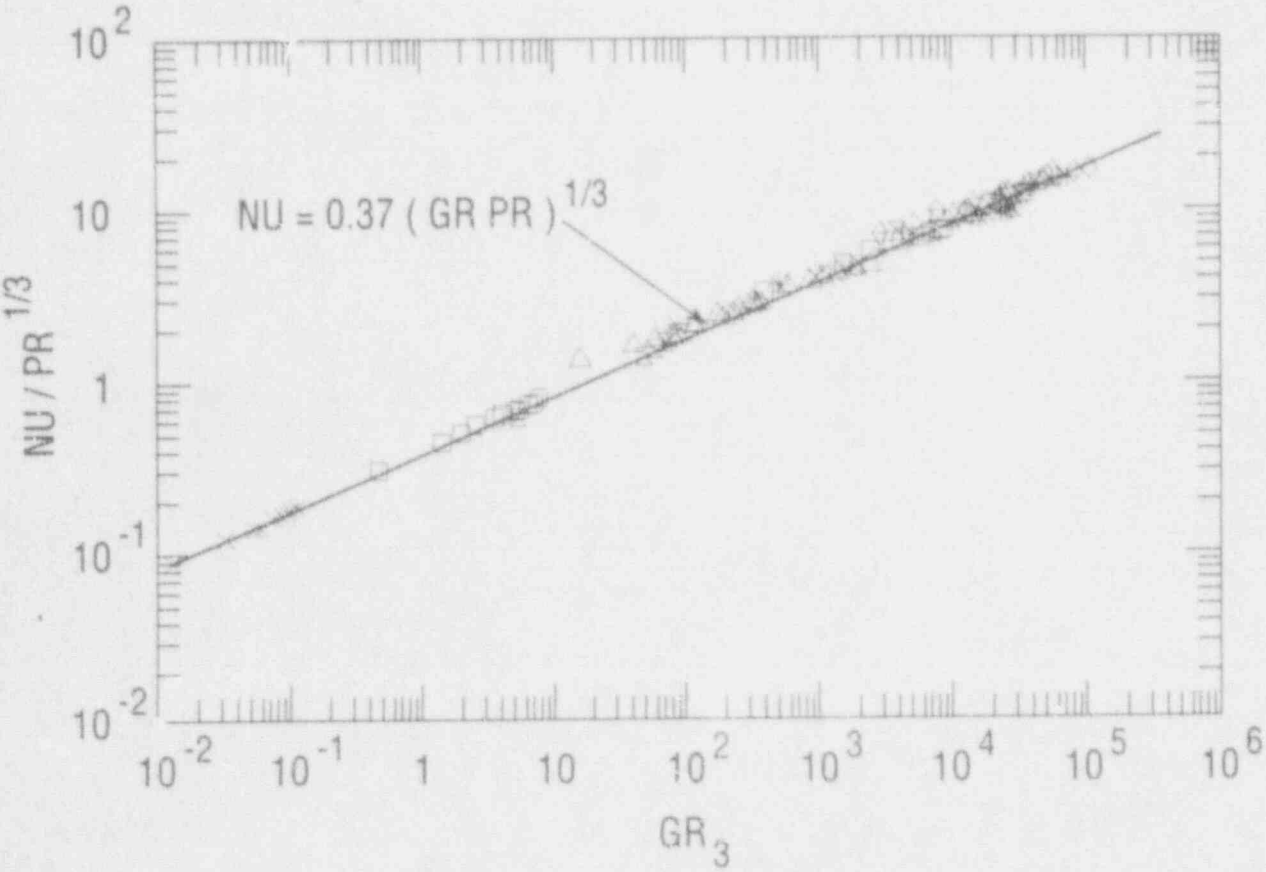

Figure 19. Dimensionless correlation of bubbling heat transfer data to a vertical wall.

6.6 Summary

Data for heat transfer from a bubbling pool to a vertical wall were presented which cover a range of Prandtl number of 2.5 - 7500. The modeling of this data can be input into the CORCON code and is directly applicable for evaluating lateral heat loads from an oxide layer to a vertical wall. The data were non-dimensionalized in a manner suggested by the analysis of Konsetov (1966). The resulting correlation was found to be a function of the Grashof number defined on the basis of void-buoyancy (Gr_3), and identical in structure to the model developed by Blottner (1979), a modified form of the Konsetov model. The resulting dimensionless model was found to cover a range of modified Grashof number from 10^{-2} to 10^{5}. Additional work would be necessary to develop a lateral heat transfer model from a bubbling metal layer to a vertical wall. Such a model would be useful for CORCON analyses of metallic layers.

7. HEAT TRANSFER FROM A HORIZONTAL BUBBLING SURFACE TO AN OVERLYING POOL

In addition to the enhanced lateral heat transfer from a bubbling pool to vertical sidewalls, it is of interest to examine the effect of gas bubbling on the downward heat transfer from the bubbling pool to the base when the gas bubbling is through the base. This is primarily of interest when considering hypothetical core melt accidents in nuclear reactors. If a reactor core becomes molten and penetrates the reactor vessel, it may attack the concrete basemat of the containment. The ablating concrete would release non-condensable gases that rise through the molten pool. It is important to know the heat transfer rate from the molten pool to the bubbling concrete surface in order to accurately calculate the rate of ablation of the concrete.

7.1 Background

Heat transfer to a gas-evolving surface from an overlying pool was initially modeled as if there were a stable gas film between the surface and the pool. This situation is similar to film boiling as shown by Benjamin (1979). In film boiling on a horizontal flat plate or heat transfer through a stable gas film, as in the sublimation of ice under a pool of water (Dhir et al., 1977; Reimann and Alsmeyer, 1982), the gas is released in a fixed geometrical pattern where the relative bubble locations are governed by the Taylor instability theory. Recently, Bradley (1988) suggested that heat transfer from an overlying pool to an outgassing surface is distinctly different than from simple gas film models. He found that the gas release from a concrete surface is less than required to form a gas film, and intermittent pool-concrete contact would occur. In this case, the heat transfer would be strongly dependent upon the liquid-solid contacts and the increased movement of liquid past the heat transfer surface caused by the bubbling action.

Sims and Duffield (1971) attempted to correlate porous and drilled surface bubbling heat transfer with nucleate boiling to explain the hydrodynamic aspects of the heat transfer mechanisms in nucleate boiling. They found that when the latent heat transport is small porous surfaces do imitate nucleate boiling, but that all their drilled surface data poorly modeled nucleate boiling since "the number of bubble generating sites does not vary with the amount of gas leaving the heat transfer surface." Kutateladze and Malenkov (1976) used several drilled heat transfer surfaces with varying hole densities, 4 to 400 sites/cm^2. They showed that as the number of holes increased, the heat transfer coefficient of a drilled plate approached that of a porous surface which in turn could be equated to nucleate boiling under a limited range of superficial gas velocities.

A complicating factor in trying to understand the heat transfer mechanisms in bubbling is the interaction between bubbles as they leave the surface. When the bubbling sites are far enough away, the inter-bubble effects can be neglected. Without the inter-bubble interactions, only the effect of the bubbles jetting into the overlying pool on the surface heat transfer needs to be studied. An important question is how far away the bubbling sites have to be from each other in order to neglect inter-bubble effects.

Bard and Leonard (1967) showed that the effect of bubbling from a single

orifice on the local heat transfer decreases inversely with the distance from the orifice. They noted that for distances along a surface greater than 10 mm from the center of an orifice of 1 mm or less in diameter, the heat transfer was not affected by the presence of the bubble. This was confirmed by several nucleate boiling studies dealing with nucleation site densities on horizontal surfaces (Tien, 1962; Lienhard, 1963; Kurihara and Myers, 1960). Lienhard found that when the nucleation site density is less than approximately 0.32 sites/cm^2, the sites cease to influence one another. This site density leads to a bubble influence area on the heat transfer surface which, if assumed circular, has a radius of 10 mm, corroborating the observations of Bard and Leonard (1967). Therefore, if the bubbling sites are located far enough away from each other, the main contribution to the surface heat transfer is due to the movement of the fluid on that surface by the stirring action caused by the bubbles.

Konsetov (1966) proposed that heat transfer from a surface in a bubbling pool is due primarily to the action of turbulent eddies. He stated that approximately one-third of the heat was removed by flow normal to the surface and the remaining heat by the parallel movement of the eddies. Interestingly, Konsetov (1966) made no mention about the orientation of the heat transfer surface in the pool, whether the bubbles were emanating from the heat transfer surface or from another source, or about the specific shape of the surface. He developed a correlation using the data from two bubbling pool studies, Fair et al. (1962) and Kolbel et al. (1958). Both studies measured the heat transfer from vertical cylinders in deep pools and the bubbling came from a different source lower in the pool. The phrase "deep" means that the pool height is equal to or greater than its width. Using their data, Konsetov (1966) developed a correlation which accounted for the void fraction in the bubbling pool as a function of the superficial gas velocity and a range of sizes for the turbulent eddies. From data which covered a range of dynamic viscosity of over three orders of magnitude he developed the following heat transfer relationship,

$$h/k\ (\nu^2/g)^{1/3}\ Pr^{-1/3}\ (\mu_w/\mu)^{0.14} = 0.25\ \alpha^{1/3} \tag{40}$$

where α is the void fraction. The void fraction was empirically determined by Kutateladze, as shown in Konsetov (1966), to be:

$$\alpha = 0.4[j_g^{2/3}\ (g\ \sigma/[\rho_\ell - \rho_g])^{-1/6}\ (\rho_\ell/\rho_g)^{0.15}] \tag{41}$$

Konsetov evaluated Equation (41) for an unspecified gas-liquid system and, upon substitution into Equation (40) arrived at the following equation for the bubbling heat transfer coefficient:

$$h(W/m^2K) = 0.20[k\ j_g^{0.22}\ Pr^{1/3}\ (\mu/\mu_w)^{0.14}\ (g/\nu^2)^{1/3}] \tag{42}$$

It should be pointed out that this formula is quite insensitive to variations in the properties in Equation (41) and is applicable to a wide range of fluids. The correlation coefficient in Equation (42) is not dimensionless; it has units of $(m/s)^{0.22}$ and requires the other variables to be of consistent units. In this correlation all properties are calculated at the pool temperature unless indicated otherwise.

Duignan et al. (1990) examined the heat transfer rate from a horizontal bubbling surface when the bubble sites are "sparsely" located. A bubble site density of 0.11 sites/cm^2 was chosen to approximate the spacing of bubbles

generated by a Taylor instability mechanism. The interdependence of the bubbles should be minimized and the predominant heat transfer mechanism should be the stirring action created by the bubbling jets into the pool. Their study is described in some detail below.

7.2 Experiment

The apparatus consisted of two 6.35-mm thick stainless steel plates that sandwiched a flexible electrical heater in a horizontal position. A vertical 101.6-mm inside diameter quartz tube was mounted over the top plate and was filled to varying heights of water. The pool height was adjusted by changing the height of a makeup reservoir which was maintained at the pool temperature. The two steel plates had nine 1-mm holes which were drilled in a square geometry with the closest inter-hole spacing being 27.2 mm to conform with previously assumed bubble locations (Benjamin, 1979). These drilled holes were fed by a gas-filled plenum. The entire apparatus was insulated so that heat flow radially outward and downward was negligible in comparison to the upward flow through the bubbling pool. The upper heat transfer plate had twelve type-K thermocouples. They were positioned and installed in order to determine the average heat flux through the plate and the average surface temperature. After the gas flow was established through the apparatus, it was filled with water to a predetermined height. The heating coil maintained a constant heat flux through the heat transfer plate of approximately 26 kW/m^2 for all the experimental runs.

7.3 Results

Figure 20 shows the deep pool data of Duignan (1990) over the entire range of superficial gas velocities. Over that range the heat transfer coefficient varied only about 20%, demonstrating only a small dependence of the heat transfer coefficient on the superficial gas velocity. These data are for pool heights greater than the pool diameter, which was 10.2 cm. Included in Figure 20 are the water pool data of Kolbel et al. (1958) and the correlation of Fair et al. (1962). Even though these studies involved heat transfer surfaces that were neither flat, horizontal, nor the source of the bubbling, as was the case in the Duignan's study, their data agree reasonably well with Duignan's measurements in both magnitude and trend. Konsetov's (1966) turbulent heat transfer model seems to predict Duignan's heat transfer data. The correlation coefficient in Equation (42) was re-calculated by Duignan for his data and found to be 0.28. As previously mentioned, the constant that Konsetov obtained was 0.20. This observation is consistent with the observation of Greene (1989) who found that, on the average, the measured bubbling heat transfer coefficient from a water pool to a vertical boundary exceeded the Konsetov model prediction by a similar amount.

An interesting result shown in Figure 20 is that for superficial gas velocities greater than 0.6 cm/s, the heat transfer from a solid surface to a liquid pool is neither dependent on the orientation of the heat transfer surface, horizontal or vertical, nor on the location of the bubbling source; that is, whether the bubbles pass through the heat transfer surface itself or come from some other, lower, surface. These results support the following observations: the bubbles that are leaving the heat transfer surface do not contribute to the local heat transfer when they are "sparsely" located, the role of the superficial gas velocity is to maintain the liquid pool turbulence, and the pool is deep

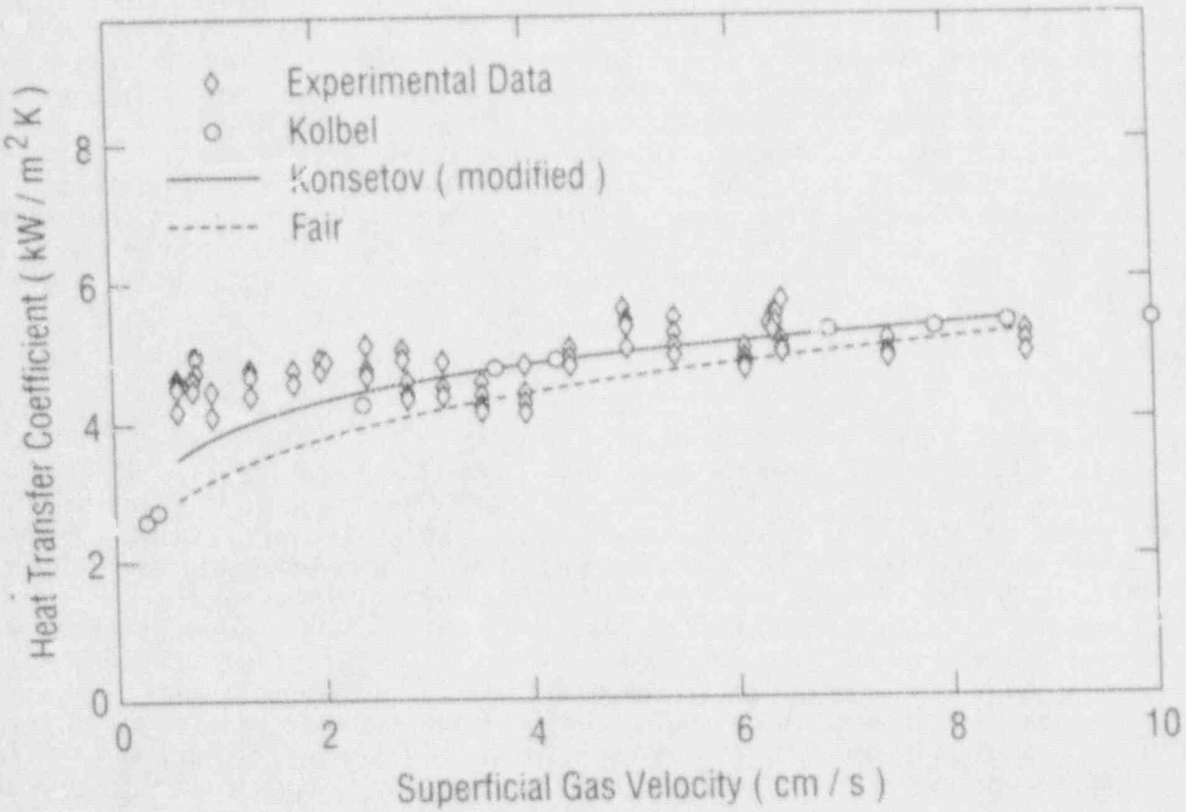

Figure 20. Heat transfer coefficient from a horizontal bubbling surface vs. superficial gas velocity.

enough to not affect the turbulent structure in the pool.

The first observation is substantiated by a criterion developed by Kutateladze and Styrikovich, as found in Wallis (1969). They showed that when the gas leaving an orifice exceeds a critical velocity, it no longer forms bubbles at the orifice but forms a jet which breaks into bubbles later in the pool. Applying the Kutateladze and Styrikovich criterion to the present tests predicts a superficial gas velocity of approximately 2.8 cm/s in the present apparatus for transition from discreet bubbles to jet flow from the drilled orifices. Since there was no discernible change in the heat transfer coefficient at that gas velocity, this suggests that the bubbles which form and break off from an orifice do not control the heat transfer from that surface when they are located far enough away from each other.

The second observation is supported by the result that the heat transfer coefficient is not strongly dependent upon the superficial gas velocity. It is observed that for j_g greater than 2 cm/s the data are bounded by Konsetov's turbulent pool model which would suggest that the liquid pool was turbulent.

The third observation was investigated by varying the pool height. The Konsetov model assumes that the characteristic length scale, the average size of a turbulent eddy, is a constant; he assumed it only to be a function of the inside diameter of the pool. Figure 21 shows that the heat transfer coefficient was not affected by changing the pool height as long as the height was at least 60% of the diameter. Below that level, the heat transfer coefficient appeared to be directly proportional to the pool height. This decrease in heat transfer may have been caused by a reduction in the average turbulent eddy size, a reduction in eddy motion due to the smaller pool, or a combination of both effects.

Heat transfer measurements could not be made accurately for pool heights lower than approximately 2.5 cm because of the difficulty in maintaining a constant liquid height and the violent splashing of the liquid from the bubbling pool. The dependence of the heat transfer coefficient on the pool height, as shown in Figure 21, was measured at a constant superficial gas velocity of 6.4 cm/s. This dependence was also investigated at lower gas velocities. Although the data base for the lower superficial gas runs was much smaller and had considerably more scatter than the data in Figure 21, the heat transfer coefficient was found to behave similarly.

7.4 Summary

For a bubble site density of 0.11 sites/cm^2, the overall heat transfer mechanism in pool bubbling was not affected by the formation of the bubbles at the surface. The heat transfer appeared to be a function of the turbulence generated by the bubble action in the pool. The Konsetov turbulent heat transfer model, developed for a heat transfer surface in a bubbling pool where the bubbles come from below the surface, predicted the heat transfer with bubbling through the surface, as long as the bubbling sites were sparsely located. For the present data, changing the coefficient in Equation (42) to 0.28 gave a best-fit to the data.

Heat transfer in a bubbling pool has been found to be a function of the

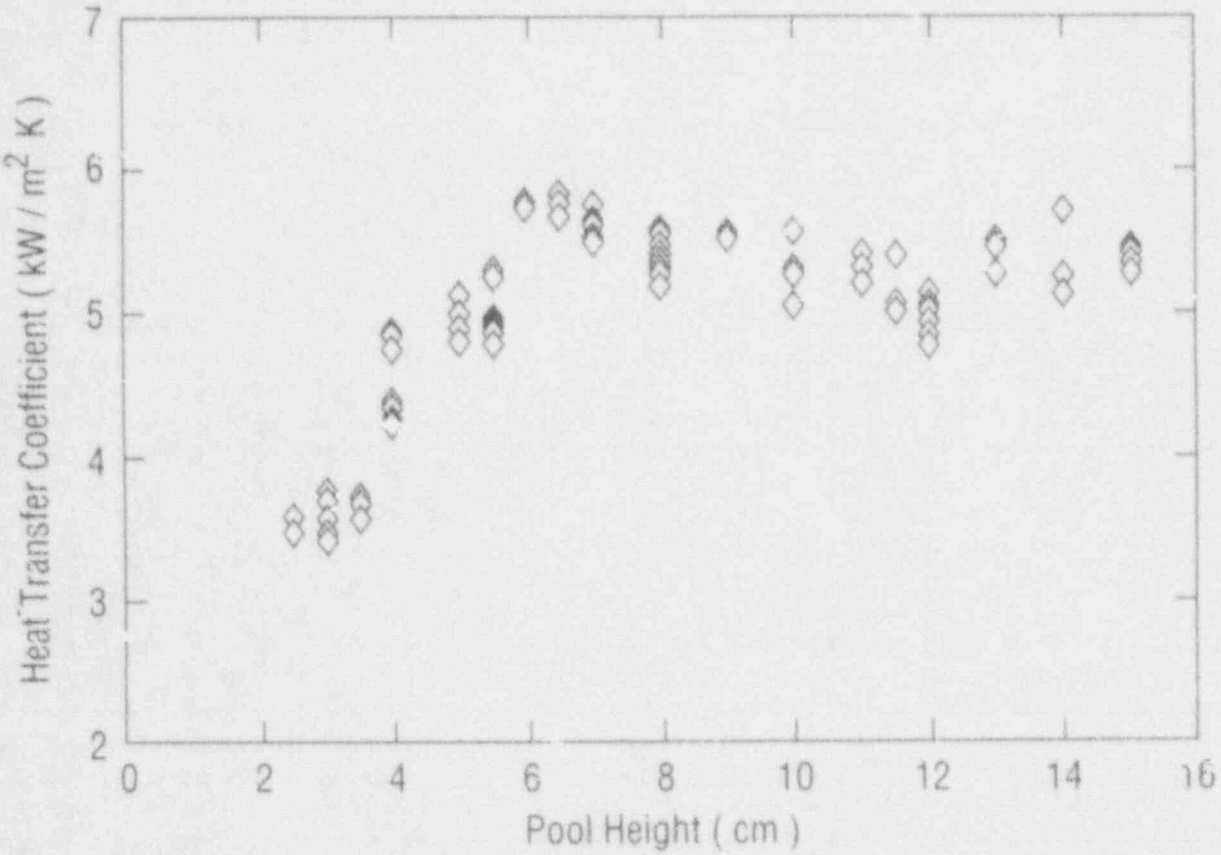

Figure 21. The effect of pool height on the heat transfer coefficient from a horizontal bubbling surface at a constant superficial gas velocity.

pool height if the pool height is lower than 60% of the pool diameter. This is rigorously true for the study of Duignan et al. (1990) which utilized a pool 10.2 cm in diameter with a bubbling site density of 0.11 site/cm^2. For pool heights greater than 60% of the diameter, the heat transfer coefficient (at a fixed superficial gas velocity) is a constant. For a deep pool (pool height greater than 60% of the vessel diameter), the heat transfer coefficient is a weak function of the superficial gas velocity, for j_g greater than 0.6 cm/s.

Molten core-concrete interactions are generally considered to be deep in the above sense. The heat transfer model and data that have been developed in this section are available for comparison to the present downward heat transfer modeling in CORCON. The CORCON code clearly does not recognize this depth-dependence of the downward heat transfer coefficient to a bubbling surface. This may be important in circumstances in which molten core debris is spread out to shallow depths and in contact with structures, such as a Mark I steel containment shell.

8. DRAG AND INSTABILITY OF LIQUID DROPLETS SETTLING IN A CONTINUOUS FLUID

In the case of severe core meltdown accidents in nuclear power reactors, the public risk is a direct function of the physical threat to the reactor containment and the release of radionuclides from the molten core to the environment during the stage of the accident termed the molten core-concrete interaction (MCCI) stage. The MCCI presupposes that the core meltdown has proceeded uninterrupted, that the high temperature core-melt has penetrated the reactor pressure vessel, and that the core has been deposited on the concrete floor below. Heat transfer from the molten core debris is sufficient to melt the concrete, which will then release H_2O and CO_2 gases due to the decomposition of hydroxides and carbonates in the concrete as well as the vaporization of water. As these gases rise through the molten pool of core debris, they can reactor exothermically with molten metals in the pool, releasing more energy into the core debris, converting H_2O and CO_2 into H_2 and CO, and chemically transforming some condensed phase radionuclides into intermediate volatile species by reactive vaporization. Since the core debris consists of molten oxides (UO_2, ZrO_2, FeO, etc.) and molten metals (Zr, Fe, Ni, Cr, etc.) which are immiscible, the molten pool would be vertically stratified in the absence of the gas bubbling action of the concrete decomposition gases. It is the action of the rising gas bubbles that enhances the boundary surface (bottom and side) and interfacial heat transfer rates and that drives the entrainment mass transport across the interface between the stratified layers of oxides and metals. If the rising gas bubbles are not able to entrain the lower liquid into the upper layer, the pool will remain stratified.

To determine the configuration of multi-fluid pools with bubbling-induced mass entrainment across the liquid-liquid interface, it is necessary to address the motion of the entrained liquid drops as they resettle downwards under the action of gravity. In the absence of entrainment, the pool will remain stratified as seen in Figure 14a. If the rate of settling of the entrained drops can balance the rate of entrainment driven by the rising gas bubbles, the pool can take on an equilibrium mixture, as seen in Figure 14b. If the rate of settling cannot keep pace with the rate of entrainment, the lower fluid will continue to be pumped into the upper layer until the pool would become fully mixed and the concept of layers becomes irrelevant (Figure 14c). In this section we will examine the drag characteristics of solid spheres and liquid droplets.

Studies of the relationship between the terminal velocity and drag coefficient of spheres falling in a semi-infinite medium have been numerous. The broad scope of applications for such research, from the analysis of particle motion in fluids to the study of phenomena such as rainfall and boiling, is a clear indication as to the importance of this field of study. A review of the literature indicates that there exists a substantial body of work devoted to the study of both solid spheres and liquid droplets. We will discuss the existing data and the data from our studies over a wide range of Reynolds number, and compare the data with the predictions of existing drag correlations. In addition, the onset of droplet deformation and oscillation will be discussed and the effect upon the droplet drag will be demonstrated.

8.1 Background

The construction of a force balance on a sphere moving at a constant terminal velocity, u, results in the following expression for the drag coefficient,

$$C_d = \frac{4g}{3u_d^2}\left(\frac{\rho_d - \rho_\ell}{\rho_\ell}\right) \tag{43}$$

which is usually presented as a function of the Reynolds number, defined as,

$$Re = \frac{u_d d}{\nu_\ell} \tag{44}$$

These relationships will be needed in the following discussion.

8.1.1 Solid Spheres

A number of investigators have undertaken to develop a general correlation between the drag coefficient and Reynolds number for solid spheres. Barnea and Mizrahi (1973) studied single-particle and multi-particle fluidization and sedimentation systems, and synthesized data from 12 different sources. They proposed the following simplified correlation,

$$C_d = \left[0.63 + \frac{4.8}{\sqrt{Re}}\right]^2 , \qquad 10^{-3} < Re < 2x10^5 \tag{45}$$

Zanker (1980) used their work as the basis for the development of nomographs for determining particle settling velocities. Turton and Levenspiel (1986), in order to simplify a 10-polynomial regression correlation that had been proposed by Clift et al. (1978), developed the following relationship,

$$C_d = \frac{24}{Re}\left[1 + 0.173\ Re^{0.657}\right] + \frac{0.413}{1 + 16300\ Re^{-1.09}} , \qquad 10 < Re < 2x10^5 \tag{46}$$

which was found to correlate the existing data with better accuracy than the cumbersome set of equations suggested by Clift. In addition, Flemmer and Banks (1986), modifying the traditional Oseen (1927) approximation using a regression technique, proposed the following empirical correlation for a settling sphere,

$$C_d = \frac{24}{Re} \cdot 10^E , \qquad 10^{-4} < Re < 3x10^5 \tag{47}$$

$$\text{where } E = 0.261\ Re^{0.369} - 0.105\ Re^{0.431} - \frac{0.124}{1 + (\text{Log } Re)^2} \tag{48}$$

8.1.2 Liquid Droplets

A number of authors have examined the motion of liquid droplets falling in liquid-filled test columns. Hu and Kintner (1955) studied droplets of ten organic fluids falling in a square, water-filled column whose temperature was maintained to within ± 0.5°C. The study covered a Reynolds number range of 10 - 2000. The authors observed that there was little evidence of surface flow or internal circulation effects below a Reynolds number of 300, since the C_d vs. Re curve in this range was nearly identical to that for solid spheres. Beyond this Reynolds number range, droplet behavior departed from the predictions of solid sphere theory. A peak diameter corresponding to the maximum droplet velocity was observed in each system studied, and it was found that droplet drag increased rapidly if the Reynolds number were to exceed the critical Reynolds number based on this peak diameter and velocity. The authors calculated the Weber number based on these values for peak diameter and velocity for each system, and presented the following average critical value, $We_{cr} = 3.58$, where the Weber number is defined as,

$$We = \frac{\rho_\ell u_d^2 d}{\sigma} \tag{49}$$

and σ is the interfacial tension between the droplet and the continuous liquid. They concluded that droplet oscillation induced at this peak velocity was the primary cause for this rapid increase in droplet drag, and that droplet deformation was secondary. The authors proposed an empirical dimensionless physical property group, P, defined as,

$$P = \frac{3\ Re^4}{4\ C_d We^3} \tag{50}$$

and found that the data from all but one of their fluid systems collapsed to one curve when presented in the following format,

$$\left[Cd \cdot We \cdot P^{0.15}\right] \quad vs. \quad \left[Re / P^{0.1}\right] \tag{51}$$

Winnikow and Chao (1986) performed a similar study examining droplets of four organic liquids over a Reynolds number range of 100 to 1000. The experiments were performed at room temperature in a four inch square water-filled test column. Similar to Hu and Kintner (1955), the authors identified three distinct regions in the drag coefficient vs. Reynolds number relationship. For Reynolds numbers less than 1.0, the liquid droplets were observed to maintain their spherical shape, and the data for each system were found to be in excellent agreement with the Stokes solution for solid spheres. A transition region was indicated for 80 < Re < 300, in which droplet deformation became apparent and the measured drag coefficients were higher or lower (depending on the particular fluid involved) than those for solid spheres of equivalent diameter. A third region, beginning at Reynolds numbers between 700 to 900, marked the onset of droplet oscillation and a sharp increase in droplet drag with a slight increase in the Reynolds number. The authors noted that the minimum drag and maximum droplet terminal velocity coincided with this onset of oscillation, as had been found by Hu and Kintner. They hypothesized that this increase in droplet drag

was due to increased pressure drag resulting from droplet deformation and a shift in the position of boundary layer separation. The continued increase in droplet drag was attributed to the combined effect of deformation-induced form drag and droplet oscillation. They proposed an average critical Weber number of 4.08 as an indication of the onset of liquid droplet oscillation. This compared favorably with the value of 3.58 proposed by Hu and Kintner.

Beard and Pruppacher (1969) studied water droplets injected into a wind tunnel with a hypodermic needle. The air speed in the tunnel was adjusted until droplets of a certain size became suspended, at which point the droplet terminal velocity and tunnel air speed were equal. Droplet diameters were determined by photographic analysis. The authors' study covered a Reynolds number range of 0.2 to 200, and they proposed the following correlations for determining droplet drag as a function of Reynolds number,

$$\frac{D}{D_s} = \begin{cases} 1 + 0.102\ Re^{0.955}, & 0.2 < Re < 2.0 \\ 1 + 0.115\ Re^{0.802}, & 2.0 < Re < 21.0 \\ 1 + 0.189\ Re^{0.632}, & 21.0 < Re < 200.0 \end{cases} \quad (52)$$

where D is the measured droplet drag and D_s is the Stokes drag for a solid sphere at the same Reynolds number. The results agreed quite well with those of prior studies involving both solid spheres and liquid droplets over a comparable Reynolds number range. For Reynolds numbers greater than 200, the droplet drag was observed to increase due to distortions from the spherical shape. As a result these equations were not recommended for Reynolds numbers greater than 200 nor for the case of droplets which are experiencing distortion or oscillation, whichever comes first.

Klee and Treybal (1956) examined both rising and falling droplets for eleven fluids in a square test column. The study covered a Reynolds number range from one to 2000. The authors identified two distinct regions in plotting the droplet velocity vs. diameter, and noted that the maximum point in each curve corresponded to the point at which droplet oscillation developed. Droplet drag coefficients were consistently found to be smaller than the values predicted for solid spheres, a phenomenon which the authors attributed to the oscillation and internal circulation present in a droplet. The interfacial tension between the dispersed and continuous phase liquids was found to be a controlling parameter for droplet stability. The authors presented the following equations relating Re, C_d, and We,

$$Re = 22.2\ C_d^{-5.18}\ We^{-0.169} \quad \text{(Region I)} \quad (53)$$

$$Re = 0.00418\ C_d^{2.91}\ We^{-1.81} \quad \text{(Region II)} \quad (54)$$

where I and II refer to their regions of observed droplet stability and oscillation, respectively. The critical Weber number at which the droplets deviated from solid sphere drag was found to be, on the average, approximately equal to 8.21. This result was in good agreement with the observations of Hu et al. and Winnikow and Chao, who reported average values of the critical Weber

number of 3.58 and 4.08, respectively (for organic droplets settling in water). Once again, however, the range of the critical Reynolds number over which the droplet drag coefficient was observed to deviate from solid sphere data was small, in the range 300-600.

Similar studies were performed by Licht and Narasimhamurty (1955) and by Krishna et al. (1959), who studied liquid droplets of six fluids and 31 fluids, respectively. The droplets were of various organic liquids and the continuous fluid was once again water, just as in the studies of Klee, Winnikow, and Hu that were discussed previously. (Recall that in the study of Beard, the droplet was water and the continuous fluid was air.) In both these studies, the measured droplet drag coefficient was observed to conform closely to the established theory for solid spheres at low Reynolds numers. Departure from solid sphere drag behavior once again occurred in a narrow range of the droplet Reynolds number; the critical Reynolds number reported for the drag deviation was in the range 600-1000 for Licht and 500-1000 for Krishna. For Krishna's data, the critical Weber number for the departure of drag from solid sphere drag (an average of 31 data points) was found to be 4.04, in remarkable agreement with the result of Winnikow and Chao (1986) of 4.08. Closer examination, however, suggests that this good agreement, particularly between the results of Hu and Kintner (1955), Winnikow and Chao (1986), and Krishna et al. (1959), may be a result of the narrow range of variation in physical properties of the fluids used in these three studies, i.e., all three used very similar droplet fluids settling in a water column. As a result of this limitation, it is suspected that the critical Reynolds and Weber numbers observed, and the correlations developed on the basis of these data may be applicable only to the narrow category of organic liquid drops settling in water.

8.2 Experiment

Droplet settling studies were conducted with eight different pairs of fluids in order to further examine the droplet drag-Reynolds number functional relationship. Liquids utilized for the droplet phase included water, water/$CuSO_4$, bromoform, and mercury; liquids utilized for the continuous phase included 10 and 100 cs. silicone oils, hexane, and water. The fluid pairs were chosen in an attempt to encompass the widest range possible for the appropriate dimensionless scaling parameters. The parameters that are most important are the droplet Reynolds number, Weber number, and drag coefficient. The physical property groupings that are embedded in each of these dimensionless scaling parameters are listed in Table 8 along with the range of the property grouping that was spanned by the chosen fluid pairs. As is shown in Table 8, the property groups were varied by as much as a factor of 400, and a characteristic value for NPP conditions was in the range covered by the experiments. The actual ranges of the dimensionless scaling parameters, Reynolds number, Weber number, and drag coefficient, are shown in Table 9. The resulting ranges of these variables was as wide as practically possible and is expected to cover the range for NPP conditions that may be encountered. The droplet volume was varied over the range 1 $\mu\ell$ to 6 mℓ; combined with the variations in liquid properties, this resulted in a data base for the droplet drag coefficient covering seven orders of magnitude in Reynolds number, from 10^{-3} to 10^{4}.

In order to measure the terminal velocities of the droplets, droplets of precise volumes were placed in a Teflon cup at the top of the liquid-filled test

Table 8

Ranges of Appropriate Property Groups
for Droplet Settling

Property Group	Experimental Range	Characteristic NPP Value
$Re \sim \nu_\ell^{-1}$ (cs^{-1})	0.96 - 198.0	1.0
$We \sim \frac{\rho_\ell}{\sigma}$ $(\frac{s^2}{cm^3})$	0.002 - 0.33	0.01
$C_d \sim \frac{\rho_d - \rho_\ell}{\rho_\ell}$	0.036 - 13.4	0.3

Table 9

Ranges of Dimensionless Scaling Parameters
for Droplet Settling

Dimensionless Group	Experimental Range	NPP Condition
Re	10^3 - 10^4	To Be
We	2 - 50	Determined By
C_d	0.3 - 100	CORCON Analysis

column. The descent of the droplet was electronically timed as it traversed a fixed course (1 meter) inscribed on the column's outer surface. The time of flight for twenty separate trials for each droplet volume was then averaged, and this average time was used to calculate an average terminal velocity. Precise measurements were made of the physical properties for each of the fluids studied over a temperature range appropriate to the droplet settling data (20-40°C). Temperature-dependent values of density, interfacial tension, and viscosity were used to calculate the Reynolds number, Weber number, and the droplet drag coefficient.

8.3 Experimental Results

The experimentally measured drag coefficient data for four of the droplet systems are illustrated in Figure 22. These droplets were observed to remain spherical during the fall period, and the measured drag coefficients were found to agree well with established models for solid sphere drag; shown in Figure 22 are the Stokes flow model for Reynolds numbers less than 0.1 and the correlations of Beard et al. (1969) for Reynolds numbers in the range 0.2 to 200 (Eqn. 52), shown here extrapolated to Re = 1000. These data are in excellent agreement with the droplet drag data of Hu and Kintner (1955), Licht et al. (1955), and Krishna et al. (1959) for Reynolds numbers below the values of the critical Reynolds number for droplet oscillation observed in each of these studies.

Previous studies have shown that, at the onset of droplet oscillation, the droplet drag suddenly departs from the solid sphere drag curve (this will be called the critical drag coefficient) and increases rapidly with a further increase in the Reynolds number. This Reynolds number has been called the critical Reynolds number, and was measured by previous investigators to lie in the range 500-1000. For nearly all these data, the corresponding critical Weber number for the onset of this phenomenon was measured to be approximately equal to four. The data for seven series of experiments from the present study are shown in Figure 23. These data were intended to cover the widest possible range of Reynolds number and Weber number, in order to test the observations of other investigators concerning the critical Reynolds number and Weber number for the onset of oscillation and drag enhancement. As is shown in the figure, the data for five of the seven fluid pairs followed the stable drag curve of Beard et al. (1969) over a range of Reynolds number of 0.2-1000. However, depending upon the fluid pair tested, deviation from the Beard model was observed to suddenly begin at Reynolds numbers as low as eight and as high as 1000. As shown in Figure 23, six of the seven fluid pairs tested experienced this departure from stable drag. Interestingly, no droplet system tested in the present study, nor from any of the previous studies cited, were able to exceed a Reynolds number of 1000 without experiencing drag departure from the stable drag curve.

In previous studies, it has been reported that the point of droplet oscillation and drag enhancement coincided with a value of the droplet Weber number approximately equal to four. However, in the present study, the critical Weber number was found to cover a much wider range than previously reported, a range of 2-50. The relationship between the critical droplet Reynolds number and critical Weber number for the onset of droplet oscillation and departure from stable drag is shown in Figure 24. It is apparent from this figure that nearly all the previous data experienced drag enhancement at a Weber number of four and in a range of Reynolds number of 400-1500. The present data, however, demonstrated this behavior for Weber numbers over the range 2-50 and Reynolds

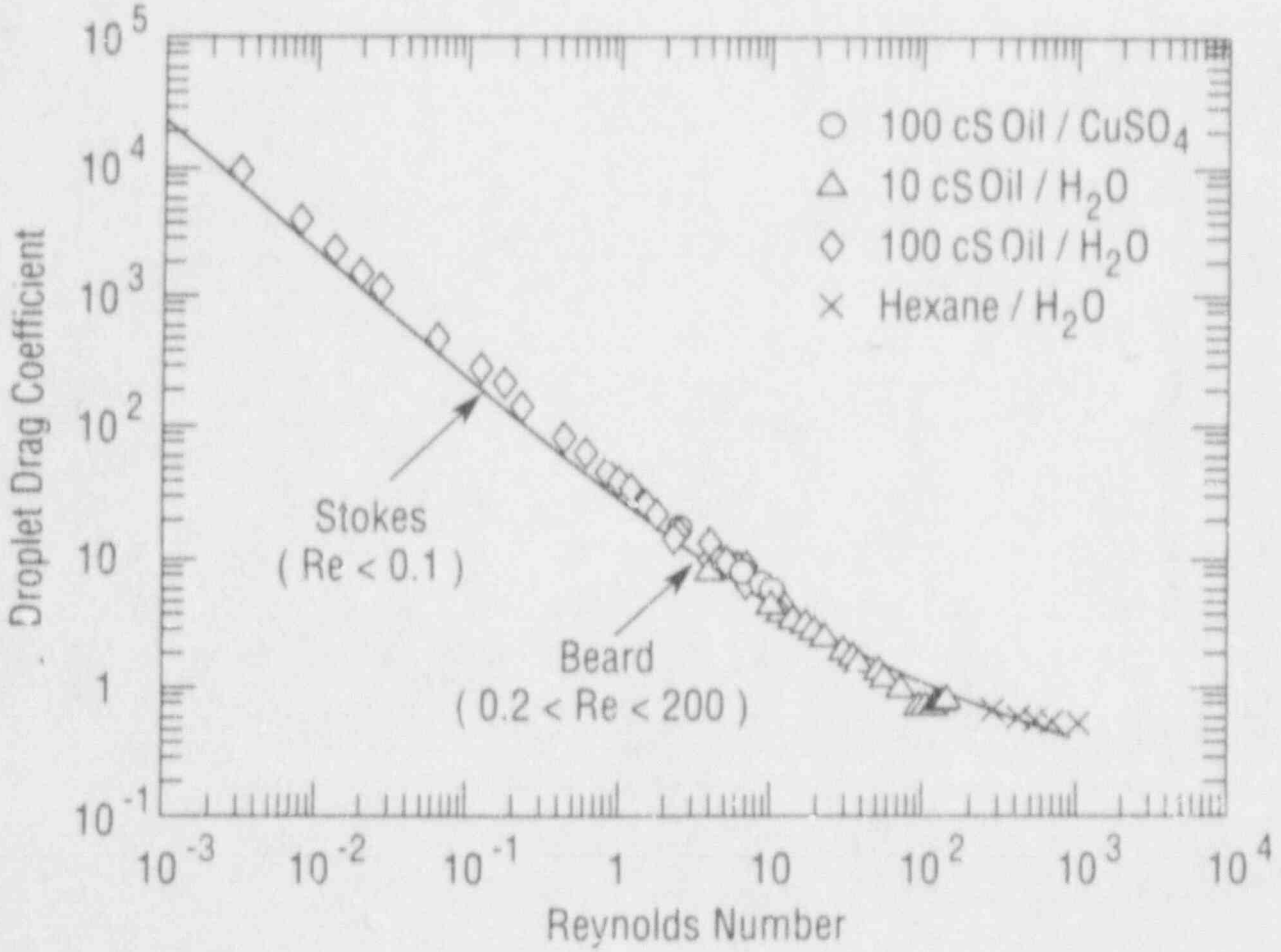

Figure 22. Drag coefficients vs. Reynolds number for stable liquid drops settling in a liquid column.

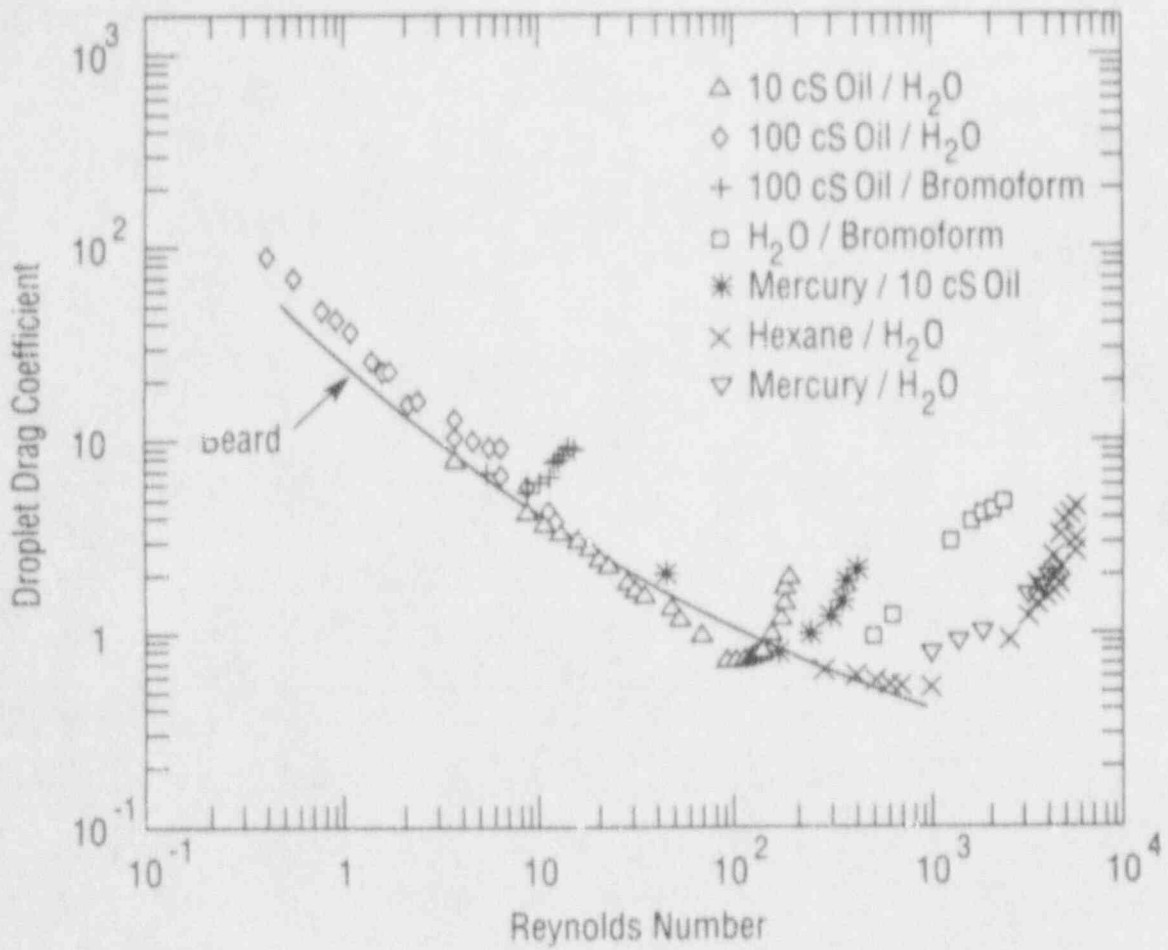

Figure 23. Effect of oscillation and instability on the droplet drag coefficient.

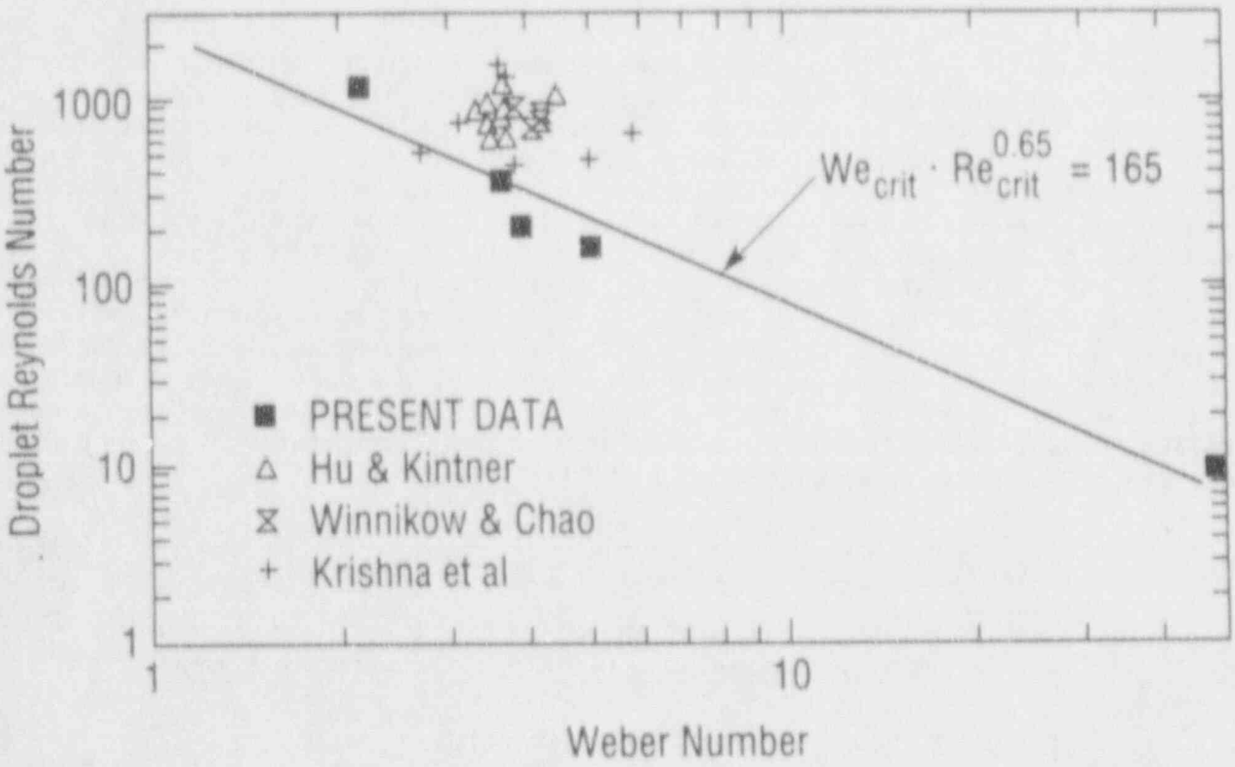

Figure 24. Critical droplet Reynolds number vs. critical Weber number for onset of droplet oscillation and deviation from stable drag.

numbers from less than ten to greater than 1000. From the present data, a correlation relationship between the Reynolds number and Weber number at this point of departure from stable drag was calculated as shown below,

$$We_{crit} * Re_{crit}^{0.65} = 165 \quad (55)$$

It is clear that for values of $We*Re^{0.65}$ less than 165, a particular droplet-continuous liquid pair would be stable, and the droplet drag would be well characterized by any of the solid sphere drag models. As the critical value of $We*Re^{0.65}$ is approached, the droplet would begin to experience oscillation and deformation. For values greater than 165, extensive droplet oscillation and deformation would result in an increase in the droplet drag far above that for an equivalent spherical drop as the Reynolds number were to increase.

Liquid droplets for which the value of $We*Re^{0.65}$ exceeds 165 will have deviated from the stable drag curve and the trend of the droplet drag coefficient will be to increase with increasing Reynolds number. The data from the present study that evidenced this behavior as shown in Figure 23 are those that depart from the Beard line and move up and to the right. As shown in the figure, this behavior was found to occur for Reynolds numbers as low as eight. It is evident that many droplet systems may experience this drag enhancement and that for practical applications, the unstable drag regime, described by $We*Re^{0.65}$ greater than 165, may be the dominant regime. In order to develop an empirical model for the data in this regime (for $We*Re^{0.65} > 165$), the droplet drag coefficients and droplet Reynolds numbers for these data were normalized by the corresponding critical values for departure from stable drag which were previously determined and shown in Figure 24. From the normalized data, a functional empirical relationship between the droplet drag coefficients and Reynolds numbers was calculated by least squares regression analysis and is given by,

$$C_d/C_{d,crit} = [Re/Re_{crit}]^{1.12} \quad (56)$$

The normalized data are shown along with Eqn. 56 in Figure 25. This is the drag relationship that is appropriate for droplet systems for which $We*Re^{0.65}$ exceeds 165.

8.4 Summary

Data for droplet drag have been found to agree well with established solid sphere or spherical droplet models and correlations as long as the droplets maintained their spherical shape while settling under the influence of gravity. At the Reynolds and Weber numbers indicative of the onset of droplet oscillation and deformation, the drag coefficients for the droplets were observed to suddenly depart from the solid sphere drag curve and increase with increasing Reynolds number. This sudden departure from classical drag has been found to occur for Reynolds and Weber numbers over the ranges 10-1000 and 2-50, respectively. No stable drag data were found for Reynolds number greater than approximately 1000. It was found that the parameter, $We*Re^{0.65}$, at this critical point was approximately 165. For values less than this criterion, the droplet drag was stable and agreed well with spherical drop models; for values greater than this criterion, the droplet drag departed from stable drag models and the drag

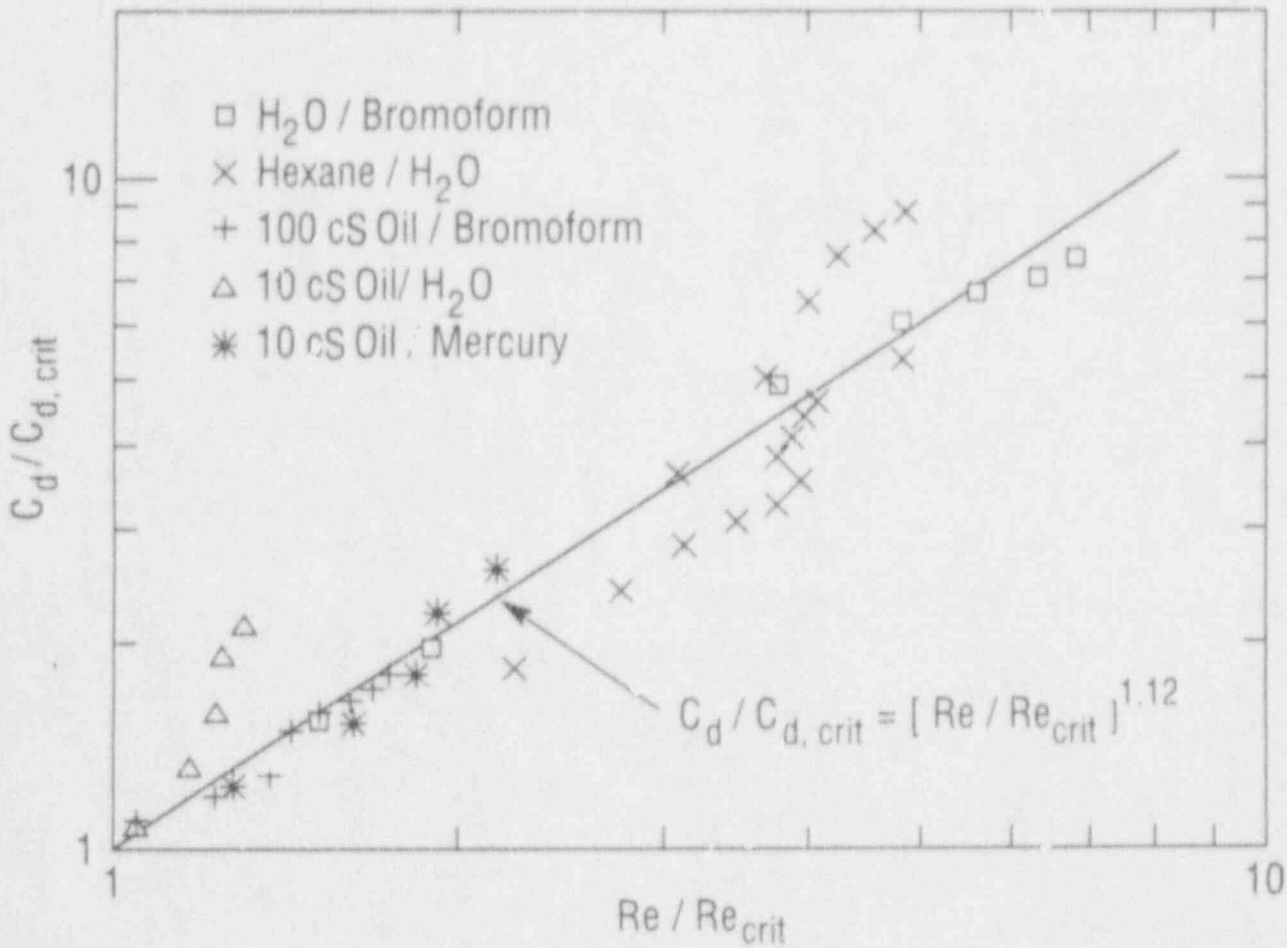

Figure 25. Correlation of unstable drag data.

coefficient increased with increasing Reynolds number.

When the droplet drag coefficients and Reynolds numbers in the unstable drag regime were normalized by the corresponding critical values for the departure from stable drag, the normalized droplet drag coefficient was found to correlate well to the normalized droplet Reynolds number.

These models for stable and unstable droplet drag and the criterion for transition from stable to unstable drag are appropriate for implementation into the CORCON-MOD3 computer code for the modeling of molten core-concrete interactions. Once these models have been implemented, the code capability to specify the configuration of the molten core debris, i.e., stratified, heterogenously mixed, or homogeneously mixed, will be complete and integral testing of the computer code predictions will be possible.

9. CONCLUDING REMARKS

This report has been prepared with the intention of presenting an introduction to the problems posed by heat, mass, and momentum transfer in multi-fluid bubbling pools. A survey of contributions in each of the seven technical areas that were discussed has been presented, along with a more in-depth discussion of the investigations undertaken by the author and co-workers. It is clear from this review that this field of heat, mass, and momentum transfer in multi-fluid bubbling pools has not been the subject of extensive research, and may represent a fertile research area for those who find its remaining problems interesting. Nevertheless, the existing contributions have been significant, and a comprehensive set of models have been developed which, when applied to the analysis of multi-fluid bubbling pools, yield reliable results. At this time, the remaining uncertainties present an immediate opportunity for research by investigators who are so inclined.

One issue which needs to be explored is the effect of wide-spread bubbling upon the entrainment onset and entrainment rate models. You recall these models were based upon data and analyses of single-bubble systems. A similar situation exists for the study of droplet drag and settling and the onset of droplet instability; the work which was reported here was similarly based upon single-droplet studies. The study of bubbling heat transfer to vertical boundaries has an impressive data base, covering a range of Prandtl number from 2.5 to 7500. However, there is no data for bubbling heat transfer from liquid metal pools (low Prandtl number). This same situation exists for horizontal bubbling surfaces as well; all the data is for water. Finally, nearly all the studies presented represented single-bubble or droplet systems or pools in the bubbly flow regime. Little is known concerning the applicability of these models at higher gas injection rates, rates at which the bubbling pools could be in churn-turbulent flow.

REFERENCES

Bard, Y. and E. F. Leonard, "Heat Transfer in Simulated Boiling," Int. J. Heat Mass Transfer, 10, 1727 (1967).

Barnea, E. and J. Mizrahi, "General Correlation for Fluidization and Sedimentation," The Chemical Engineering Journal, 5, 171 (1973).

Beard, K. V. and H. R. Pruppacher, "A Determination of the Terminal Velocity and Drag of Small Water Drops by Means of a Wind Tunnel," Journal of Atmospheric Sciences, 26, 1066 (1969).

Benjamin, A. S., "Core-Concrete Interfacial Heat Transfer and Molten Pool Dynamics," Trans. Am. Nucl. Soc., 33, 527 (1979).

Blottner, F. G., "Hydrodynamics and Heat Transfer Characteristics of Liquid Pools With Bubble Agitation," NUREG/CR-0944 (1979).

Bradley, D. R., "Modelling of Heat Transfer between Core Debris and Concrete," 1988 National Heat Transfer Conference, ANS Proceedings, 3, 37 (1988).

Cheung, F. B., G. Leinweber, and D. R. Pedersen, "Bubble-Induced Mixing of Two Horizontal Liquid Layers with Non-Uniform Gas Injection at the Bottom," Proceedings of the Sixth Information Exchange Meeting on Debris Coolability, EPRI NP-4455 (1986).

Clift, R., J. R. Grace and M. E. Weber, Bubbles, Drops, and Particles, Academic Press, New York (1978).

Dhir, V. K., J. N. Castle and I. Catton, "Role of Taylor Instability on Sublimation of a Horizontal Slab of Dry Ice," J. Heat Transfer, 99, 411 (1977).

Duignan, M. R., G. A. Greene and T. F. Irvine, Jr., "Heat Transfer from a Horizontal Bubbling Surface to an Overlying Water Pool," Chem. Eng. Comm., 87, 185 (1990).

Epstein, M., D. J. Petrie, J. H. Linehan, G. A. Lambert, and D. M. Cho, "Incipient Stratification and Mixing in Aerated Liquid-Liquid or Liquid-Solid Mixtures," Chem. Eng. Sci., 36, 784 (1981).

Fair, J. R., A. J. Lambright, and J. W. Andersen, "Heat Transfer and Gas Holdup in a Sparged Contactor," Ind. Eng. Chem., Process Des. Dev., 1, 33 (1962).

Flemmer, R. L. C. and C. L. Banks, "On the Drag Coefficient of a Sphere," Power Technology, 48, 217 (1986).

Gonzalez, F. and M. Corradini, "Experimental Study of Pool Entrainment and Mixing Between Two Immiscible Liquids with Gas Injection," Proceedings of the CSNI Specialists' Meeting on Core Debris-Concrete Interactions, EPRI NP-5054-SR (1987).

REFERENCES (continued)

Greene, G. A., O. C. Jones, Jr., and N. Abuaf, "Correlation of Local Heat Flux from Inclined Volume-Heated Pools in Bubbly Flow," Proceedings of Nineteenth National Heat Transfer Conference, ASME Paper No. 80-HT-91 (1980).

Greene, G.A. and C.E. Schwarz, "An Approximate Model for Calculating Overall Heat Transfer Between Overlying Immiscible Liquid Layers with Bubble Induced Liquid Entrainment," Proceedings Fifth Post Accident Heat Removal Information Exchange Meeting, Karlsruhe, FRG, p. 251 (1982).

Greene, G. A., J. C. Chen, and M. T. Conlin, "Onset of Entrainment Between Immiscible Liquid Layers Due to Rising Gas Bubbles," Int. J. Heat Mass Transfer, 31, 1309 (1988a).

Greene, G. A. and T. F. Irvine, Jr., "Heat Transfer Between Stratified Immiscible Liquid Layers Driven by Gas Bubbling Across the Interface," 1988 National Heat Transfer Conference, ANS Proceedings 3, 31 (1988b).

Greene, G. A., "Heat Transfer from a Liquid Pool in the Bubbly Flow Regime to a Vertical Boundary," 1989 National Heat Transfer Conference, AIChE Symposium Series 269, 85, 223 (1989).

Greene, G. A., J. C. Chen, and T. F. Irvine, Jr., "Heat Transfer Between Overlying Immiscible Liquids Due to Bubbling-Induced Mass Entrainment Across the Interface," Proceedings Ninth International Heat Transfer Conference, Jerusalem, Israel, 3, 467 (1990).

Greene, G. A., J. C. Chen, and M. T. Conlin, "Bubble-Induced Entrainment Between Stratified Liquid Layers," Int. J. Heat Mass Transfer, 34, 149 (1991).

Hart, W. F., "Heat Transfer in Bubble-Agitated Systems: A General Correlation," Ind. Eng. Chem., Process Des. Dev., 15, 109 (1976).

Hu, S. and R. C. Kintner, "The Fall of Single Liquid Drops Through Water," AIChE Journal, 1, 42 (1955).

Klee, A. and R. E. Treybal, "Rate of Rise or Fall of Liquid Drops," AIChE Journal, 2, 444 (1956).

Kolbel, H., W. Siemes, R. Maas, and K. Muller, "Warmeubergang and Blasensaulen," Chem. Ing. Tech., 30, 400 (1958).

Konsetov, V. V., "Heat Transfer During Bubbling of Gas Through Liquid," Int. J. Heat Mass Transfer, 9, 1103 (1966).

Krishna, P. M., D. Venkateswarlu and G. S. R. Narasimhamurty, "Fall of Liquid Drops in Water: Drag Coefficients, Peak Velocities, and Maximum Drop Sizes," J. Chem. Engr. Data, 4, 340 (1959).

Kurihara, H. M. and J. E. Myers, "The Effects of Superheat and Surface Roughness on Boiling Coefficients," AIChE Journal, 6, 83 (1960).

Kutateladze, S. S. and I. G. Malenkov, "Fluid- and Gas Dynamical Aspects of Heat Transfer in the Injection Bubbling and Boiling of Liquids," High Temperature, 14, 703 (1976).

Lee, M. and M. S. Kazimi, "Interfacial Heat Transfer Between Bubble Agitated Immiscible Liquid Layers," Proceedings Sixth Information Exchange Meeting on Debris Coolability, UCLA, EPRI NP-4455 (1984).

Licht W. and G. S. R. Narasimhamurty, "Rate of Fall of Single Liquid Droplets," AIChE Journal, 1, 366 (1955).

Lienhard, J. H., "A Semi-Rational Nucleate Boiling Heat Flux Correlation," Int. J. Heat Mass Transfer, 6, 215 (1963).

Mercier, J. L., F. M. da Cunha, J. C. Teixeira, and M. P. Scofield, "Influence of Enveloping Water Layer on the Rise of Air Bubbles in Newtonian Fluids," J. Applied Mechanics, 96, 29 (1974).

Mori, Y. H., K. Komotori, K. Higeta, and J. Inada, "Rising Behavior of Air Bubbles in Superposed Liquid Layers," Canadian J. Chem. Engrg., 55, 9 (1977).

Oseen, C. W., Hydrodynamik, Lipzig: Akad. Verlag. (1927).

Poggi, D., R. Minto, and W. G. Davenport, "Mechanisms of Metal Entrapment in Slag," J. Metals, 21, 40 (1969).

Porter, W. F., F. E. Richardson, and K. N. Subramanian, "Some Studies of Mass Transfer Across Interfaces Agitated by Bubbles," In Heat and Mass Transfer in Process Metallurgy (edited by A.W.D. Hills), Ch. 3. The Institution of Mining and Metallurgy, London (1966).

Reimann, M. and H. Alsmeyer, "Hydrodynamics and Heat Transfer Processes of Dry Ice Slabs Sublimating in Liquid Pools," Proceedings Seventh International Heat Transfer Conference, Munich, Germany, 4, 167 (1982).

Sims, G. E. and P. L. Duffield, "Comparison of Heat-Transfer Coefficients in Pool Barbotage and Saturated Pool Boiling," Trans. Can. Soc. Mech. Eng., Canada, 14, 1 (1971).

Suo-Anttila, A. J., "The Mixing of Immiscible Liquid Layers by Gas Bubbling," NUREG/CR-5219 (1988).

Suter, A. and G. Yadigaroglu, "Bubble-Driven Mixing of the Oxidic and Metallic Phases During MCCI," Trans. Am. Nucl. Soc., 56, 401 (1988).

Szekely, J., "Mathematical Model for Heat or Mass Transfer at the Bubble-Stirred Interface of Two Immiscible Liquids," Int. J. Heat Mass Transfer, 6, 417 (1963).

Tien, C. L., "A Hydrodynamic Model for Nucleate Pool Boiling," Int. J. Heat Mass Transfer, 5, 533 (1962).

Turton, R. and O. Levenspiel, "A Short Note on the Drag Correlation for Spheres," Power Technology, 47, 83 (1986).

Veeraburus, M. and W. O. Philbrook, "Observations on Liquid-Liquid Mass Transfer with Bubble Stirring," in Physical Chemistry of Process Metallurgy, (G. St. Pierre, ed.), p. 559, Interscience Publishers, New York (1959).

Wallis, G. B., One-Dimensional Two-Phase Flow, McGraw-Hill, New York (1969).

Werle, H., "Enhancement of Heat Transfer Between Two Horizontal Liquid Layers by Gas Injection at the Bottom," Nuclear Technology., 59, 160 (1982).

Winnikow, S. and B. T. Chao, "Droplet Motion in Purified Systems," Physics of Fluids, 9, 50 (1966).

Zanker, A., "Nomographs Determine Settling Velocities for Solid-Liquid Systems," Chemical Engineering, p. 147 (May 19, 1980).

NRC FORM 335 (2-89) NRCM 1102, 3201, 3202

U.S. NUCLEAR REGULATORY COMMISSION

BIBLIOGRAPHIC DATA SHEET

(See instructions on the reverse)

1. REPORT NUMBER (Assigned by NRC, Add Vol., Supp., Rev., and Addendum Numbers, if any.)

NUREG/CR-5875
BNL-NUREG-52325

2. TITLE AND SUBTITLE

Experimental Modeling of Heat and Mass Transfer in a Two-Fluid Bubbling Pool with Application to Molten Core-Concrete Interactions

3. DATE REPORT PUBLISHED

MONTH: June
YEAR: 1992

4. FIN OR GRANT NUMBER

L1259

5. AUTHOR(S)

George Alanson Greene

6. TYPE OF REPORT

Technical

7. PERIOD COVERED (Inclusive Dates)

8. PERFORMING ORGANIZATION – NAME AND ADDRESS (If NRC, provide Division, Office or Region, U.S. Nuclear Regulatory Commission, and mailing address; if contractor, provide name and mailing address.)

Brookhaven National Laboratory
Upton, NY 11973

9. SPONSORING ORGANIZATION – NAME AND ADDRESS (If NRC, type "Same as above"; if contractor, provide NRC Division, Office or Region, U.S. Nuclear Regulatory Commission, and mailing address.)

Division of Systems Research
Office of Nuclear Regulatory Research
U.S. Nuclear Regulatory Commission
Washington, DC 20555

10. SUPPLEMENTARY NOTES

11. ABSTRACT (200 words or less)

This report describes the results of seven series of experiments conducted to investigate heat and mass transfer phenomena in multicomponent bubbling pools with application to the modeling of interlayer heat and mass transfer between immiscible liquid layers and interfacial heat transfer to vertical and horizontal boundaries for the CORCON computer code. Criteria for the onset of entrainment between immiscible liquids, as well as the rate of entrainment and the rate of settling are developed, which are applicable for modeling of mass transport during core-concrete interactions. Heat transfer models are developed for the case of stratified layers as well as the case with mass entrainment between the layers. Finally, models for heat transfer with bubbling to horizontal, drilled surfaces as well as bubbling along vertical surfaces are presented which are appropriate for boundary heat transfer analyses during molten core-concrete interactions.

12. KEY WORDS/DESCRIPTORS (List words or phrases that will assist researchers in locating the report.)

Meltdowns - concretes, Heat Transfer, Mass Transfer, Reactor Accidents - fluid-structure interactions, Corium, Boiling, Bubbles, Reactor Accidents - reactor core disruption, C Codes, Entrainment, Gas Production Rates

13. AVAILABILITY STATEMENT

Unlimited

14. SECURITY CLASSIFICATION

(This Page) Unclassified

(This Report) Unclassified

15. NUMBER OF PAGES

16. PRICE

THIS DOCUMENT WAS PRINTED USING RECYCLED PAPER

UNITED STATES
NUCLEAR RE' 'LATORY COMMISSION
WASHINGT N, D.C. 20555-0001

OFFICIAL BUSINESS
PENALTY FOR PRIVATE USE, $300

SPECIAL FOURTH-CLASS RATE
POSTAGE AND FEES PAID
USNRC
PERMIT NO. G-67

UNITED STATES
NUCLEAR REGULATORY COMMISSION
WASHINGTON, D.C. 20555-0001

OFFICIAL BUSINESS
PENALTY FOR PRIVATE USE, $300

SPECIAL FOURTH-CLASS RATE
POSTAGE AND FEES PAID
USNRC
PERMIT NO. G-67